NUCLEIC ACID PURIFICATION AND ANALYSIS BY ISOTACHOPHORESIS

A dissertation
submitted to the Department of Mechanical Engineering
and the committee of graduate studies
of Stanford University
in partial fulfillment of the requirements
for the degree of doctor of philosophy

Alexandre Louis André Persat

December 2010

This dissertation is online at: http://purl.stanford.edu/pd941xj1045

I certify that I have read this dissertation and that, in my opinion, it is fully adequate in scope and quality as a dissertation for the degree of Doctor of Philosophy.

Juan Santiago, Primary Adviser

I certify that I have read this dissertation and that, in my opinion, it is fully adequate in scope and quality as a dissertation for the degree of Doctor of Philosophy.

Stephen Quake

I certify that I have read this dissertation and that, in my opinion, it is fully adequate in scope and quality as a dissertation for the degree of Doctor of Philosophy.

Eric Shaqfeh

Approved for the Stanford University Committee on Graduate Studies.

Patricia J. Gumport, Vice Provost Graduate Education

This signature page was generated electronically upon submission of this dissertation in electronic format. An original signed hard copy of the signature page is on file in University Archives.

Abstract

Microfluidics has recently enabled new capabilities in life sciences research. By leveraging physics at the microscale, novel miniaturized methods and devices provide fundamental improvements over traditional assays including higher sensitivity, massive parallelization, speed and automation. For example, nucleic acid analyses such as PCR or capillary electrophoresis are now commonly executed on microfluidic platforms. However, extracting and isolating a set of molecules of interest from a biological sample remains a widespread challenge, in particular when the target is a nucleic acid; such sample preparation has been identified as the "weak link" of microfluidics.[1] Moreover, the discovery of classes of small RNA such as microRNA[2] (miRNA) has revealed the limitations of benchtop preparation methods.[3] This work tackles these issues by leveraging an electrophoretic focusing method, isotachophoresis (ITP), to perform selective focusing of specific nucleic acid molecules contained in complex mixtures. This includes extraction of genomic DNA from blood and isolation of miRNA from total RNA. Also, we leverage the unique physics of ITP to perform simultaneous purification and analysis of these molecules, thus enabling automated analysis at unprecedented speed.

ITP is a robust electrophoretic preconcentration technique which generates strong electric field gradients, and enables selective focusing and separation of charged species based on their electrophoretic mobilities. In this

work, we show that we can extract and purify genomic DNA from chemically lysed whole blood samples by carefully controlling ITP electrolyte chemistry to achieve selective focusing of genetic material. We show that ITP outputs PCR-compatible DNA with high efficiency in about 1 min. This novel sample preparation technique allows for efficient, fast, and automated purification of DNA from 10 nL to 1 µL of biological fluids.

We also demonstrate that ITP focusing of microRNA – short (~22 nt), non-coding RNA regulating gene expression – enables quantification and sequence specific detection. We leverage both the selective and preconcentration capability of ITP for the quantification of global miRNA abundance. This allows for the measurement of RNA silencing activity in specific cells or tissues. We have optimized ITP chemistry and used a multi-stage injection strategy to selectively preconcentrate and quantify RNA shorter than 40 nt. We discuss results of miRNA quantification for a wide variety of samples. Additionally, we show that the combination of selective ITP focusing with simultaneous hybridization with molecular beacons is an efficient method for detection and quantitation of specific miRNA sequences. We demonstrate the efficacy of this assay for the detection of a liver specific miRNA. Finally, we show that we can use ITP to perform polymerase chain reaction in isothermal conditions by creating a cycles of chemicals mimicking thermal cycling.

Acknowledgements

I have spent an unforgettable time at Stanford. There, my passion for science as been continuously growing. I am grateful to the people who have helped me discover that scientific research could be so thrilling.

I would like to thank my advisor Juan Santiago for his mentorship and help in accomplishing this work. For his permanent support, I will always be indebted to him. Juan gave me the opportunity to innovate and work independently. He is highly dedicated to his students and strives to transmit his enthusiasm for science. I admire Juan's achievements, and for me his career in academia is a model of success. I also thank the other members of my reading committee, Stephen Quake and Eric Shaqfeh, who provided invaluable advice on my research.

I have received precious help from numerous members of the Santiago lab. I particularly thank David Huber and Tomoyuki Morita for training me to a wide variety of lab techniques in my first year of graduate school. I have used their teachings throughout my doctoral studies. I am also very grateful to CC, who keeps the lab running and is so devoted to students.

I made great friends in the lab. I have spent days and nights researching by Elia, Ray, Cullen, Shawn, Tom, Tarun and Dan. They are all brilliant researchers and amazing people. I sincerely hope our roads will cross in the future. I also want to thank my friends Aurel and Alice who helped me staying French, and Justin for his refreshing authenticity.

Lastly, I would like to thank my family. Laura's love and support gave me the motivation and inspiration to achieve this work. Also, I would not have been able to go through this time without the constant support of my parents and my sister. To them, I dedicate this dissertation.

Table of Contents

List of Figures

List of Tables

Chapter I. Introduction

I.1 Background

Electrophoresis

Under the influence of an electric field, a charged compound is subject to a Coulomb's force inducing its motion. In a fluid, this migration is termed electrophoresis, and generally refers to the displacement of ions. In solution, electrophoresis results from the balance between a coulomb's force driving the charge and a drag force that opposes its motion.[4] After a brief charge relaxation time[5] (typically a few microseconds), the charged species reaches a steady drift velocity, the electrophoretic velocity $\vec{u}_{\text{eph}}$, that is proportional to the electric field $\vec{E}$. The factor of proportionality is referred to as the electrophoretic mobility v_{eph} and is characteristic of the species:

$$\vec{u}_{\text{eph}} = v_{\text{eph}}\vec{E}\,.$$

The electrophoretic mobility is here a signed quantity that depends on multiple parameters including the charge and size of the ion and the viscosity of the solvent.[4] The chemistry of the solution can strongly affect the charge of the ion (*e.g.* via acid-base reactions) and therefore can dramatically affect its mobility.[6] Such dependence is the key to electrophoretic analysis which, in optimized chemical conditions, allows for the separation of a large number of charged species.[7]

Capillary electrophoresis

Capillary electrophoresis (CE) is a ubiquitous separation technique in chemical and biomedical analysis.[7] Optimization of CE system has allowed for separation of a variety of compounds including explosives,[8] toxins,[9] proteins,[10] and nucleic acids[11] at high resolution. CE can be combined with ultra-sensitive detection systems such as laser induced fluorescence,[12] requires only small amounts of sample and has potential for parallelization.[13] More recently, the development of CE on planar microchips has reduced the laboratory footprint of CE systems and even enabled portability, automation and parallelization while further reducing reagent use.[14] A large panel of techniques based on CE has made it an even more generally applicable separation method. For instance, micellar electrokinetic chromatography is attractive for the analysis of hydrophobic or neutral compounds,[15] capillary isoelectric focusing is widely applicable to separation of proteins,[16] and isotachophoresis allows for the preconcentration and separation of trace analytes.[17-19]

Life scientists have adopted CE for multiple types of nucleic acid analysis. For example, CE and its microchip version have been applied to sequencing,[20] analysis of polymerase chain reaction (PCR) products,[21] and assessment of RNA quality,[22] For highest performance, CE of nucleic acids leverages the sieving capability of polymers dissolved in the separation buffer. Multiple commercial CE systems (*e.g.* the Agilent LabChip bioanalyzer system) can

perform on a single instrument various types of nucleic acid separation assays with a high level of automation and sensitivity.

Isotachophoresis

Isotachophoresis (ITP) is a well established electrophoretic separation and preconcentration technique.[23,24] It leverages a heterogeneous buffer system with distinct electrophoretic mobilities to generate strong electric field gradients. In most cases, designing an ITP experiment consists in selecting a leading and trailing electrolyte (LE and TE) with respectively greater and lesser electrophoretic mobility than the analyte's. We describe two ITP modes **Figure I-1**. In **Figure I-1**a, the analyte is injected between LE and TE within the separation channel (finite injection ITP) or alternately in **Figure I-1**b, the analyte is dissolved in one of the electrolytes, here the TE, before creating an initial interface between LE and TE (single interface ITP). Upon application of an electric field, ionic species reorganize into contiguous zones of increasing effective electrophoretic mobility from TE to LE, allowing analyte focusing.

The ITP interface is self-sharpening,[25] and the main features of ITP focusing include:

- Preconcentration. Focusing species accumulate at the ITP interface, greatly increasing their concentration, up to a million-fold.[26] Preconcentration is typically used prior separation of focused analytes to increase assay sensitivity.[18]
- Separation. While analytes focused in "peak mode" do not separate, the use of spacers (ions whose mobility ranges between two analyte's) in

"plateau mode" enables simultaneous preconcentration and separation.[19, 27, 28] Selective focusing. Species whose mobilities are smaller than the trailing ion's or greater than the leading ion's do not focus. Therefore, optimization of ITP chemistry (*e.g.* careful selection ot leading and trailing ion) enables focusing of one species while leaving other species unfocused.[29]

- Protection from dispersion. The self-sharpening ITP interface creates a focused sample zone whose axial width can be on the order of 10 μm. This protects the sample from dispersion into a volume smaller than 100 pL (in a typical 100 μm deep and wide channel).

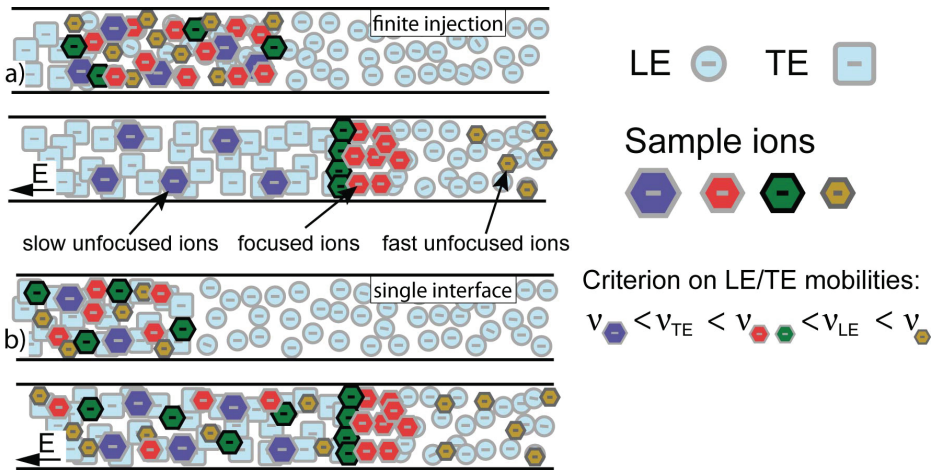

Figure I-1: Schematic representation of ITP with sample containing four different ions injected within the leading electrolyte (LE). In (a), we show finite injection ITP where the sample is initially injected between LE and TE and in (b) single interface ITP where the sample is dissolved in TE. Two ions (mid-sized red and green hexagons) have mobilities bound by those of the TE and LE. Upon application of an electric field, these two targeted ionic species focus, generally in order of increasing electrophoretic mobilities. Here, we depict the selective focusing of two target sample analytes (mid-sized green and red hexagons). Species which have mobilities lower than the TE (here large blue hexagons) or higher than the LE (small yellow hexagons) do not focus.

While ITP has been widely used as an efficient preconcentration method for the analysis of a wide variety of compounds,[23] it has not yet been efficiently adapted to life sciences assays. For example ITP of nucleic acids has been limited to the focusing of DNA fragments prior CE.[30] While it yields large preconcentration factors for DNA, ITP combined with CE has a limited use for the analysis of PCR products, which does not necessarily require high sensitivity.

Surprisingly, the unique features of ITP physics described above have only been marginally used to design novel assays. In particular, the selectivity of ITP, *i.e.* the ability to focus one species while leaving others unfocused, has only been used for fractionation of proteins from a mixture.[31] Also, to our knowledge, the protection from dispersion has only been utilized twice to perform chemical reactions: for immunoassays,[32] and as a way of bringing and mixing reagents together.[33] In this work, we will leverage the unique features of ITP described above, in particular the selective focusing as a way of purifying nucleic acids and the protection from dispersion as a way of using the ITP interface as a small reactor.

I.2 Organization of the thesis

In Chapter II, we describe a sample preparation technique that leverages ITP to extract and purify DNA from blood. We discuss how selection of a suitable buffer system enables purification of nucleic acids to yield a sample ready for analysis. In Chapter III, we show that ITP can be used to isolate and

quantify a single type of nucleic acids, here microRNA (miRNA). We show that such use of ITP allows for quantification global miRNA levels in total RNA as a measurement of RNA silencing activity. Then, we demonstrate that ITP can be used to perform chemical reactions with simultaneous focusing. In Chapter IV, we show combination of selective miRNA focusing with hybridization of molecular beacons for sequence selective detection. In Chapter V, we demonstrate that ITP focusing and separation of nucleic acids can be used to carry out polymerase chain reaction (PCR) at constant temperature by cycling chemical concentrations. Appendices provide supplementary description and discussions of methods used in the thesis, including flow control, design of lysis chemistry for ITP purification and injection protocols.

I.3 Scientific contributions

First, the purification of nucleic acids using ITP is a novel method which that allows for significantly faster sample preparation from minute amounts of sample compared to existing purification techniques.[29] A patent application related to this invention is currently under review.[34] Also, the precise isolation of the short RNA using ITP enables measurements directly targeting miRNA. In particular, our ITP based quantitation is the unique method for measurement of global miRNA abundance.[35] To achieve this, we designed a novel ITP protocol that leverages multiple zones with distinct chemical compositions to combine selectivity and sensitivity, which we filed for

provisional patent application.[36] Besides competing with traditional miRNA analysis methods, the combination of precise ITP isolation with molecular beacon hybridization allows for miRNA profiling at unprecedented speeds.[37] Finally, We have performed PCR with ITP and chemical cycling which enables isothermal reaction, relaxing the requirement of thermal control and reagent thermostability.[38] We filed a patent application for this invention.[39]

Chapter II. Purification of nucleic acids by isotachophoresis

The contents of this chapter were previously published by Persat, Marshall and Santiago (2009)[29] and are reproduces here with minor modifications.

II.1 Introduction

Microfluidics has become an alternative to traditional techniques for biological and medical analysis; and offers the use of small reagent volumes, fast analyses, and potential for parallelization.[40] PCR,[41] capillary electrophoresis,[42] immunoassays,[43] and many other analytical techniques used in biology and medicine have been successfully miniaturized. However, sample preparation is often still a challenge and a limiting factor in the capability of many devices,[1] so that most miniaturized systems have used prepurified, ideal samples as analyte. One important application is the purification of nucleic acids (NA) from complex biological samples. We here demonstrate a simple, fast, efficient and sensitive technique for the purification of NA from whole blood which leverages the physicochemistry of ITP.

The traditional method for nucleic acid purification is based solid phase extraction (SPE).[44] Nucleic acids dissolved in a low pH, high ionic strength buffer have high affinity for a hydrophobic surface such as silica. In SPE, nucleic acids are released in such buffer and flowed through a silica column to which they bind. The column is then washed with ethanol (where NA have low solubility) and finally the NA are eluted in a low ionic strength solution, typically

deionized water. Commercial spin columns such as the QIAGEN kits (Valencia, CA) are now the standard methods for purification of NA. [45]

The implementation of NA purification in microchip format has been limited to the miniaturization of SPE. Extensive work by Landers and co-workers has shown successful microchip integration of SPE with application to purification of DNA,[46] RNA,[47] and successful integration with on-chip PCR.[21] While micro-SPE shows excellent efficiency and throughput,[45] the process requires specialized materials and fabrication (*e.g.* micropillars or packing of silica beads). Further, the typical SPE protocol involves three successive steps (loading, washing, elution), requires bulk flow control, and uses a PCR inhibiting chemistry (*e.g.* chaotropic agents, organic solvents).[45]

Similarly, purification of NA in microfluidic device with paramagnetic beads involves usage of significant off-chip instrumentation such as magnets and networks of valves.[48]

ITP has been marginally used as a sample purification method.[49, 50] For instance, Caslavska *et al.*[31] used recycling ITP to simultaneously purify, isolate and fractionate proteins from a mixture, but not from a crude biological sample. Kondratova *et al.*[51] concentrated and isolated DNA from blood plasma and urine by agarose gel ITP with applications to cancer diagnosis. In this work, the authors only recovered extracellular NAs therefore excluding genomic material. Also, performing ITP on an agarose gel does not allow for miniaturization or integration with other on-chip modules for automation, and require further extraction and purification from the gel slab. More recently,

Schoch *et al.*[52] isolated short nucleic acids from cultured cells by ITP at low pH in a pluronic sieving matrix. The use of an LE with low pH reduced the effective charge of proteins while leaving the mobility of nucleic acids nearly unchanged. While this technique was efficient for isolation of short nucleic acids, Schoch *et al.* have not applied this concept to the extraction of genomic DNA from biological fluids and have not verified purity of the isolated sample. To our knowledge ITP has never been applied to sample preparation from biological fluids for genomic analysis or to sample preparation of blood.

We here present and demonstrate an ITP-based purification method for extracting genomic DNA from a biological fluid. We perform ITP focusing in free solution and use a small injected volume (order 10 nL) of whole blood lysate as sample. We leverage the selectivity of ITP focusing to concentrate NA in a sharp zone while rejecting most proteins and other unwanted compounds. We first determine extraction efficiency to evaluate the performance of the technique. We then demonstrate ITP purification of genomic DNA from whole blood and assess its performance with this difficult sample. Finally, we recover the genetic material and perform off-chip PCR to assess the quality of the ITP purification process.

II.2 Materials and Methods

Microchip preparation.

We performed on-chip experiments in an off the shelf microchip with 90 μm wide (50 μm mask width) by 20 μm deep borosilicate microchannels in

a simple cross geometry (model NS12A, Caliper Life Sciences, Mountain View CA, *cf.* Figure II-1). The injection channel is 1.5 cm long (with an approximate volume of 25 nL) and the separation is channel 4.5 cm long. We treated the channels with the silanizing agent Sigmacote (Sigma, MO) as follows. We first rinsed the channel 10 min with a 1:1 methanol hydrochloric acid solution, followed by 10 min of concentrated sulfuric acid. This rinsing step removes species for the glass surface that potentially inhibit the silanization, such as metal ions. We then rinsed the channels with deionized water for 2 min or more, and dried thoroughly with a vacuum. Next, we applied the silanizing solution for about 10 min. We then rinsed the channels with hexane and deionized water. This modification creates a hydrophobic layer on the microchannel surface which allows for reduction of adsorption of proteins from lysate on the channel walls and for electroosmotic flow reduction. To avoid cross contamination, we rinsed the chip between each experiment as follows: 2 min with a 1:10 (v/v) household bleach solution (Clorox, CA), 2 min with deionized water, and 2 min with leading electrolyte buffer (see below). Bleach is an efficient reagent for the degradation of DNA.[53]

Sample lysis.

Blood samples from a healthy donor were collected in heparin tubes and stored in 2 mL aliquots at -80ºC. Before each set of experiments, we thawed one blood aliquot and prepared a stock of lysis buffer containing 1% Triton X-100 (Sigma, MO) in 50 mM Tris hydrochloride at pH = 8.2. We diluted 10 µL of whole blood and 4 µL of proteinase K (RNA grade, Invitrogen, CA) in 86 µL

of lysis buffer. We then incubated the lysate 10 min at 56ºC in a water bath. In the case of the second control in **Figure II-5** (third bar in the plot), we added 4 U of deoxyribonuclease I (DNase I, amplification grade, Invitrogen, CA) to the lysate and incubated 15 min at room temperature prior to proteinase K treatment. To quantify the ITP extraction efficiency, we diluted a commercial standard solution of λ-DNA (0.333 mg.mL^{-1}, Invitrogen, CA) in lysis buffer and used this as a standard sample. All solutions were prepared with DNase/RNase free deionized water (Gibco, CA).

Isotachophoresis-based purification.

Leading (LE) and trailing electrolytes (TE) were respectively 50 mM Tris titrated with hydrochloric acid to pH = 8.2 and 50 mM Tris titrated with HEPES to pH = 7.8. LE and TE each contained 1x SYBR Green I (Invitrogen, CA) for fluorescence visualization and on-chip DNA quantitation. We obtained best results adding also 0.1% Triton X-100 to reduce electroosmotic flow and protein adsorption (in conjunction with silanization treatment).

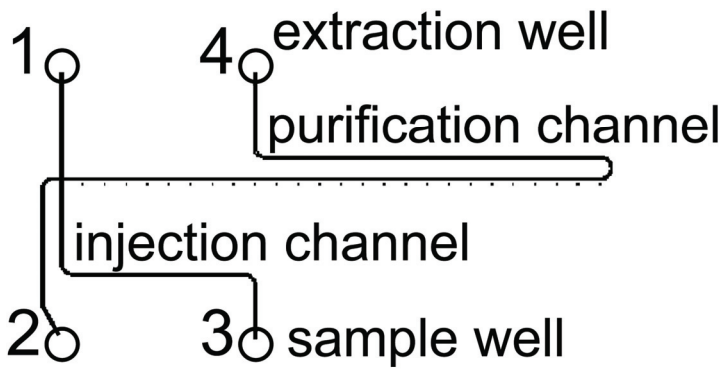

Figure II-1: design of the chip used to perform the ITP based purification. Sample is injected from reservoir 3 by applying a vacuum at 2.

For each experiment, we first filled all four channels and reservoirs (*cf.* Figure II-1) with LE. We emptied reservoir 3 with a vacuum, and pipetted 1 μL of lysate into that reservoir. We then applied a vacuum to reservoir 2, generating flow from reservoirs 1, 3 and 4 to 2, which fills the injection channel with lysate (~25 nL) while the separation channel remains filled with LE. We carefully removed the lysate remaining in reservoir 3 with a vacuum. We only used a light vacuum to avoid generating flow in the injection channel, which could remove some of the injected lysate. We then rinsed reservoir 3 where we finally pipette 10 μL of TE. We then immediately applied electric field between 3 and 4 (500 V) with a sourcemeter (model 2410, Keithley, Cleveland OH) controlled via Matlab (the Mathworks, Natick, MA) to carry out the purification. We used fluorescence visualization of used the current signal to locate the ITP interface in the channel (see Figure II-2). We used this same injection protocol for the extraction efficiency quantifications performed with λ-DNA.

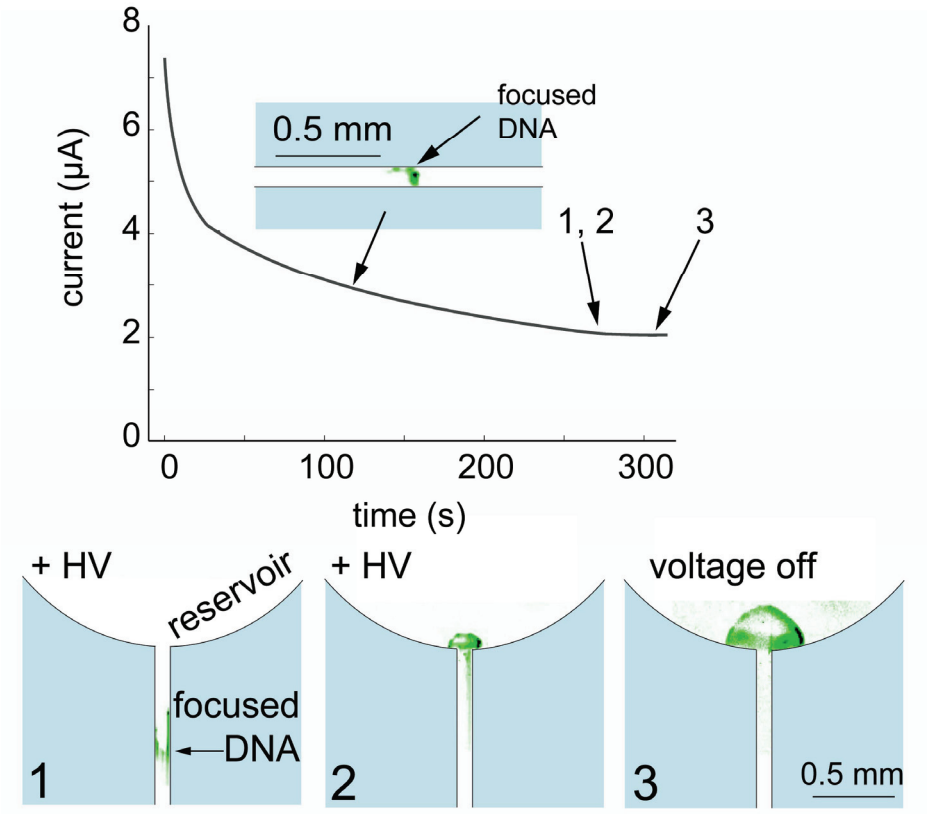

Figure II-2: Localization and extraction of the ITP purified NA. We track the location of the focused NA ITP zone by either monitoring ionic current or by fluorescence visualization. Above, we show a measured current trace obtained from a constant voltage ITP extraction experiment where the sample is λ-DNA. We acquired the current trace by interfacing the sourcemeter with MATLAB using a GPIB card (National Instruments, TX). The current decreases monotonically as the ITP interface advances within the channel, as the relatively low conductivity TE replaces the high conductivity LE. At the moment where the current reaches a plateau (here near t = 260 s), the purification channel is entirely filled with TE and the ITP interface has reached the anode reservoir. Above the current plot, is an actual image of focused DNA in the microchannel (with a superposed schematic of walls). At the bottom, we show actual fluorescence images corresponding to the same experiment. Image 1 shows the focused DNA approaching the reservoir. Image 2 shows an image of the same location just after the interface enters the reservoir. Image 3 shows the reservoir about 20 s later, where the purified NA has migrated into the reservoir. These three instances in time are highlighted in the current plot. Either or both current monitoring and fluorescence visualization can be used to track the position of the NA during the purification process.

Visualization.

We performed on-chip visualization on an inverted epifluorescent microscope equipped with a 4x (Plan APO, N.A. = 0.2, Nikon, Japan) or a 10x objective (Plan APO, N.A. = 0.45); a mercury light source (Ushio, Japan); a filter cube (exciter/emitter 485/535 nm, Omega, VT); and a 0.6x demagnification lens (model RD060-CMT, Diagnostic Instruments, MI). We acquired images with a CCD camera (Cascade 512F, Roper Scientific) controlled with the software Winview32 (Princeton Instruments, Trenton, NJ).

On-chip quantitation.

We quantified the amount of DNA extracted from whole blood in the ITP-focused zone by first calibrating our fluorescence measurement. For the calibration, we used a control solution of genomic DNA purified from blood with the DNeasy blood and tissue purification kit (QIAGEN, Hercules, CA) according to the manufacturer's instructions. We measured its DNA concentration with a Nanodrop 1000 spectrophotometer (Thermo Scientific, MA) and prepared a 1.42 $\mu g.mL^{-1}$ standard solution stained with 1x SYBR Green I in LE. We acquired images of the fluorescent profile of this standard filling the purification channel (but without performing ITP). Using these images, we were able to relate peak areas to DNA mass in the ITP experiments. We used the fluorescent profile of the channel filled with standard corrected for background intensity as a flat field image. A frame of the ITP experimental data was corrected for background and normalized with the flat field. We sum the intensity of all pixels in this frame to get the amount

of DNA in terms of standard units of the calibration solution. We then converted the number to DNA mass by multiplying with the amount of DNA in the channel (calculated assuming a rectangular channel cross-section). We also performed this calibration with a solution of λ-DNA.

Off-chip PCR.

We tracked the position of the focused zone in the channel by directly visualizing the focused species or by monitoring current transients (see Figure II-2). After the ITP interface exited the purification channel, we collected the liquid from reservoir 4 (~2 μL) with a standard pipettor into a PCR tube containing 5 μL of 2x Fast SYBR Green I master mix (Applied Biosystems, CA), 0.1 μM primers (Invitrogen, CA) targeting a 201 bp fragment of the BRCA2 gene (forward primer: 5'-CAC CTT GTG ATG TTA GTT TGG A-3'; reverse primer: 5'-TGG AAA AGA CTT GCT TGG TAC T-3'), and filled the rest of the reaction tube with deionized water up to 10 μL. We summarize this procedure in Figure II-3. All PCR reactions were prepared in a UV-sterilized fume hood to avoid contamination and allow sensitive amplification without false positives. We performed off-chip real-time PCR on an ABI 7500 Fast thermocycler with the following thermal profile: 20 s initial hold at 95˚C, 40 cycles composed of 3 s denaturation at 95˚C followed by 30 s annealing and extension at 60˚C. We performed real-time monitoring of the reaction with SYBR Green I (included in the PCR master mix) and used the PCR curves to assess success of amplification, without performing quantitative PCR. We systematically compared the amplification result to a negative control (without

DNA in the reaction tube) and to a control where we used non-purified lysate as template. For all reaction products, we performed post-PCR dissociation curve analyses on the same instrument.

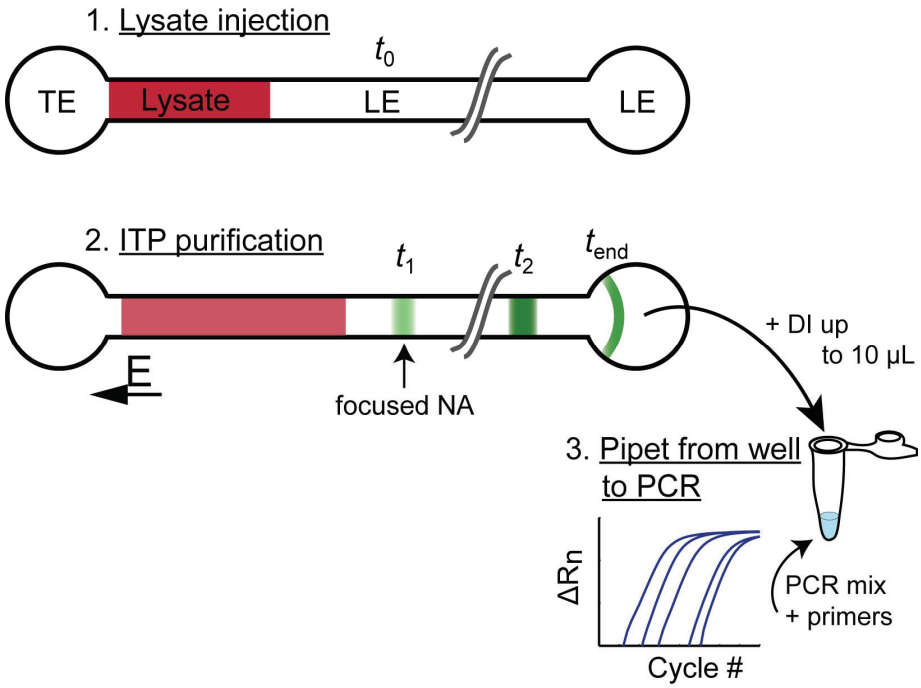

Figure II-3: Schematic of the workflow of the ITP-based purification with off-chip PCR. The lysate is initially hydrodynamically injected between LE and TE. Upon application of an electric field, NAs focus and migrate towards the anode in a sharp concentrated zone. When the focused NA enter the anode reservoir, we pipet all of the solution out of the reservoir (~ 2 µL), add it to the PCR mix, and perform real-time PCR.

II.3 Results and discussion

Principle of ITP purification.

Our purification method relies on the ability of ITP to separate and focus species based on their effective electrophoretic mobilities.[17, 27] We depict the ITP-based purification in Figure II-4. We select LE and TE with effective

mobilities[6] respectively higher and lower than that of the target nucleic acids (NA). Upon application of an electric field, NA molecules focus between TE and LE in a sharp concentrated zone. Species with smaller effective mobilities than the TE migrate into the channel but lag behind and do not focus. Faster species overspeed the sample zone and also do not focus. Overspeeding species can only slightly contaminate the ITP zone as they overlap with the ITP zone, but remain unfocused and therefore have low concentration. At moderate pH and in free solution, DNA has relatively large magnitude (negative) mobility compared to a vast number of polypeptides,[54, 55] so the mobility of the TE effectively determines purification selectivity. In this work, we also use proteinase K to release DNA from histones (see below), which also effectively digest most proteins in solution into shorter fragments.

There are an abundance of PCR inhibitors in blood (*e.g.* hemoglobin, immunoglobulin G, lactoferrin), making it a challenging sample for a NA purification technique.[56] If we define a pure sample as a sample that is PCR compatible, performing DNA extraction from blood is therefore one of the most stringent tests for purification. In our protocol, we use proteinase K to release DNA from its binding proteins, which has also the effect of degrading nearly all proteins, including the ones that potentially inhibit PCR, into short polypeptides.[57] But proteinase K is itself a PCR inhibitor.[58] We compensate for this by operating with an ITP chemistry where proteinase K (pI = 8.9)[57] does no focus. The LE is titrated to pH = 8.2, lower than the isoelectric point of proteinase K. so that this protein is effectively positively charged. During

the ITP process, the pH in the adjusted TE is nearly the same as the initial value in the LE. Proteinase K is therefore kept away from the sample zone as it electromigrates in the opposite direction, and stays in the TE reservoir. The combination of proteinase K and ITP-based purification effectively removes PCR inhibiting species and other polypeptides from the lysate.

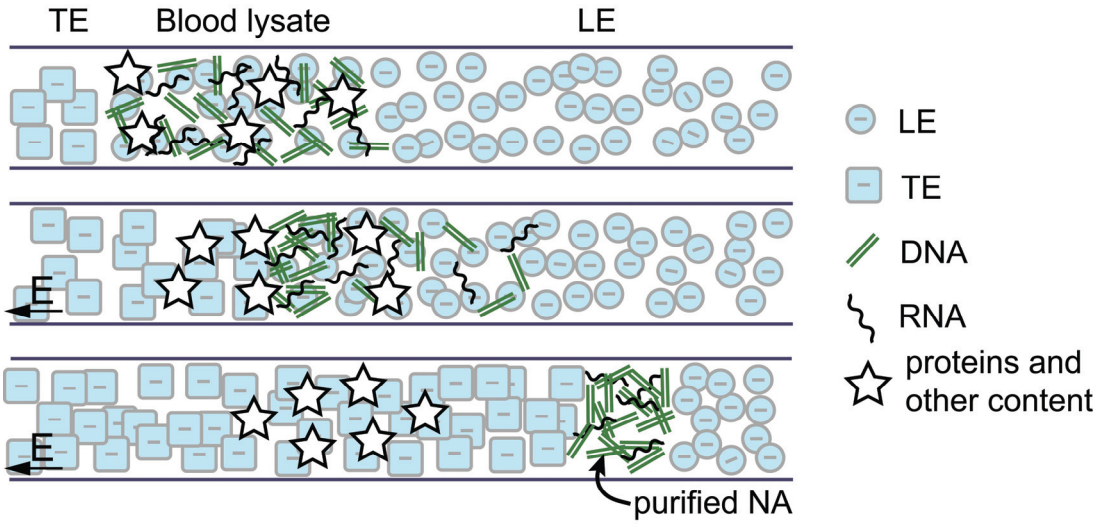

Figure II-4: Schematic of the ITP-based NA purification from a complex biological sample like blood lysate. We select LE and TE with mobilities respectively larger and smaller than NA. The TE needs to have larger mobility than proteins (and other contents) present in blood lysate. We inject a finite plug of lysate between TE and LE. Upon application of an electric field, NA focus between LE and TE, while proteins cannot focus as they travel slower than the ITP interface. After sufficient time, the ITP zone contains only pure NA extracted from the lysate.

Lysis

There exist a wide variety of lysis methods for the preparation of nucleic acids from biological fluids (see Appendix D).[59] The typical lysis method for blood is the selective lysis of white blood cells after selective lysis of red blood cells. The red blood cells (which do not contain genetic material) are first

lysed using a first lysis buffer, without lysis of leukocytes. The first lysate is then centrifuged and the supernatant discarded to yield a concentrated solution of white blood cells, free of red blood cells. Finally, white blood cells are lysed for example using a surfactant. In this work, we performed full lysis of whole blood without selectivity, thus avoiding additional manual steps and centrifugation.

We carefully chose the chemical lysis agent to avoid possible contamination. The surfactant Triton X-100 is an efficient lysis agent for eukaryotic cells, and has the advantage of being PCR friendly.[60] We have found Triton-X does not appreciably alter proteinase K function or modify protein mobilities. This is in contrast to, for example, the popular bacterial lysis agent sodium dodecyl sulfate (SDS). SDS disrupts the cell membrane, but also denatures proteins and significantly increases protein effective charge.[61] Moreover, Triton X-100 is a neutral (zwitterionic) surfactant, and therefore does neither electromigrate nor is focused by ITP. Our lysis buffer also avoids chaotropic agents which at significant ionic strengths can interfere with ITP dynamics (*e.g.* high concentration guanidine hydrochloride[62, 63]). Chaotropic agents are useful ad versatile lysis agents and their combination with solid phase extraction is a powerful extraction tool, but are difficult to implement in ITP without significant dilution.

Extraction efficiency

In our purification procedure, there are at least two extraction efficiencies of interest: the fraction of DNA purified and focused via ITP from the amount

injected into the channel, and the amount of DNA extracted from the chip and delivered to PCR versus the amount of DNA in the lysate dispensed into the chip. To characterize the former, we applied our technique to a solution of λ-DNA of known concentration. We injected 10 pg of λ-DNA on-chip and performed the ITP purification as described in the experimental section. We determined the amount of focused DNA by quantifying SYBR Green I fluorescence and comparing it to the standard (see calibration section above). We measured the mean fraction of extracted DNA (*vs.* amount injected into the channel, calculated based on stock concentration of λ-DNA and on calculated injection channel volume) as 1.03 ± 0.06 (N = 3). This approximately complete extraction is at least as good as traditional extraction methods (*e.g.* QIAGEN kits) and state-of-the-art micro-solid phase extraction devices.[45] We estimate that we extract out of the chip (and deliver to the PCR) approximately all of the DNA which we focus on chip.

Our injection protocol currently processes a small amount of the 1 μL lysate sample volume dispensed into the chip. We process only 25 nL of sample, which is 1/40th of the volume dispensed into the chip. Processing such a small fraction of lysate significantly decreases the global extraction yield. While this remains acceptable in some applications (given the efficiency associated with injection is precisely known), it might represent a drawback for application requiring large amounts of nucleic acids or high throughput. However, we decided to use a chip with such small channel volume for convenience and availability, but we estimate a much higher sample fraction

can be processed by modifying the chip design. For example, a custom chip with a relatively large 1 μL injection channel can be designed. Alternately, a larger fraction of sample dispensed into the chip presumably can be processed using a small reservoir volume and a nanoliter fluid dispenser.

Extraction time

In ITP, migration velocity is directly proportional to current.[27] Consequently, the duration of purification depends on applied voltage and channel geometry. In our conditions, a typical purification lasts about 250 s for an applied voltage of 500 V (*cf*. Figure II-2), which is fast compared to a typical micro-SPE process.[46] Increasing applied voltage can be used effectively to reduce this time. As a demonstration of the potential speed of the purification process, we also performed experiments with an applied voltage of 3 kV using lambda λ-DNA as sample. This higher applied potential yielded extraction in 56 s in average (N = 3), without undue joule heating. This extraction time is by far shorter than any other nucleic acid extraction technique.

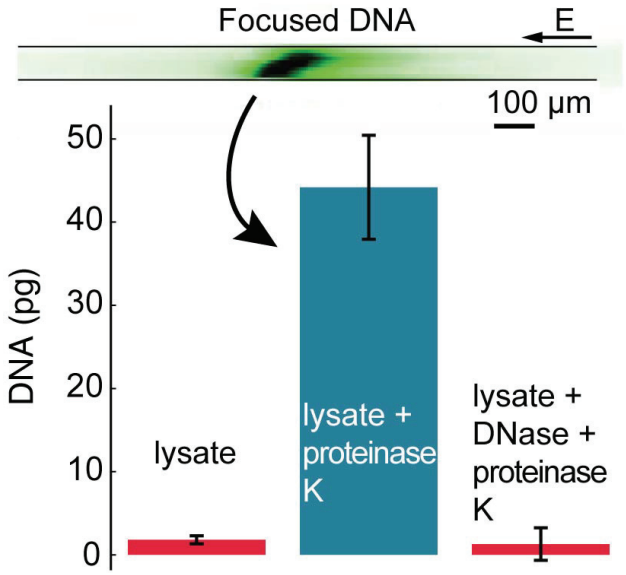

Figure II-5: Experimental demonstrations of ITP-based NA purification from human blood. The bars show mean values of NA mass purified from blood lysate, as calculated from the fluorescence intensity profile. We show results from three sets of experiments. ITP purification of pure lysate yields little or no signal, and therefore little or no extraction of NA. The lysate pretreated with proteinase K shows significant signal enhancement over the previous case. We show an image of ITP-focused DNA zone above the bar graph. The amount of focused DNA is 44.2 ± 6.2 pg. As a control, we performed the extraction with a lysate treated with first DNase and then proteinase K, which significantly lowers the focused DNA mass. Together, these show that the ITP purification method efficiently extracts DNA from human blood lysate. We injected 2.5 nL of blood, which contain between 65 and 162 pg of DNA, so that our purification efficiency for a blood sample ranges between 30 and 70%. Uncertainty bars represent uncertainty in measured mass of DNA with 95% confidence interval. The three sets are results from N = 2, 9, and 2 repetitions, respectively.

ITP-based purification from whole blood results

We show examples of DNA purifications from a whole blood lysate in **Figure II-5**. Here we present purifications of DNA from about 2.5 nL of whole blood (25 nL of blood lysate). We show three sets of experiments: purified blood lysate, blood lysate treated with proteinase K, and blood lysate treated

first with DNase and then proteinase K. We used SYBR Green I fluorescence measurements to estimate the amount of DNA recovered in the ITP zone. The amount of DNA recovered without proteinase K is negligible (on the same order as the negative control). In these runs we also observed a large amount of debris (micrometer-size fluorescent particles) migrating into the separation channel, which could eventually clog the chip. On the other hand, the mass of focused DNA is significant when performing the assay on a lysate initially treated with proteinase K. The third set of results shows ITP purification of a lysate treated with DNase prior to proteinase K treatment. DNase is a enzyme that specifically digests DNA without damaging proteins. This control case shows low DNA recovery, as expected, and shows that the fluorescence from the previous case is actually due to recovery of DNA. From observation of these three experiments, we hypothesize that DNA binding proteins (in particular histones[64]) significantly reduce the electrophoretic mobility of DNA by increasing the hydrodynamic Stokes' drag of the DNA-protein complex. If the mobility of the DNA-protein complex is smaller than the mobility of the TE, DNA does not focus and cannot be purified. If the protein bound to DNA increases significantly drag and is positively charged, the trailing ion must have a relatively smaller electrophoretic mobility than the complex, and a suitable ITP chemistry that will focus DNA becomes non-selective. Proteinase K effectively releases DNA from binding proteins allowing selective focusing and purification. Together, these experiments show that our fluorescence

signal is due to focused DNA from the lysate samples, and that the extraction process is suitably repeatable with the combination of proteinase K treatment.

The fluorescence measurements from **Figure II-5** show that we focused about 44 ± 6 pg (N = 9) of DNA from the initial 2.5 nL of whole blood (25 nL of lysate). A nanoliter of blood from a healthy human contains 4 to 10 white blood cells, and each human diploid cell contains about 6.6 pg of DNA.[64] We therefore estimate that the efficiency of ITP purification of blood ranges between 30% and 70%, which competes with both batch and microchip-based SPE methods.[45]

Finally, we collected extracted genetic material (with a pipettor at reservoir 4) and performed PCR analyses to verify that (i) we effectively purified DNA from the human blood sample, and (ii) the purified DNA is free of PCR inhibitors. We show real-time PCR amplification curves in **Figure II-6**. Real-time fluorescence monitoring shows repeatable amplification signal with a threshold cycle of $C_t = 30.9 \pm 0.4$ (N = 4); while the negative control showed negligible amplification after 40 cycles. This is in contrast to results obtained with an equivalent, unpurified amount of blood lysate (25 nL, obtained by dilution), for which PCR was clearly inhibited (negligible amplification after 40 cycles).

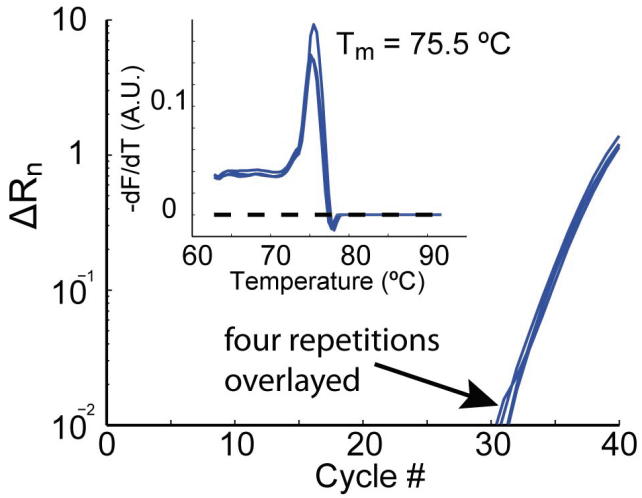

Figure II-6: Real time PCR amplification of ITP purified DNA from human blood. We present a schematic of the extraction–PCR protocol in Figure II-3. The amplification curve shows repeatable amplification of the extraction product (here four repetitions, threshold cycle C_t = 30.9 ± 0.4). Negative controls and PCR from equivalent amount of lysate showed no amplification after 40 cycles. We therefore successfully purified DNA from whole blood to obtain PCR-ready NA in a PCR-friendly buffer. The inset shows post-PCR dissociation curve (derivative of SYBR Green I fluorescence). The melting temperature of the PCR product equals that of the positive control. The dashed line corresponds to melting curves of negative controls.

We also performed dissociation curve analysis of the PCR products from all samples as additional identification of the target. The melting temperature of the PCR product of the ITP-purified samples and a positive control were equal (T_m = 75.5ºC, see dissociation curves on the inset of **Figure II-6**). The experiments show that we successfully and repeatably purified DNA from whole blood and recovered genomic DNA free of PCR inhibitors.

II.4 Conclusions

We described a novel technique for the purification of NA from biological samples using ITP. We leveraged the focusing and separating power of ITP

to purify and extract DNA from proteins and other sample contents. We demonstrated ITP-based purification of NA from whole blood. After chemical lysis and proteinase K treatment, we extracted DNA from a few nanoliters of sample. The efficiency of the ITP based purification (versus injected sample) ranges between 30 and 70% for whole blood and reaches 100% for λ-DNA, which rivals with other microchip purification techniques as summarized in **Table II-1**. ITP-based purification is a fast and simple technique for the purification of NA from small volumes of biological samples (1 to 100 nL), results in negligible PCR inhibitors and uses a PCR friendly chemistry. We here proved the efficacy of this technique to extract DNA from 10 to 25 cells, and therefore hypothesize that sample preparation from a single cell is possible. Finally, the ITP based purification is performed in a single step, enabling automated and multiplexed analysis.

Table II-1: Comparison of efficiencies, purification times and throughput of isotachophoresis based DNA purification with the traditional QIAGEN and solid phase extraction.

	QIAGEN spin column	Microfluidic SPE[45]	ITP
Efficiency for prepurified L-DNA	80-100%	30-85%	100%
Efficiency for whole blood			30 to 70% (based on typical white blood cell concentration range)
Purification time	~ 20 min	~ 20 min	~ 1 min
Volume dispensed	> 50 µL	20 µL	1 µL
Volume processed			25 nL

Chapter III. Global quantification of microRNA using isotachophoresis

The contents of this chapter were previously published by Persat, Chivukula, Mendell and Santiago (2010)[35] and are reproduced here with minor modifications.

III.1 Introduction

microRNAs (miRNAs) are a class of 18 to 24 nucleotide (nt) non-coding RNAs that regulate gene expression via sequence-specific interactions with messenger RNAs.[2] Several hundred miRNAs are encoded in the human genome and dozens have now been shown to regulate a diverse variety of cellular processes, both in normal physiology and in disease. [65] For example, the miRNA let-7 was shown to regulate the transition between larval and adult stage in *Caenorhabdis elegans*.[2] Also, mir-26a is ubiquitously expressed in human cells but is downregulated in lung cancer.[2]

Understanding the genesis and mode of action of miRNA is key to accurate quantification. We show a schematic of miRNA biogenesis in **Figure III-1**. microRNAs are liberated from long, RNA Polymerase II transcribed precursors (pri-miRNA) by a series of sequential endonuclease-mediated cleavage events and are turned over by mechanisms that remain poorly characterized.[2] Evidence is now accumulating that miRNA biogenesis is subject to regulation, allowing cells to selectively control the production of these small RNAs and thereby titrate their regulatory activity. For example,

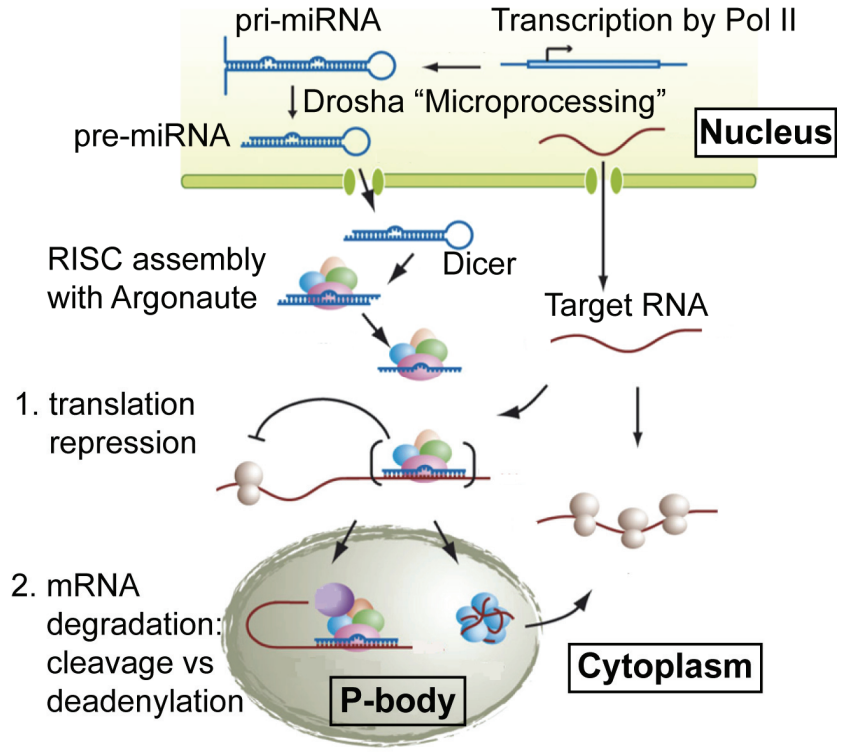

Figure III-1: miRNA biogenesis and mode of action. miRNAs are transcribed from polymerase II promoters to yield pri-miRNA transcripts. These undergo cleavage by the RNA endonuclease Drosha in the so-called "micro-processing" step, producing the approximately 80 nt long pre-miRNA. Following cytoplasmic export, the RNA endonuclease Dicer cleaves the "loop" to produce the double stranded miRNA intermediate. The non-coding miRNA* strand undergoes degradation, while the coding miRNA strand is incorporated into the RISC complex with Argonaute proteins, where duplex formation with target mRNAs and either translational repression or mRNA degradation/de-adenylation occurs. Adapted from [68]

recent studies have demonstrated that the expression of many miRNAs increases during early embryonic development.[66] Conversely, miRNA abundance is globally reduced in a wide variety of human cancers. [65] Moreover, it was recently demonstrated that global miRNA abundance increases as cells are grown to high density in culture.[67] These findings highlight the need for accurate, high-throughput methods to quantify the global

abundance of miRNAs in total RNA samples derived from diverse sources. Such methodology would greatly facilitate investigation of the mechanisms that regulate miRNA biogenesis and the settings in which these pathways operate.

To investigate the correlation between miRNA expression and cell density, Hwang *et al*.[67] used microarrays and northern blots to analyze RNA samples from various culture conditions. These techniques allow for quantitation of specific miRNA individually. Monitoring global miRNA abundance with northern blot and microarrays therefore requires profiling a large number of miRNAs. These measurements therefore require large amounts of sample and do not necessarily include all miRNAs. Moreover, northern blots do not allow for absolute quantification of miRNAs. A commercial electrophoresis system for quantification of small RNAs was reported recently.[69] A kit specific for the analysis of small RNAs (Agilent's "RNA small" kit) is combined with the Agilent Bioanalyzer electrophoresis system. The RNA small kit is optimized for high resolution separation of RNA shorter than 200 nt long. The CE can be performed on total RNA or on isolated small RNA. The miRNA analysis if performed by observation of the electropherogram at early migration times. miRNA concentration is obtained by integration of the electropherogram signal corresponding to RNA size up to 40 nt long. We show an example electropherogram for human kidney (Ambion, Austin, TX) in **Figure III-2**. By accounting for RNA longer than the range of miRNA, this instrument generally overestimates miRNA abundance.[70] Moreover, the measurement may suffer

the same effect from the dispersion of longer RNA (in particular abundant transfer RNA) into the range of measurement. We here demonstrate a technique which allows fast, accurate and absolute measurement of global miRNA levels from small amounts of total RNA using highly selective multi-stage on-chip isotachophoresis (ITP).

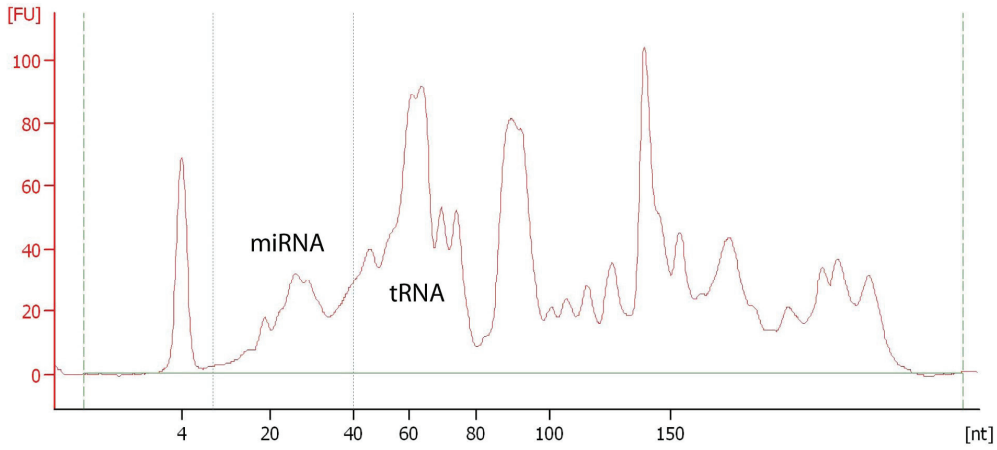

Figure III-2: Electropherogram of small RNA from human kidney using the Agient's RNA small kit on the Bioanalyzer system. This system integrates the electropherogram signal at small migration times to measure global miRNA abundance.

As discussed in the previous chapters, in ITP, species with mobilities smaller than the TE or greater than LE will not focus. We have used this selectivity to extract PCR-compatible genomic DNA samples from whole blood as discussed above,[29] and to isolate short nucleic acids from cell lysate.[52] In this work, we use the selectivity of ITP to focus exclusively miRNA from total RNA while leaving longer RNA molecules unfocused. We then quantify the

amount of focused sample by fluorescence to obtain an absolute measurement of the global amount of miRNA in the sample of interest.

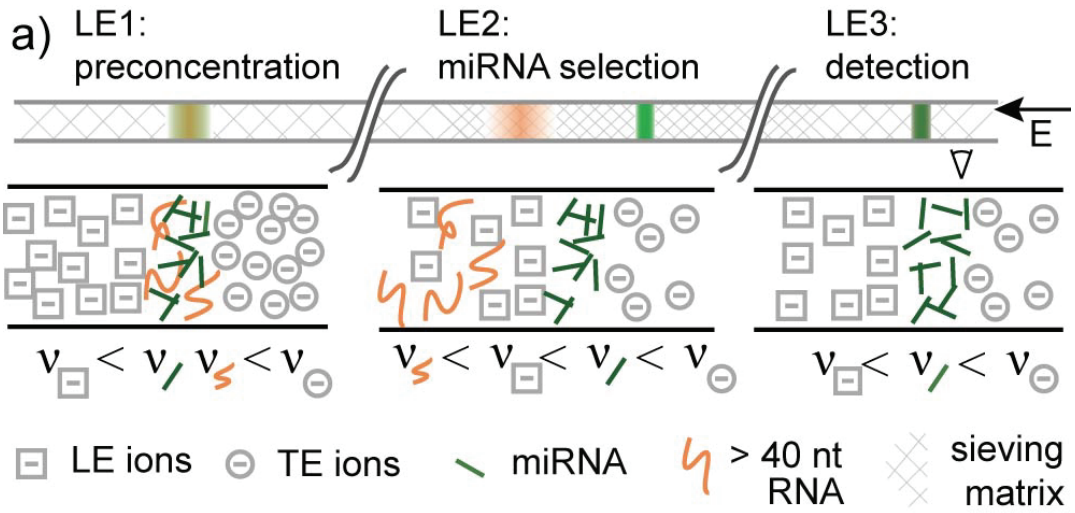

Figure III-3: Schematic of three-zone ITP for the selective focusing and quantification of miRNA. LE1 (left) contains high leading ion concentration and to yield high electric field gradient between the TE reservoir and the adjusted TE in the channel. LE1 has also low concentration of sieving polymer matrix (depicted by widely space cross hatching) to allow for high flux of miRNA to the ITP interface, as the mobility of RNA is larger at lower polymer concentration. LE2 (middle) contains a high concentration sieving matrix and smaller ionic strength to increase separation resolution and defocus 40 nt or longer RNA while keeping miRNA focused. Finally, LE3 has reduced denaturant and polymer concentration to increase sensitivity of the fluorescence detection.

Our ITP assay relies on the length dependence of the electrophoretic mobility of RNA. In free solution, the mobility of nucleic acids only slightly increases with length.[55] The length dependence of RNA mobility in free solution is therefore small and does not allow for high resolution separations. However, the mobility of polyelectrolytes is dramatically affected by the addition of a polymer to the separation buffer. In a dilute or semi-dilute polymer matrix, nucleic acids migrate via an entanglement mechanism which

causes their mobility to decrease with length.[71] Also, increasing concentration of polymer in the separation buffer globally decreases the mobility of all lengths on NAs. Because dilute and semi-dilute polymer solutions have low viscosity and do not always require cross-linking, they have been widely used for DNA and RNA electrophoresis in microchip format.[71, 72] We use polyvinylpyrrolidone (PVP) as polymer sieving matrix. PVP is a low viscosity polymer that has been previously used for DNA sequencing[73] and for electrophoresis of miRNA.[74] This polymer yields sufficiently high resolution in the low RNA range to perform selective focusing extraction of miRNA. Additionally, PVP efficiently reduces electroosmotic flow.

A cell contains on the order of 10 pg of RNA. Figure III-4 shows the size distribution of different types of RNA in order of mass abundance in total RNA. Ribosomal RNA (rRNA) and transfer RNA (tRNA) are at least 80 nt long, and constitutes more than 95% by mass of total RNA.[64] Messenger RNA (mRNA) are typically longer and in low abundance. miRNA is the shortest class of RNA in the cell (along with siRNA) and is expected to have significantly lower abundance than tRNA or rRNA. Pre-miRNA, the precursor of miRNA, is at least 70 nt long. Quantification of miRNA is therefore equivalent to measurement of the abundance of RNA shorter than approximately 60 nt in a total RNA sample.

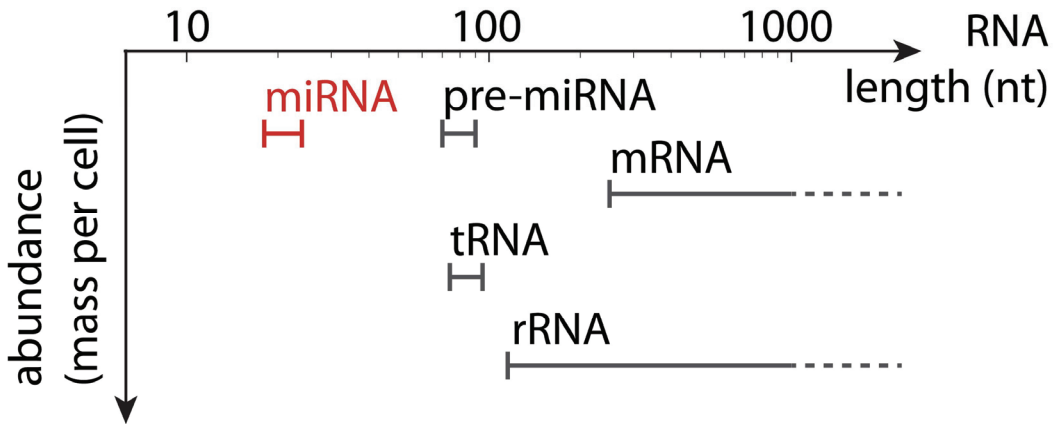

Figure III-4: Size distribution of commonly abundant RNA. Each horizontal bar shows the interval of length of the type of RNA. The vertical position indicates the abundance of the corresponding RNA in mass per cell. miRNAs are the shortest known RNA moleculaes (18 to 24 nt long) but have low mass concentration. Among the small RNA (shorter than 200 nt), the most abundant class is transfer RNA (70 to 90 nt long). The shortest ribosomal RNA (rRNA) is the 115 nt long 5S rRNA and messenger RNA (mRNA) is at least 300 nt long. To perform accurate global quantification of miRNA, the ITP chemistry must be optimized to a cutoff length in the 40-60 nt range.

III.2 Description of the assay

High selectivity in ITP can be achieved by tuning the concentration of sieving matrix in the LE such that the mobility of miRNA is only slightly larger, and that the mobility of longer RNA is slightly smaller than the TE mobility. However, this implies that unfocused miRNA in the TE migrates at nearly the same speed as the ITP interface; thus resulting in slow focusing rate and a low level of preconcentration and sensitivity.[27] Also, denaturing conditions are required for high selectivity, but can interfere with quantum yield and affinity of fluorescent reporters. To achieve both high selectivity and high sensitivity, we have designed an ITP assay with multiple zones of varying sieving matrix and

denaturant concentrations. These are established using three initial LE zones. We know of no other work using such multistage sieving matrix ITP. We first describe our assay qualitatively, and then describe the injection protocol and the specific chemistry of the LE zones and TE.

In the microfluidic chip, we establish three initial LE zones arranged in series along the separation channel. We also suppress electroosmotic flow so that these initial zones of neutral species do not migrate under the influence of the electric field during the ITP process. The zones only slowly diffuse into each other. Initial LE zones 1, 2 and 3 have different initial concentrations of chloride (leading ion) C_{Cl^-}, polymer sieving matrix C_p, and denaturant C_d. Our sample is initially mixed uniformly with TE, and dispensed into the TE reservoir. Figure III-5 depicts the sample migration through the three zones. Sample travels behind LE ions but through three stationary regions of sieving matrix and denaturant (each electrically neutral) established by the initial condition.

The initial zone LE1 has low C_p, resulting in miRNA mobility significantly larger than that of the TE and increased miRNA flux to the ITP interface. High C_{Cl^-} in LE1 also enhances preconcentration by "cascade" effect.[75] The initial zone LE2 has high C_p for selective focusing of miRNA and defocusing of longer RNA. This transition is shown in Figure III-3, where the narrow green band represents miRNA and the dispersed orange band is longer RNA. The spatial temporal diagram of Figure III-5 is an experimental demonstration of

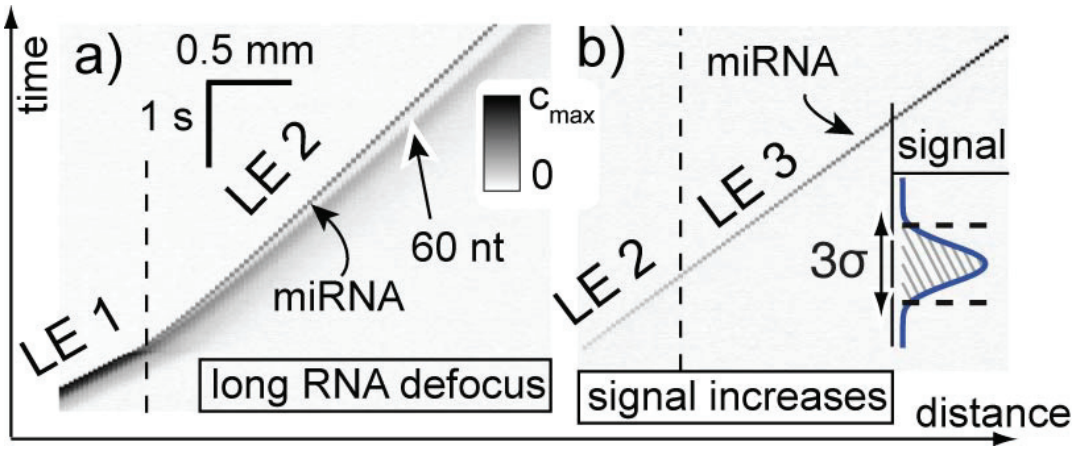

Figure III-5: Experimental demonstrations of the transitions between successive ITP stages shown in Figure III-3. An experimental demonstration of the defocusing is shown in the spatiotemporal diagram (a) showing channel-width-averaged fluorescence intensity (inverted grey scale) versus axial channel distance and time. Here, a mixture of 22 nt and 60 nt long RNA focus in LE1, but only the 22 nt RNA remains focused in LE2. In (b), the LE3 zone (right) has reduced denaturant concentration enabling higher fluorescence for sensitive quantification of the selectively focused miRNA. The latter experiment's spatio-temporal diagram shows transition of a 22 nt RNA focused peak from low fluorescence in LE2 to significantly larger fluorescence in LE3.

this process, where we focused 22 nt and 60 nt long RNA in zone LE1 and selectively defocused the 60 nt long RNA in zone 2.

The mobility of RNA is strongly affected by its secondary structure, requiring use of denaturing agents.[76] Denaturing agents in the separation buffer significantly increase the resolution of RNA electrophoresis. Also, strong denaturing condition in the sample's buffer is beneficial to resolution. Here, we use a standard denaturing agent, urea, in the LE1 and LE2 zones to increase separation resolution for greater accuracy. However, we measured a significant decrease in fluorescence of the RNA intercalating dye at high urea

concentration (7 M). Consequently, we use reduced denaturing conditions (low C_d, here 2 M) in LE3, so this last section acts as a detection zone. An experimental demonstration of the transition between LE2 and LE3 zones is shown in the spatial temporal diagram of Figure III-5, where we only focus the 22 nt long RNA which remains focused but whose fluorescence signal significantly increases in the LE3 zone.

III.3 Materials and methods

We performed the ITP experiment in a microchip containing an 8 cm long microchannel with multiple T-junctions (*cf.* Figure III-6). Details of our confocal optical setup are provided in Supplementary Information. Briefly, we performed visualizations on an inverted epifluorescence microscope equipped with a diode laser, and measured fluorescence intensity using a photomultiplier tube. We calculated fluorescence intensity by integrating the ITP zone signal peak (*cf.* Supplementary Information).

We performed visualizations on an inverted epifluorescence microscope (Eclipse TE200, Nikon, Japan) with 488 nm diode laser illumination (Stradus 488, Vortran, Sacramento, CA). The laser was coupled to the microscope using a set of mirror and 1 in. diameter adapters (SM1 series, Thorlabs, Newton, NJ). We used a filter cube (exciter/emitter 482/536 nm, dichroic reflection band 446 nm to 500 nm, model FITC-3540B, Semrock, Rochester, NY) and a 60x water immersion objective (N.A. = 1.0, Fluor, Nikon, Japan) for fluorescence imaging. For quantitative the detection system, we assembled a

custom confocal setup by coupling to a 150 μm pinhole placed at the image focal plane to reduce noise created by out of focus light. The light coming out of the pinhole was then refocused on the surface of the detector using two biconcave lenses (f = 25.4 mm, Thorlabs, Newton, NJ). Pinhole and lenses were mounted in a 1 in. diameter tube (SM1 series, Thorlabs, Newton, NJ) with a C-mount adapter to couple with the detector module. We measured fluorescence intensity using a photomultiplier tube (H7422-40, Hamamatsu Photonics, Japan) set to 900 V. We mounted the PMT, pinhole and lenses assembly on a micropositioning stage to perform precise alignment with incident light from the microscope. Signal was converted using an amplifier/converter unit (C7319, Hamamatsu, Japan) with gain set to 10^6, filtered using an low pass RC circuit (RC = 1.2 ms) and acquired using a DAQ card (NI USB-6211, National Instruments, Austin, TX) controlled with Matlab (The Mathworks, Natick, MA). We performed all measurements at 90 kS/s and filtered signal with a 1500 points moving average. We calculated fluorescence intensity by fitting a Gaussian to the ITP peak, then integrating the signal in the ITP peak (from the raw data) over one and a half standard deviations above and below the position of the maximum of the fit.

Alternately, for the spatial temporal diagrams of Figure III-5, we used a 488 nm collimated diode light source for illumination (Thorlabs, Newton, NJ), a 4x objective (N.A. = 0.2, Plan Apo, Nikon) and acquired images using a cooled CCD camera (cascade 512F, Photometrics, Tucson, AZ) controlled with Winview32 (Princeton Instruments, Trenton, NJ). The plots are width-

averaged fluorescence intensity versus time and distance along the separation channel. We inverted the gray scale so that dark regions correspond to high-intensity fluorescence from intercalated RNA

Reagents

For control experiments, we used HPLC purified synthetic miRNAs, 40 nt and 60 nt long RNA (Integrated DNA Technologies, Coralville, IA) whose sequences are given in Table III-1, and yeast tRNA (Invitrogen, Carlsbad, CA). We used an equimolar mixture of 735 synthetic miRNAs (mirVana miRNA reference panel v9.1, Ambion, Austin, TX) to generate the calibration curves of Figure III-9. For the validation and demonstration of quantification assay (Figure III-11), we purified RNA from subconfluent and confluent HeLa and Hepa1-6 cells using Trizol (Invitrogen; see Hwang *et al*. for description of the culture method[67]). We measured total RNA concentration with a NanoDrop 2000 spectrophotometer (Thermo Scientific, Rockford, IL) and diluted all stock solutions to 0.5 $\mu g.\mu l^{-1}$ before storage at -80°C. Before running each ITP experiment, we diluted the specified RNA sample into 100 µL of TE. This sample/TE mixture was then denatured in a 70°C water bath for 5 min to ensure full disruption of RNA secondary structures and placed on ice.

The LEs all contain DNase, RNase free Tris hydrochloride (pH = 8.0, Invitrogen, Carlsbad, CA), urea (EMD biosciences, Gibbstown, NJ), polyvinylpyrrolidone (PVP, M.W. = 1,000,000, Polysciences Inc., Warrington, PA). LE1 and 2 were prepared from a stock solution of 8 M urea and 6.8% w/v PVP. We provide details of concentrations for each LE in Table III-2. For

RNA quantitation, we used 500 nM SYTO RNAselect dye (Invitrogen), except for the spatial temporal diagrams of Figure III-5 where we used 1x SYBR Green II (Invitrogen). The TE is a solution of 92.5% v/v formamide (Invitrogen) containing 5 mM Tris (Sigma-Aldrich, Saint Louis, MO) and 2.5 mM Caproic acid (Fluka, Milwaukee, WI). All solutions were made using DNase RNase free water (Gibco, Carlsbad, CA).

Oligo length (name)	Sequence (5' to 3')
23 nt (mir-17)	CAAAGUGCUUACAGUGCAGGUAG
40 nt	CUGUGACACUUCAAACUCGUACCGUGAGUAAUA AUGCGCC
60 nt	CAUUAUUACUUUUGGUACGCGCUGUGAC ACUUCAAACUCGUACCGUGAGUAAUAAUGCGC
22 nt (mir-126)	UCGUACCGUGAGUAAUAAUGCG
22 nt (complementary to mir-126)	CGCAUUAUUACUCACGGUACGA

Table III-1: Sequences of oligoribonucleotides used in this work for calibration experiments.

	Tris hydrochloride, pH = 8.0	PVP (M.W. = 1,000,000)	Urea	SYTO RNAselect
LE1	100 mM	0.5% w/v	7 M	500 nM
LE2	20 mM	5.5% w/v (varies in fig. 2)	7 M	500 nM
LE3	20 mM	3% w/v	2 M	500 nM

Table III-2: Detailed composition of LE1, 2 and 3.

Injection protocol

Here, we describe the strategy to prepare the chip for miRNA quantitation. The off-the-shelf chip design (model NS260, Caliper LS, Mountain View, CA) is shown in Figure III-6 Before each set of experiments, we first precondition the chip by rinsing the channels successively with 100 mM sodium hydroxide

for 5 min, deionized (DI) water for 1 min, 100 mM hydrochloric acid for 5 min, and DI water for 1 min. We then add the different LEs to reservoirs 1 to 8 as described in step 1 of Table III-3 below and apply vacuum to reservoirs 3 and 7 for 5 min. These initial rinsing and filling steps are useful to suppress and stabilize electroosmotic flow in the borosilicate chip during the ITP experiments.

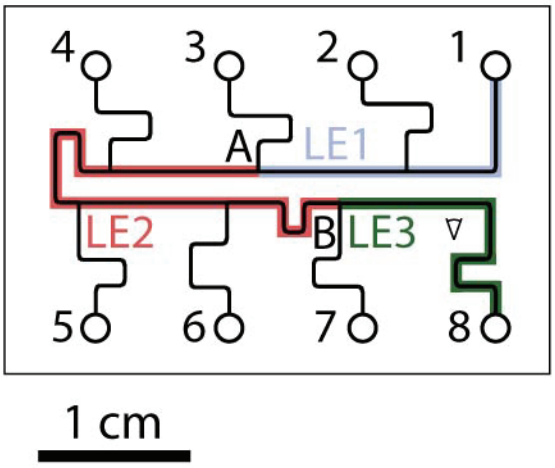

Figure III-6: Design of the caliper NS260 chip. Before each experiment, we fill the microchannels with LE1, 2 and 3 according to the sequence described in Table III-3. The three LE zones are highlighted for clarity

To prepare each experiment, we load LE1 in reservoirs 1, 2 and 3, LE2 in 4, 5 and 6 and LE3 in 7 and 8. All reservoirs contain 5 µL of their respective LE, except 8 that contains 10 µL of LE3. We then apply vacuum to reservoirs 3 and 7. This generates flow in the microchannel network so that the channel connecting reservoir 1 and intersection A fills with LE1, the segment A-B fills with LE2 and B to reservoir 8 fills with LE3. Figure III-6 shows the resulting train of three LE zones after this step, where LE1 is in gray, LE2 in red and

LE3 in green. After 2 min of this vacuuming step, we rinse reservoir 1 with deionized water. We then add 10 µL of the mixture of sample in TE in reservoir 1, and finally apply 3 kV in 8 and ground 1 to initiate ITP and stop voltage after the ITP interface has reached the detector. We summarize the injection procedure to create the initial multi-stage LE train in Table III-3.

We use a slightly larger volume of buffers in 1 and 8 in order to generate a slight pressure driven flow into the branches connecting the separation channel to reservoirs 2 to 7. This flow overcomes diffusion of leading ions present in these branches after the ITP interface has passed the corresponding intersection. That way, we avoid leading ions leaking into the TE region which could break the ITP condition and defocus miRNA unintentionally. We also recognize that when the ITP interface crosses a channel intersection (*e.g.* at point A), a small part of the focused sample flows into the branch (A to 3). We measured that this loss was reproducible across experiment and it did not significantly decrease sensitivity of our assay (but could impart isolation efficiency in case this technique is used for miRNA extraction).

Reservoir	1	2	3	4	5	6	7	8
Step 1	LE1, 5 µl	LE1, 5 µl	LE1, 5 µl	LE2, 5 µl	LE2, 5 µl	LE2, 5 µl	LE3, 5 µl	LE3, 10 µl
Step 2			Vacuum 2 min				Vacuum 2 min	
Step 3	Empty, rinse, add 10 µl TE+sample							
Step 4	GND							+ 3 kV

Table III-3: Summary of the injection protocol to setup the multi-stage ITP for miRNA quantitation.

III.4 Results and discussion

Buffer design for high selectivity

To perform exquisitely selective miRNA focusing, we first chose a TE whose mobility was smaller than the mobility of short nucleic acids (for zero C_p),[55] and chose nominal values for C_p in LE1, 2 and 3. We selected caproic (hexanoic) acid as trailing ion and used 0.5% w/v in LE1, which is sufficient to suppress electroosmotic flow while keeping high flux of miRNA sample to the ITP interface. We selected 3% w/v PVP in LE3. We then performed a series of experiments with increasing C_p (and decreasing local RNA mobility[71]) in LE2. Such titration allowed tuning of the cut-off focusing length (length below which RNA focuses).

In Figure III-7, we show results of three sets of titration experiments using 23 and 40 nt synthetic oligoribonucleotides and yeast tRNA. We used a 40 nt long synthetic oligo to simulate RNA longer than miRNA, and tRNA (80 nt in average[64]) to verify that highly abundant short RNAs with strong secondary structures do not interfere with our measurement. The titration aimed at finding a C_p that allows miRNA to focus but reject 40 mer and tRNA. For all three RNAs, the amount of focused RNA gradually decreased with increasing PVP initial concentration in LE2. This is consistent with a global decrease of nucleic acid electrophoretic mobility, and associated decreased flux of RNA to the ITP interface.[27] At 3% w/v PVP concentration, there was significant

focusing of all three RNA samples. Increasing PVP concentration to 4% w/v resulted in defocusing of tRNA, shown by the drop in tRNA signal to the baseline value. 40 nt RNA was rejected at 5% w/v PVP. Meanwhile, the amount of 23 nt long RNA remained significant at all concentrations. In particular, at 5.5% w/v PVP, the measured (baseline) fluorescence intensity of the 40 nt RNA case was only 12% of the fluorescence of miRNA, but exceeded 60% of miRNA at 4% w/v PVP (see inset of Figure III-7). We

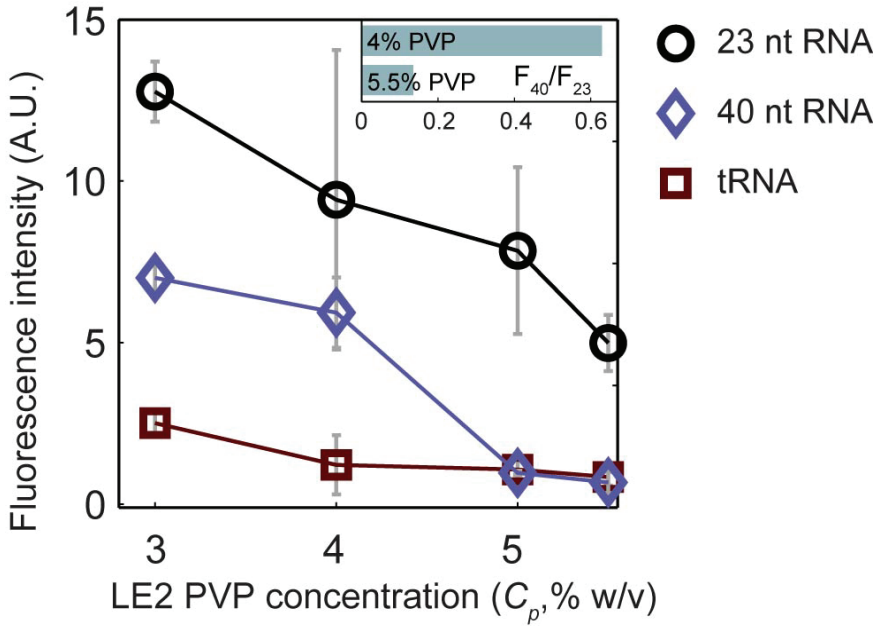

Figure III-7: Demonstration of selectivity of miRNA focusing. We performed ITP experiments using 23 nt and 40 nt long synthetic RNA and yeast tRNA dissolved in the TE. We report total fluorescence intensity in the focused zone for increasing polymer concentration in LE2. All RNA focus at 3% w/v PVP. At 5% w/v and above, we observe significant focusing of the 23 nt RNA while both 40 nt and tRNA are rejected from ITP focusing. The inset shows a horizontal bar chart of 40-nt-to-23-nt signal ratio (F_{40}/F_{23}). At 4% w/v PVP, F_{40}/F_{23} is greater than 0.6, but drops down to 0.12 at 5.5% w/v. We chose to use 5.5% w/v PVP in LE2 for selective focusing of miRNA.

attribute most of the residual fluorescence at 5.5% w/v to fluorescence contamination (see below) and synthesis byproducts remaining after purification of the 40 mer despite HPLC purification. This titration shows refined selective focusing of miRNA with an LE2 with 5.5% w/v PVP and an RNA cutoff length between about 24 and 39 nt. The results also show that secondary structure of tRNA had no discernable effect on assay selectivity.

Additionally, we explored the effect of possible miRNA base pairing on our fluorescence signal. Base pairing can strongly enhance quantum yield of typical intercalating dyes,[77] and so reduces quantitation accuracy. Base pairing can occur between miRNA and its "star" sequence or with siRNA.[2] To control this, under sufficiently denaturing conditions, we performed selective

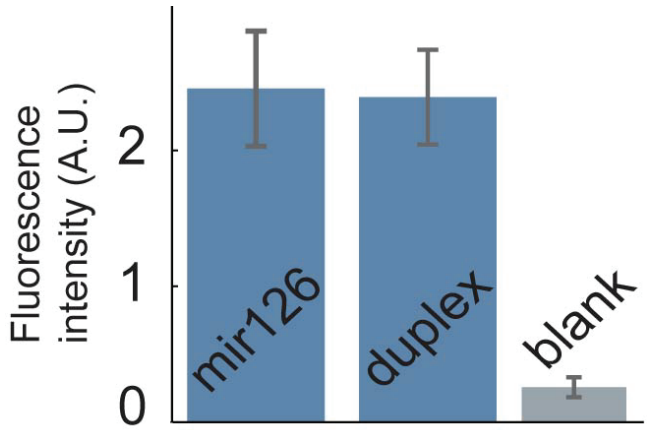

Figure III-8: Effect of potential base pairing on miRNA fluorescence in ITP. We verified that potential base pairing of miRNA does not affect fluorescence. We show results of selective focusing of mir-126 (5 pg.µl-1 in TE) and of an equimolar mixture of mir-126 and its complementary oligoribonucleotide (each at 2.5 pg.µl-1). There is no significant difference between fluorescence of mir-126 and of the duplex, showing no bias due to base pairing. Uncertainty bars represent 95% confidence intervals.

focusing of the 22 nt long mir-126 and compared it to focusing of an equimolar mixture mir-126 and its perfect match. We compare these focusing experiments in Figure III-8. We measured no significant difference in fluorescence intensity between focusing of mir-126 and the associated duplex mixture. This shows our denaturing conditions are sufficient to disrupt miRNA base-pairing, thus avoiding bias in the miRNA quantitation.

For ITP with sample mixed in TE, focused sample amount is proportional to its initial concentration.[27] Given proper calibration, the total fluorescence intensity in the ITP zone is a measurement of the initial miRNA concentration in the TE. We used an equimolar mixture of 735 synthetic miRNAs as a standard solution. This miRNA panel is widely used as accurate reference for microarrays.[78] Using a mixture of hundreds of miRNA helps reducing possible bias from sequence specific fluorescence of the RNA dye and length. Moreover, leveraging a commercial standard is helpful for comparison of experimental results with other work.

We determined calibration curves by diluting the miRNA reference in the TE at relevant concentrations. We show a sample calibration curve on Figure III-9, where the miRNA concentration varied between 0.3 and 30 $pg.\mu l^{-1}$. We note that negative controls (experiments with no miRNA in the TE) yielded a reproducible fluorescent signal at the 0.1 $pg.\mu l^{-1}$ level. This residual fluorescence was likely due to contamination of stock chemicals as observed routinely by us and others using ITP.[79]

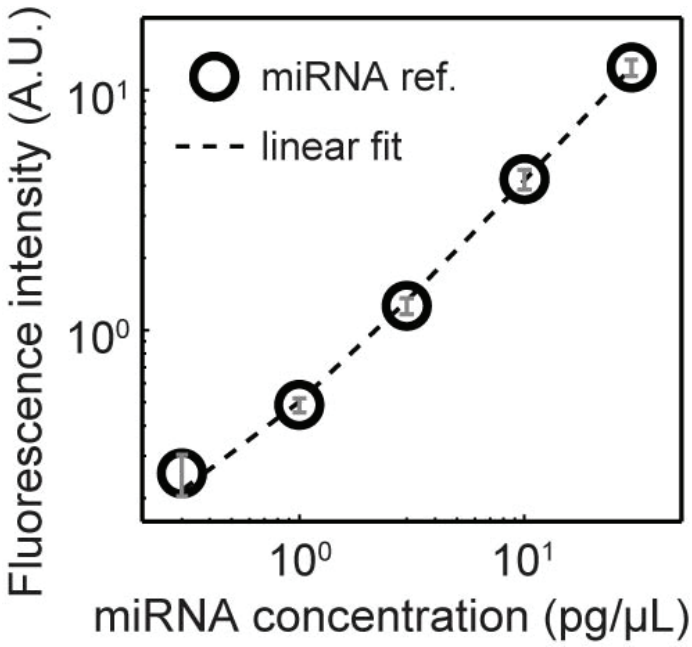

Figure III-9: Calibration curve for absolute quantification of miRNA using selective ITP. We built the calibration curve by performing selective ITP of a mixture of 735 miRNAs at a total concentration ranging between 0.3 pg.μl^{-1} and 30 pg.μl^{-1} using the RNAselect fluorescent stain. This calibration curve is used for absolute quantitation of miRNA levels from a single fluorescence measurement.

To demonstrate the efficacy and utility of our assay in a strongly relevant biological application, we quantified global miRNA levels in subconfluent and confluent cell cultures. As mentioned above, Hwang *et al*. showed that cell-cell contact activates miRNA biogenesis, resulting in greater miRNA abundance in densely-grown cultures of various cell lines.[67] We provide further independent evidence for this effect using our ITP-based selective quantitation; in particular we measured miRNA levels in total RNA extracted from HeLa and Hepa1-6 cell cultures before and at confluence.

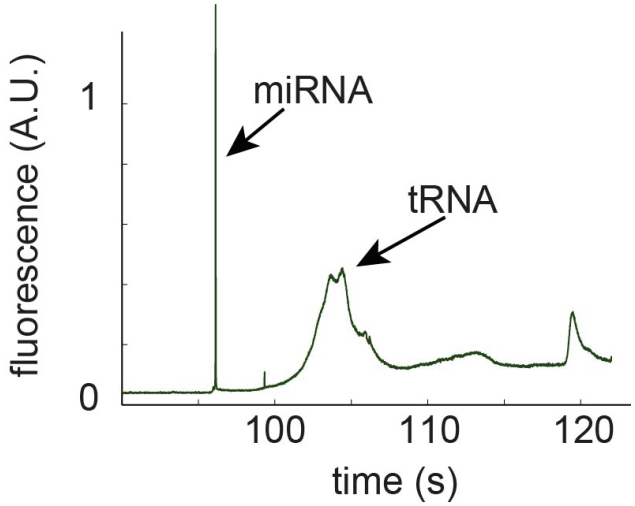

Figure III-10: Sample isotachopherogram of selective focusing of miRNA from total RNA. The sharp peak at t = 92 s corresponds to the ITP focused miRNA. This peak is approximately Gaussian with characteristic width around 20 ms. The peak(s) at larger migration times (t >100 s) corresponds to longer RNA molecules, most likely transfer RNA. For each run, we performed a Gaussian fit on the miRNA peak and integrated signal over three standard deviations, center on the peak position. This run corresponds to a typical miRNA quantitation run for Hepa1-6 cells (5 ng.μl^{-1} in the TE).

We dissolved total RNA in the TE down to 5 ng.μl^{-1} and performed miRNA quantitation with ITP as described above. We show a sample isotachopherogram in Figure III-10. The sharp, early peak corresponds to the ITP zone, and is nearly Gaussian in shape with approximately 10 ms detector width. The trailing defocused portion of the signal at larger migration times corresponds to longer RNA defocused within the LE2 zone. We attribute the first wide, diffused peak at 104 s (5 to 10 s width) to tRNA. This tRNA peak does not overlap with the focused miRNA peak and therefore does not affect quantitation. Before continuing, we note we performed similar measurements on degraded RNA samples, and these showed significant tailing of the miRNA

peak, a dispersed tRNA peak, and overlap between these. Degraded RNA samples also showed abnormally high levels of focused short RNA compared to higher quality preparations. Under such conditions, degraded RNA likely

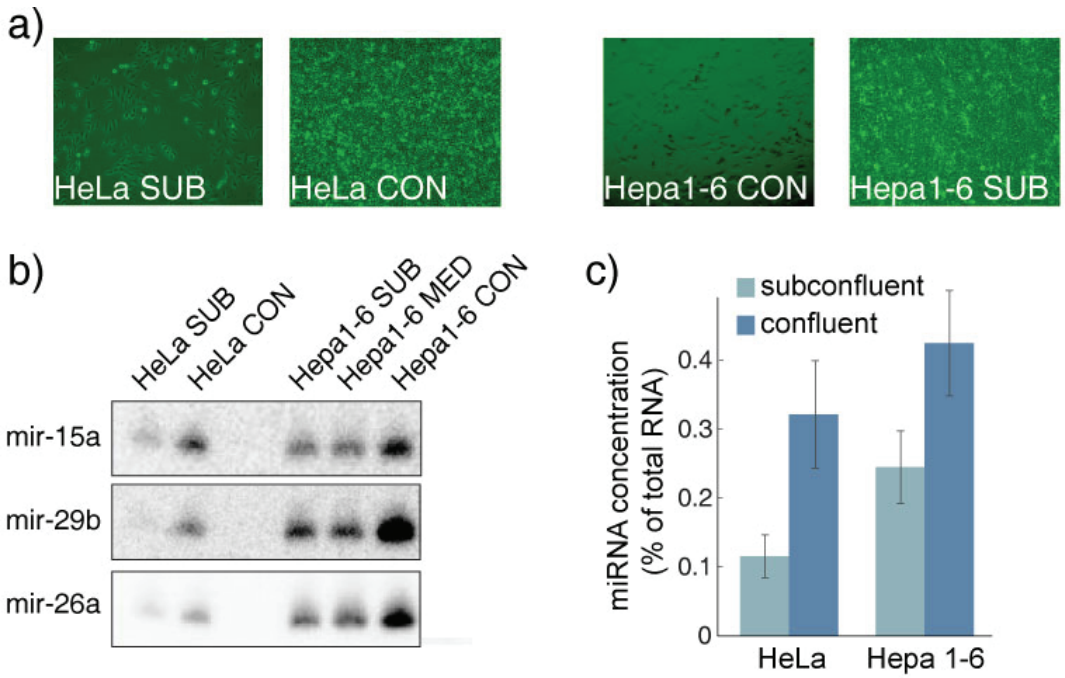

Figure III-11: Measurement of miRNA abundance in HeLa and Hepa1-6 subconfluent and confluent cell cultures. We show pictures of the four different cultures in (a), Northern blot analysis for profiling of three miRNAs in all four samples in (b), and miRNA quantitation with selective ITP in (c). Shown in (a) are pictures of cultures with distinct cell densities before RNA extraction. We also performed control experiments to verify that these specific samples have distinct miRNA expressions as shown by Hwang et al.. [67] Northern blots show increase miRNA expression with confluence for all three miRNA tested. In (c) we validate these results by comparison of miRNA levels between Hepa1-6 and HeLa cell cultures before (low density) and at confluence (high density). In this experiment, we diluted a total RNA in TE down to 5 ng.μl^{-1} and performed the ITP assay. miRNA quantitation shows that subconfluent cells have lower miRNA expression compared to the confluent cells, consistent with (b) and the work of Hwang et al..[67] This result implies that miRNA expression is not only a function of tissue type, but also of tissue density. Uncertainty bars represent the 95% confidence intervals.

produced fragments shorter than the ITP cutoff length, resulting in highly upward biased quantitation of miRNA. To avoid this bias, we systematically obtained RNA integrity numbers (RIN, measured at the at the Stanford PAN facility)[22] for all samples and performed measurements exclusively on samples with RIN greater than 9.0, which exceeds recommendations for miRNA analysis.[70]

We measured absolute miRNA abundance from total RNA from subconfluent and confluent cultures. We show results for HeLa and Hepa1-6 cells in Figure III-11, where the measurements are presented as percentage of total RNA (since total RNA concentration does not vary with cell density). In both cases, we observed a significant increase in miRNA expression between the subconfluent and confluent cultures. miRNA levels increased from 0.11% to 0.32% of total RNA in HeLa cells, and from 0.24% to 0.42% in Hepa1-6 cells. These results provide independent validation of the findings reported in Hwang *et al*.[67] and confirm the efficacy of the ITP based miRNA quantification. While relative values of miRNA levels were qualitatively similar to Hwang's study, we note that the current measurements show slightly larger concentrations of miRNA than levels estimated from microarray data.[80] We attribute this apparent discrepancy to variations of miRNA expression between different cell types and to different small RNA extraction efficiencies associated with the preparation methods.[81]

Measurement of global miRNA abundance: examples

We have measured miRNA abundance in a wide variety of samples; including from different types of cell cultures. While the interpretation of these results is outside the scope of this thesis, we here provide comments on selected examples to demonstrate the usefulness of miRNA quantitation.

We used the quantitation assay to measure miRNA abundance in E14 ES cells and summarize results in Figure III-12. We first note that the absolute value of miRNA abundance is significantly larger in the wild type than all other cultured cells we have analyzed. We hypothesize that this high absolute value of miRNA abundance maintains the undifferentiated state of stem cells by globally reducing protein expression. We performed miRNA quantitation on a cell line where the Dicer gene was knocked down (Dicer null) and compared to the wild-type (WT). Dicer is the enzyme that processes precursors into miRNA.[2] Here, we measured a 5x decrease of miRNA level between WT and Dicer null, validating the hypothesis of the function of Dicer in ES cells, and also confirming that our assay discriminates miRNA from precursors.

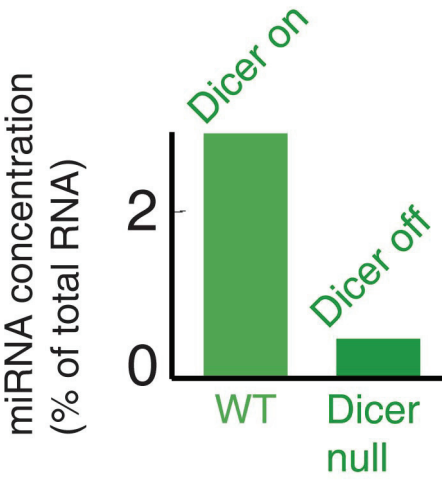

Figure III-12: Measurement of miRNA abundance in wild type (WT) and Dicer knock down (null) cultured E14 ES cells. WT cells have large absolute miRNA levels. This is consistent with stem cells maintaining their undifferentiated states with high miRNA levels. The Dicer null sample shows significantly reduces miRNA abundance (about 5-fold decrease). This is validating the function of Dicer, which processes long miRNA precursors into the mature miRNA.

We have also performed miRNA quantitation on P493 cells with increased expression of the MYC oncogene transcription factor. One of the cultures is treated with doxicylin, an antibiotic that inhibits the MYC protein. We show results of global miRNA abundance measurement in Figure III-13. The sample treated with doxycilin (+Dox) has significantly larger miRNA expression than the control (-Dox). We believe the three-fold increase in miRNA expression in treated culture is generated from the inhibition of the MYC protein that has already been shown to reduce expression of specific miRNAs.[82] This result brings additional clues to the mode of action of the MYC transcription factor in oncogenic transformation.

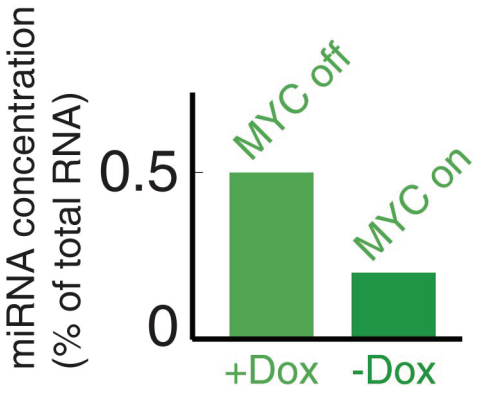

Figure III-13: Measurement of miRNA abundance in P493 cultured cells with treated with doxicylin. The cells treated with doxicylin (+Dox) have low MYC oncogene expression. Cells not treated with doxicylin (-Dox) have high expression of MYC. There is a significant decrease in miRNA abundance upon activation of MYC oncogene, showing that this transcription factor has a key role in miRNA biogenesis.

In summary, we have developed a new technique for accurate, fast, and absolute quantitative measurement of global miRNA levels with low sample consumption (*e.g.*, order 10 µl volumes with 10 to 50 ng of total RNA) based on on-chip ITP. We demonstrated the selectivity and the accuracy of the assay and showed its utility by performing global miRNA measurements on subconfluent and confluent HeLa and Hepa1-6 cell cultures. The technique is

a new, efficient tool for the investigation of the biogenesis and role of miRNAs, and its high sensitivity allows for potential application to a large variety of cells and tissues.

Chapter IV. microRNA profiling by simultaneous selective isotachophoresis and hybridization with molecular beacons

IV.1 Introduction

microRNA (miRNA) is a class of small, non-coding RNA that regulates gene expression.[2] Sequence specific binding of miRNAs to target messenger RNA transcripts induces gene silencing, via the formation of the RNA-induced silencing complex (a.k.a. RISC). miRNAs play an important role in gene regulation, both in normal pathology and disease, and therefore constitutes a potential marker for diverse cellular processes.[2] In particular, profiling miRNA is potentially a powerful diagnostics and monitoring tool for cancer.[65, 83] Novel techniques for the isolation, detection and quantification of miRNAs are now essential to unravel the functions and mode of actions of these small molecules whose analysis by traditional techniques is still limited.[3]

miRNA profiling

The most popular and well-established miRNA profiling methods are adapted from traditional nucleic acid analysis techniques.[3] These include northern blot, microarrays and stem-loop PCR. Microarrays have high throughput but require significant instrumentation, amount of sample (about 5 μg of total RNA), are time consuming and cannot distinguish miRNA from its precursor. Stem loop PCR[84] has high dynamic range and is sensitive but has low throughput and is less specific than standard PCR.[3] Lastly, northern blot has high sensitivity and allows for length discrimination of sequences, but

remains time consuming and requires large amounts of sample (generally more than 1 µg of total RNA). Northern blotting consists in gel electrophoresis for separation of total RNA with subsequent transfer to a nitrocellulose membrane, followed by hybridization with a radioactively labeled probe visualized with a scintillation counter.[85] We here adopt a similar strategy that leverages isotachophoresis (ITP) and hybridization with molecular beacons (MBs) for the profiling of miRNA in a single separation-hybridization step.

	Northern blot	qPCR	Microarray	Sequencing
Time per run	days	6 hours	2 days	1-2 weeks
Sample amount	> 1µg	500 ng	0.1 to 1 µg	0.5 to 5 µg
Dynamic range	2 log	6 log	4 log	>5 log
Sensitivity	Low	High	Moderate	High
Cost	Low	Moderate	Moderate	High
Instrumentation	Light	Moderate	Moderate	Heavy

Table IV-1: figures of merit of current techniques for miRNA profiling.

Molecular beacons

Molecular beacons are sequence specific nucleic acid probes that fluoresce upon hybridization.[86] Developed in the early years of qPCR, molecular beacons have become ideal sequence specific fluorescent reporters for nucleic acid amplifications assays and *in vivo* hybridization.[86, 87] The sequence specific fluorescence of MBs originates from its unique structure that we schematize in **Figure IV-1**. These probes are composed of four different units: (i) a nucleic acid probe sequence (the loop, up to 30 nt long) complementary to the target sequence of interest; this sequence is flanked by (ii) two, complementary self-hybridizing sequences which allow conformation of the probe into a hairpin structure, (iii) a fluorophore at the 5' end, and (iv) a

suitable quencher at the 3' end. We present a schematic of the MB hybridization reaction mechanism in **Figure IV-1**. When the molecular beacon is free in solution, it acquires a hairpin structure which brings 5' and 3' ends to proximity, so that the quencher hampers fluorescence. In the presence of a sequence complementary to the probe, the hairpin opens and hybridizes to the target. This occurs because the short stem hybrid is less stable than the longer probe-target hybrid. This "open" conformation is therefore thermodynamically favorable. In this configuration, the distance between fluorophore and quencher is sufficient to emancipate fluorescence.

The stem sequence is typically 4 to 6 bp. A stem that is too short has low melting temperature and will open too easily, reducing specificity. On the contrary, a stem that is too long will have significantly larger melting temperature and may lock, reducing affinity of the probe for the target. There is no standard stem sequence, and its design is key to hybridization specificity and sensitivity. Also, one must make sure that: the stem sequence does not cross-hybridize with the probe sequence. A good way to check for cross-hybridization is to test the MB sequence in the Zucker' folding algorithm.[88]

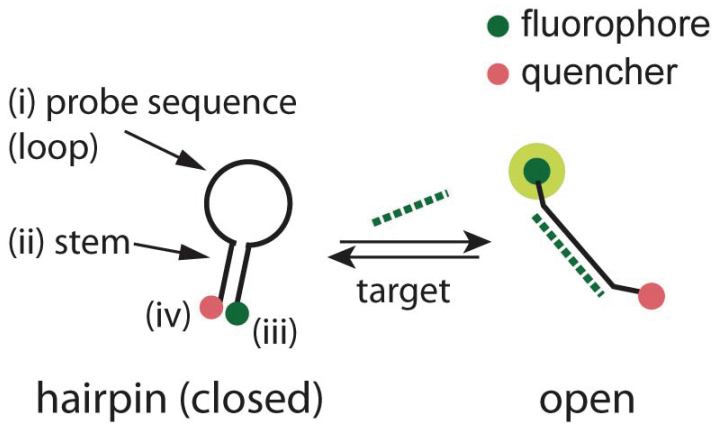

Figure IV-1: Schematic representation of components of the ITP hybridization assay. In (a), we show the structure and mode of action of molecular beacon probes. A MB is DNA molecules which includes a probe sequence that is complementary to the target of interest, flanked by two segments that are complementary to each other. One end of this short DNA is labeled with a fluorophore and the other end with an adapted quencher. The self-complementary flanking sequence hybridize to form a stem so that the MB is in a closed, "hairpin" conformation, where the probe sequence forms a loop. In this condition, quencher is close enough form the fluorophore to significantly inhibit fluorescence emission. In the presence of a complementary sequence, the MB opens to form a probe-target hybrid, which releases the fluorophore from the quencher, and induces fluorescence.

ITP for hybridization of miRNA

In the previous chapters, we have leveraged the selectivity of ITP focusing for the purification of nucleic acids,[29] and the measurement of global miRNA abundance in diverse tissues.[35] To our knowledge, ITP has been utilized twice to perform chemical reactions. Park *et al.* controlled immunoassays by ITP focusing of antibody and antigen prior separation.[32] Also, Goet and coworkers proposed ITP as a way of bringing and mixing reagents together and discussed DNA hybridization coupled with ITP without showing an experimental demonstration.[33]

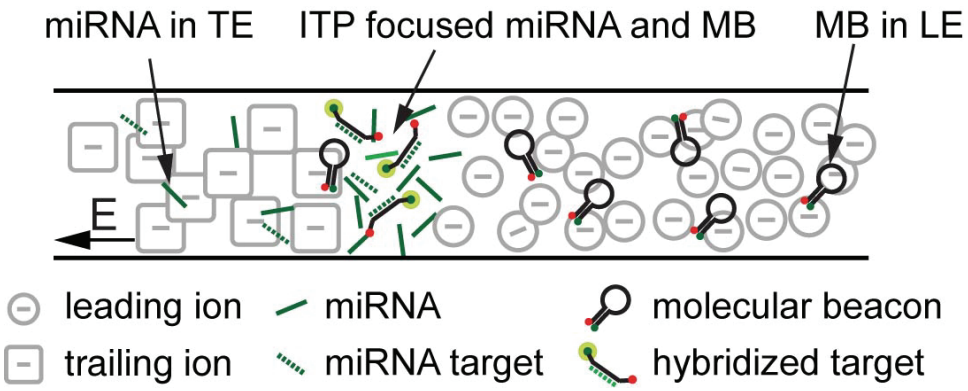

Figure IV-2: Combination od ITP and MB hybridization. Target (miRNA in this work) are initially in the TE and MB in the LE. Both MB and target electromigrate toward the interface between trailing and leading ions into the same focused zone. Within this zone, probe and target hybridize, this generates a fluorescence increase in the focused zone.

In the present work, we combine selective ITP with MB hybridization for the sequence specific detection of miRNA. In the same manner as our previous work on miRNA quantification,[35] we use a multi-stage ITP injection strategy to accomplish sensitive, selective and specific detection. We reach high sensitivity using an initial ITP preconcentration step. Selectivity for miRNAs occurs in a second ITP step with increased sieving conditions, where longer RNA molecules are excluded from the focused zone. We perform highly specific detection in a last step where MBs hybridize to target miRNA. We first report and discuss experimental conditions of the multi stage ITP hybridization assay. Then we demonstrate hybridization and show selectivity and specificity of the assay using synthetic miRNAs. We finally apply the ITP hybridization to a biologically relevant case by detecting and quantifying a specific miRNA in human liver.

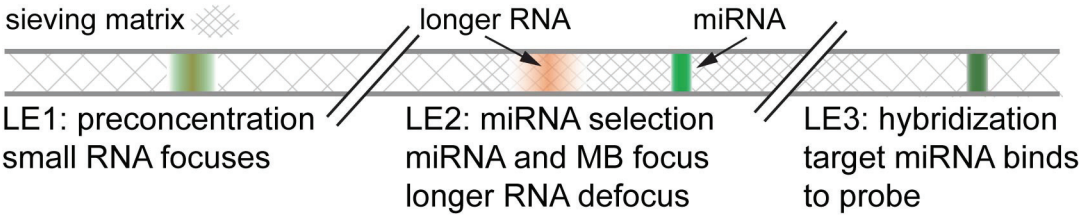

Figure IV-3: Schematic of the three-stage ITP strategy used for ITP hybridization. We initially setup three contiguous zones of LE with varying concentration of polymer, denaturant, leading ion and magnesium chloride. The first zone LE1 allows for strong preconcentration of miRNA. The second has higher polymer concentration to selectively focus miRNA. LE3 has reduced denaturing conditions to allow for specific hybridization.

IV.2 Description of the assay.

We present the concept of the ITP hybridization assay in **Figure IV-2**. Initially, MB probes targeting the miRNA of interest are dissolved in the LE, and RNA (which includes miRNA) is dissolved in the TE. Leading and trailing ions are selected so that their mobilities allow for simultaneous focusing miRNA, probe, and miRNA-probe hybrid. Under this condition, and upon application of an electric field, miRNA and MB simultaneously focus at the interface between TE and LE. In the focused zone, and under optimized conditions, miRNA hybridizes to the probe sequence of the MB which disrupts the hairpin. This yields an increase in fluorescence intensity within the ITP zone. This way, the ITP-focused zone acts as a reactor whose volume is delimited by its width and the cross sectional area of the microchannel. In our 44 μm wide, 12 μm deep channel, we estimate the volume of the ITP interface to be on the order of 10 pL, assuming a 10 μm wide ITP interface.[27] This is a significantly smaller reaction volume compared to existing microfluidic reactors,

which are at least on the order of few nanoliters,[89] and therefore has potential for improved kinetics and sensitivity.

In addition, we leverage the selectivity of ITP focusing to perform hybridization solely on the RNA length range of interest. We have used this feature of ITP to quantify global miRNA levels in diverse cell cultures.[35] Here, we selectively focus miRNA and reject all longer RNA molecules from the ITP zone. We therefore avoid bias from hybridization of long RNAs that contains identical or similar sequences, in particular we exclude the ~80 nt long miRNA precursors pre-miRNA. This selectivity combined with the simultaneous hybridization is globally similar to the process of northern blotting, which requires multiple successive steps including electrophoresis and hybridization to achieve detection.

We perform the ITP hybridization assay using electromigration through multiple zones of varying chemical concentrations. We have used a similar strategy in previous work on miRNA,[35] where the zones allowed for successive preconcentration, selection and quantification of miRNA. We created three initial contiguous LE zones arranged in series along the separation channel. Initial LE zones had distinct initial concentrations of leading ion, polymer sieving matrix, or denaturant. During ITP, the sample travels behind leading ions through the successive stationary zones. In the present work, we use three successive zones to preconcentrate small RNA, select miRNA and hybridize and detect a specific target with MBs in the ITP zone.

The function of each step is summarized in **Figure IV-3**. In the first zone LE1, we use a low polymer concentration. The mobility of miRNA increases with decreasing polymer concentration, so LE1 yields a strong flux of miRNA to the ITP interface, but at the same time focuses longer RNA molecules. Also, the slightly larger concentration of leading ions in LE1 augments preconcentration.[75] The second zone LE2 has large polymer concentration, which globally decreases mobility of RNA. This defocuses longer RNA while leaving miRNA and MB focused. Finally, LE3 has low denaturing conditions, polymer concentration, and optimized magnesium chloride concentration. These conditions enable hybridization in LE3, where miRNAs specifically bind to MBs.

IV.3 Materials and Methods

Chemicals and reagents. Leading electrolytes contain DNase RNase free Tris hydrochloride buffer (pH = 8.0, Invitrogen, Carlsbad, CA), polyvinylpyrrolidone (PVP, M.W. = 1,000,000, Polysciences Inc., Warrington, PA), urea (EMD biosciences, Gibbstown, NJ) and magnesium chloride (EMD biosciences). Concentrations in LE1, 2 and 3 are respectively 50 mM, 20 mM and 20 mM of Tris hydrochloride; 0.5% w/v, 3% w/v and 0.5% w/v of PVP, 7 M, 7 M and 2 M of urea; 0 mM, 2 mM and 2 mM of magnesium chloride. The trailing electrolyte is a solution of 5 mM Tris (Sigma-Aldrich, Saint Louis, MO), 5 mM Caproic acid (Fluka, Milwaukee, WI) in 92.5% formamide (UltraPure, Invitrogen).

Table IV-2: Sequences of oligoribonucleotides and molecular beacons used in this work. For molecular beacons, TYE 665 is a fluorophore (with spectrum similar to Cy5) and Iowa Black RQ (IBRQ) is the quencher. microRNAs and precursor are ribonucleic acids while molecular beacons are deoxyribonucleic acids. For molecular beacons, the complementary stem-forming sequence fragments are underlined.

Oligo name (length)	Sequence (5' to 3')
miR-26a (22 nt)	UUCAAGUAAUCCAGGAUAGGCU
miR-126 (22 nt)	UCGUACCGUGAGUAAUAAUGCG
miR-122 (22 nt)	UGGAGUGUGACAAUGGUGUUUG
mir-26a (77 nt) (miR-26a precursor)	GUGGCCUCGUUCAAGUAAUCCAGGAUAGGCUGUGCAG GUCCCAAUGGGCCUAUUCUUGGUUACUUGCACGGGGA CGC
miR-26a MB (34 nt)	TYE665 - CCGAGCAGCCTATCCTGGATTACTTGAAGCTCGG - IBRQ
miR-122 MB (34 nt)	TYE665 - CCGAGCCAAACACCATTGTCACACTCCAGCTCGG - IBRQ

We purchased HPLC-purified molecular beacons and synthetic miRNA from Integrated DNA Technologies (Coralville, IA). We used (DNA) molecular beacons 5'-labeled with TYE 665 fluorescent dye (excitation at 645 nm and emission at 665 nm) and 3'-labeled with Iowa Black RQ quencher (peak absorbance at 656 nm). The precursor mir-26a was synthesized and PAGE-purified by Dharmacon (Lafayette, CO). We provide the sequences of synthetic oligoribonucleotides and probes used in this work in table 1. Total RNA from normal human liver and kidney were obtained from Ambion (FirstChoice human total RNA, Austin, TX). Before each experiment, we dissolved the sample (total or synthetic RNA) to the specified concentration in 50 µL of TE, placed in a water bath at 70°C for 5 min and finally on ice until running the ITP hybridization experiment. Separately, we dissolved the MB in 500 µL of each LE.

ITP hybridization protocol

We here describe the injection protocol to perform the three stage ITP hybridization. We performed all experiments in an off-the-shelf borosilicate glass microfluidic chip (model NS260, Caliper LS, Mountain View, CA) whose design is shown on **Figure IV-4**. Its multiple T-junctions enable generation of the initial serial LE zones by vacuum filling. Initially we precondition the chip by successively flushing channels with 200 mM sodium hydroxide (5 min), deionized (DI) water (1 min), 100 mM hydrochloric acid (5 min), and DI water (1 min). We then deliver LE1 to reservoirs 1, 2 and 3, LE2 to reservoirs 4, 5 and 6 and LE3 to 7 and 8. We then apply vacuum to 3 and 7 for 5 min. These successive rinsing steps help reducing electroosmotic flow in the borosilicate chip for the subsequent experiments.

Before each experiment, all reservoirs are rinsed with DI water. We then deliver LEs to the reservoirs as described above and in **Table II-1**, and apply vacuum to 3 and 7 for 2 min. Vacuum at 3 generates the interface between LE1 and LE2 at the intersection A and vacuum at 7 creates an interface between LE2 and LE3 at the intersection B. After loading, we release vacuum, rinse reservoir 1 with DI water, and deliver the TE-sample mixture. We generate an electric field in the separation channel by applying a 3 kV voltage difference between reservoir 8 and 1 using a high voltage power supply (Labsmith, Livermore, CA). This activates ITP focusing of miRNA and MBs through the three serial zones. We eventually stop voltage after the ITP

interface has passed the detector which monitors fluorescence in the LE3 zone.

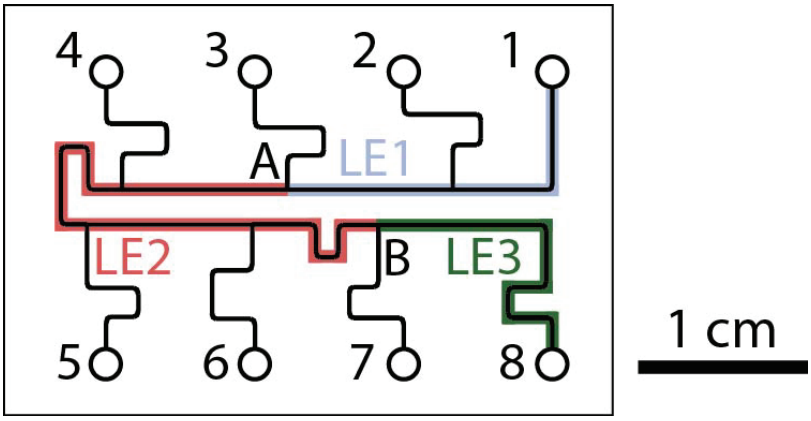

Figure IV-4: Design of the caliper NS260 borosilicate glass microchip. Before each experiment, we fill the microchannels with LE1, 2 and 3 according the sequence described in Table III-3. Channel The three LE zones are highlighted for clarity. LE1 and LE2 zones meet at A and LE2 and LE3 meet at B.

Optical setup

We acquired data on an inverted epifluorescence microscope (Eclipse TE200, Nikon, Japan) equipped with a laser diode illumination (642 nm, Stradus 642, Vortran, Sacramento, CA). Light was filtered using a standard Cy5 cube (exciter/emitter 630/695 nm, model XF110-2, Omega Optical, Brattleboro, VT) and focused though a 60x water immersion objective (N.A. = 1.0, Fluor, Nikon, Japan). To reduce noise created by out of focus light, we built a custom confocal assembly by placing a 150 µm pinhole (mounted precision pinhole, Edmund Optics, Barrington, NJ) at the image focal plane. We measured fluorescence intensity using a photomultiplier tube (PMT, model H7422-40, Hamamatsu Photonics, Japan) with voltage set to 900 V. We

converted the PMT signal using an amplifier/converter unit (C7319, Hamamatsu, Japan), and filtered it with a simple low pass RC circuit (RC = 1.2 ms). We acquired the resulting voltage signal with a DAQ card (NI USB-6211, National Instruments, Austin, TX) controlled with Matlab (The Mathworks, Natick, MA). We performed all measurements at 250 kS/s data rate and applied a 4000 points moving average to the signal for analysis. We processed the voltage trace by fitting a Gaussian function to the ITP peak. We then calculated fluorescence intensity by integrating the raw data under the fit over three standard deviations.

IV.4 Results and Discussion

Initial demonstration using synthetic miRNA. We present an initial demonstration the ITP hybridization assay in **Figure IV-5**. We perform the multi-stage ITP with 1 nM of MB targeting miR-26a in all three LEs. We compare the signal of the ITP where the TE contains 1 nM synthetic miR-26a to a negative control (with no target in the TE). We show the two resulting isotachopherograms (fluorescence versus time) in **Figure IV-5**. The black trace corresponds to the fluorescence intensity of the negative control. This trace exhibits a signal peak that we attribute to residual fluorescence from incomplete quenching of focused MB.[90] In the experiment where the TE contains 1 nM of miR-26a (gray trace), the fluorescence signal in the ITP zone increases significantly. This shows successful hybridization of the target with MBs within the focused zone. To compare the two results, we calculated the

corresponding peak areas and report them in the inset as a bar diagram. The peak area of the hybridized peak (+) is about 6.5 larger than the one of the negative control (-).

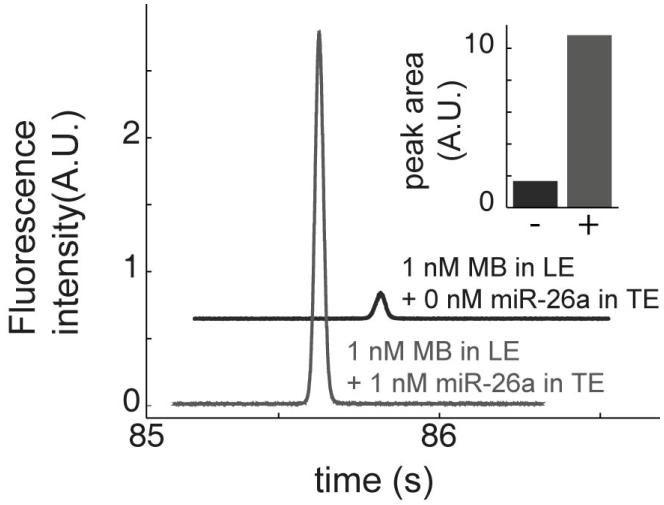

Figure IV-5: Initial demonstration of the ITP hybridization assay. We here show two isotachopherograms tracing fluorescence signal over time are 8 mm into the LE3 zone. In both experiments, the LE contains 1 nM of ME targeting miR-26a. The upper black trace corresponds to a negative control experiment where the TE does not contain any RNA. This trace exhibits a peak that corresponds to the non-deial quenching of the MB. The grey trace shows the result of ITP-hybridization where we added 1 nM of miR-26a target to the TE. The ITP peak has significantly greater amplitude compared to the negative control. This demonstrates successful combination of ITP and MB based hybridization for the detection of miRNA. We report the area of each peak in the inset. The peak area of the experiment with 1 nM target in the TE (+) is more than 6 times larger than the area of the negative control (-). We shifted the black isotachopherogram for visualization.

For an ITP hybridization experiment with a peak area *A*, we define the relative fluorescence enhancement *f* as

$$f = A/A_{nc} - 1,$$

where A_{nc} is the peak area of the negative control, *i.e.* an experiment with equal MB concentration but a blank TE. In the case presented in Figure IV-5, *f*

is approximately 5.5. *f* theoretically varies between zero (when $A = A_{nc}$) and a "saturated" value where all focused MB are open. This occurs when the amount of miRNA (*i.e.* the number of miRNA copies) in the focused zone is much larger than the amount of MBs. We note that *f* is also a function of multiple parameters including MB concentration, MB stem sequence, miRNA melting temperature and ITP chemistry.

The fluorescence enhancement of MB increases with target concentration.[90] In ITP, the amount of focused sample is a linear function of sample concentration in the TE.[27] Consequently, in the ITP hybridization assay, *f* increases with target concentration in the TE. We performed a titration experiment to illustrate the effect of sample concentration on fluorescence enhancement. In **Figure IV-6**, we report fluorescence enhancements for ITP hybridization at 100 pM MB with miR-26a concentrations ranging from 1 pM to 100 nM in the TE (circles). At low target concentration, here 1 to 10 pM, the fluorescence enhancement remains negligible. *f* significantly increases above 100 pM. The most sensitive increase occurs between 100 pM and 1 nM. Above 10 nM, *f* varies only slightly and seems to reach a plateau value, indicating saturation of MBs. The maximum value of *f* in this titration experiment is approximately 28 (at 100 nM miR-26a).

Selectivity

We now demonstrate the selectivity for miRNA of the ITP hybridization assay. Mature miRNAs are generated from processing of longer precursors,

successively the pri-miRNA and pre-miRNA. The latter is about 80 nt long and is the shortest precursor preceding full miRNA maturation.[2] Because these precursors contain the mature sequence, hybridization must be carried out exclusively on isolated miRNA as in northern blotting. We achieve this by leveraging the variation of electrophoretic mobility of RNA with length. In a polymer sieving matrix, mobility decreases with increasing polynucleotide length.[71] miRNA is the shortest class of RNA, hence its mobility is the greatest among all RNA. In particular it is greater than its precursors. Therefore, careful selection of the trailing ion allows for selective focusing of miRNA, excluding non-miRNA containing identical sequence.

To reach high selectivity, we performed calibration experiments in the same manner as we did in our previous work on miRNA isolation.[35] We first chose an initial trailing ion (here MOPS) and selected a polymer concentration in LE2 that shows focusing of miRNA and MB (separately and simultaneously). We then increased that concentration to reject pre-miRNA from the focused zone while keeping miRNA and MBs focused. We found that 3% w/v PVP in LE2 matched this requirement.

We illustrate the selectivity of this chemistry by showing results of ITP hybridization using the 77 nt long precursor of miR-26a, mir-26a, as sample (cross symbols). The enhancement *f* is globally much smaller than the signal generated by the mature miRNA. *f* remains at background level up to 1 nM mir-26a. We note a slow increase of fluorescence enhancement at large precursor concentration (above 10 nM). We attribute this residual signal to

hybridization of byproducts resulting from imperfect RNA synthesis. These byproducts include short RNA fragments containing segments of the mature sequence, which consequently hybridize with MB.

Specificity

As a last control experiment, we demonstrate that in ITP hybridization, MBs bind specifically to the correct target sequence. Molecular beacons have intrinsically high specificity,[91] we here confirm that ITP conditions does not alter this property, and we experimentally verify that the detection of the miRNA target is not biased by the presence of other miRNA. To this end, we perform ITP hybridization on a mature miRNA whose sequence does not match the MB probe. We used the MB designed for detection of miR-26a and varied the concentration of a "model" miRNA, miR-126, in the TE. The resulting titration curve is shown in **Figure IV-6** (plus symbols). At all concentrations, the fluorescence enhancement of the focused MBs nearly is null. Fluorescence in the focused ITP zone is unaffected by non-target miRNA, miR-126 does not efficiently bind to the miR-26a probe. This demonstrates that the signal of our ITP hybridization assay is solely due to the focusing of the target miRNA. However, we have not been able to show single base specificity. The length selectivity and sequence specificity of our assay shows its efficacy to precisely detect specific miRNA sequences in total RNA samples.

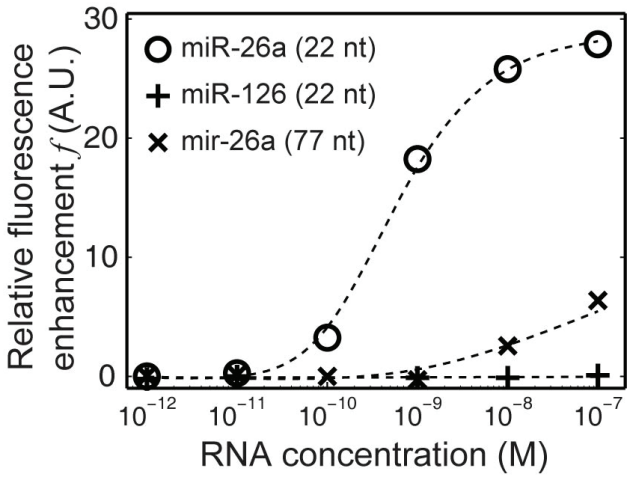

Figure IV-6: Demonstration of selectivity and specificity of the ITP hybridization assay. We performed the ITP hybridization with MB targeting miR-26a and where the TE contains miR-26a (circles), miR-126 (plus) or mir-26a (cross) at concentrations increasing from 1 pM to 100 nM. We here report relative fluorescence enhancement f as defined in the text. To improve data visualization, we fitted the data with spline functions (dashed lines). Titration with miR-26a shows the signal generated from hybridization of the perfectly matching target. Fluorescence enhancement remains small at low concentration (below 10 pM) and significantly increases at 100 pM and above. f plateaus over 10 nM, where nearly all focused MBs are open. Titration with the precursor mir-26a shows only slow increase of fluorescence with concentration. This shows that ITP in the LE2 zone excludes miRNA precursors from the focused zone, and allows for selective hybridization on miRNA. We also verified that potential unspecific hybridization was not affecting detection. We used miR-126 (whose sequence is distinct from miR-26a) as titrant, and observed that the fluorescence enhancement remained approximately null at all concentration. This confirms the specificity of MB hybridization in the ITP zone.

miR-122 profiling in human liver with ITP hybridization

To show the efficacy of the ITP hybridization in a biologically relevant case, we attempted detection of miR-122 in two human total RNA samples. We chose this liver-specific miRNA target for its large dynamic range of expression: miR-122 is highly expressed in the liver but poorly expressed in other organs.[92] Here, we diluted total RNA from human liver and kidney in TE

down to 10 ng.μL^{-1}. We then performed the ITP hybridization assay on these samples with 100 pM MBs targeting miR-122 in the LEs.

We show results of these experiments along with a negative control (blank run) in **Figure IV-7**, where we report ITP peak areas. ITP hybridization of miR-122 in kidney shows a slight increase in fluorescence (f = 0.2), which is not statistically significant compared to negative control (failed the t-test). We conclude that the amount of miR-122 in kidney is below the limit of detection of our assay. We estimate this limit to 2 pM (f > 0.4, see calibration below), which corresponds to 3,000 copies per cell (assuming 25 pg of RNA per cell). This is consistent with the amount of miR-122 measured in mouse kidney by RNase protection assay.[92] Conversely, ITP hybridization of miR-122 in liver yields significant signal enhancement (f = 1.3 ± 0.15). This indicates that miR-122 is largely expressed in liver compared to kidney, as previously demonstrated.[92]

We attempt quantification of miR-122 in liver using this measurement and leveraging a calibration curve built with synthetic miR-122, in the same manner as in **Figure IV-6**. We measured peak area of ITP hybridization of synthetic oligos dissolved at 1, 10 and 100 pM in the TE. We then perform a linear interpolation between the respective f values to yield a simple relation between fluorescence enhancement and miRNA concentration. We show a portion of this interpolation in the inset of **Figure IV-7** (grey solid line) for concentration values neighboring 10 pM. Using this calibration and the value of f found for liver (f_{liver} in inset of **Figure IV-7**), we calculated that a liver cell

contains 16,000 ± 400 copies of miR-122. This is on the same order of magnitude as RNase protection (50,000 copies per cell[92]) or RT-PCR measurements (10,000 copies per 10 pg of RNA, 25,000 copies per cell with our assumption on RNA mass per cell).[93] We believe the slight discrepancy between these three values partly arises from biological variability, differences in RNA quality,[70] or distinct efficiencies of miRNA extraction methods.[81]

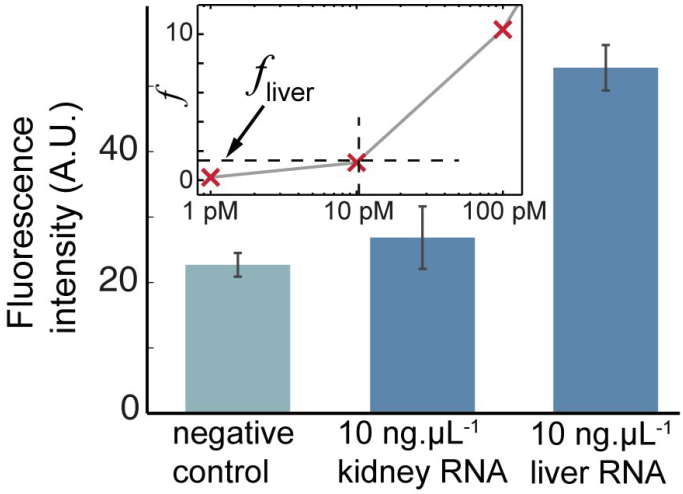

Figure IV-7: Demonstration of the ITP hybridization assay for detection and quantification of miR-122 in kidney and liver. We here report peak areas of ITP hybridization experiments where LEs initially contain 100 pM MBs targeting miR-122, and where the TE is blank (left bar) contains 10 ng.μL-1 of total RNA from human kidney (middle bar) and from human liver (right bar). The increase in fluorescence for kidney is not statistically significant, showing that our assay predicts miR-122 concentration in kidney below limit of detection (3,000 copies per cell). The peak area for liver is significantly greater, showing greater expression of miR-122. We use a calibration curve built with synthetic miR-122 to estimate target concentration from fluorescence enhancement. The solid grey line in the inset shows a calibration curve resulting from interpolation of hybridization results from synthetic miR-122 at different concentrations (red plus). We use this curve to calculate the concentration corresponding to the enhancement fliver = 1.3. We estimate this concentration to 10.3 pM, corresponding to approximately 16,000 copies per cell. Uncertainty bars represent 95% confidence intervals.

IV.5 Conclusion

We presented, characterized and demonstrated an assay for the detection and quantification of miRNA targets in total RNA samples based on selective ITP focusing of miRNA coupled with MB hybridization. We showed that ITP hybridization enabled selective detection of miRNA and could distinguish miRNA from its precursors. We also showed that the specificity of MBs is unaffected by coupling hybridization with ITP. Finally, we demonstrated the efficacy of the assay for the detection of miRNA targets in total RNA. We successfully detected miR-122 in liver and validated this result by measuring reduced expression in kidney. Using calibration experiments, we calculated the amount of miR-122 in liver; our estimate is in fair agreement with measurements performed with other quantification methods. ITP hybridization is therefore a fast (< 2 min), low cost (~$50 per chip, standard epifluorescence microscope), sensitive (down to 3,000 copies per cell) microfluidic method for miRNA profiling with about three decade dynamic range, and that uses small amounts of sample (100 ng of RNA). We hypothesize that further optimization of ITP and MB chemistries could significantly enhance sensitivity and reach the 100 copies per cell level.

Chapter V. Isothermal, chemical cycling polymerase chain reaction

The contents of this chapter were previously published in conference proceedings by Persat, and Santiago (2007-08)[38] and are reproduced here with minor modifications.

V.1 Introduction

Polymerase chain reaction (PCR)

The polymerase chain reaction (PCR) is a ubiquitous profiling and diagnosis method in biology and medicine. PCR is now the gold standard for nucleic acid analysis and its versatility and sensitivity enable a wide variety of applications. These include gene expression analysis, diagnosis of hereditary disease, pathogen detection, etc. Multiple nucleic acid analysis techniques have been derived from PCR. One of the most attractive variations is real-

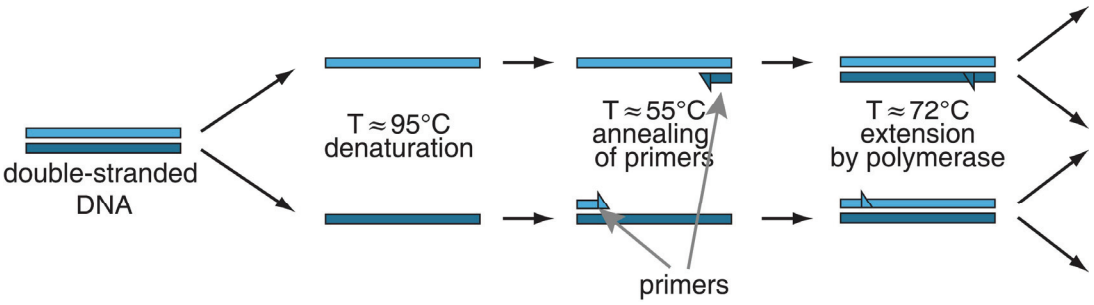

Figure V-1: Schematic of thermal cycling PCR. The double stranded DNA template is initially denatured into tow complementary strands, typically at 95C. In a second step, the two strands anneal a primer flanking the sequence of interest. Lastly, a polymerase extends the primers to generate two copies of the initial template sequence.

time PCR that allows for quantitation of nucleic acid targets in a sample of interest. More recently, the development of digital PCR has enabled detection at the single molecule level.

In PCR, a target nucleic acid undergoes a chain of reaction cycles. Each cycle is a three-step process: a sequence of denaturation, primer annealing and extension. We schematize the process of PCR in **Figure V-1**. Denaturation corresponds to the separation of the two strands of DNA template via disruption of hydrogen bonding, generally performed at elevated temperature (95°C). The annealing step consists in the hybridization of primers at sites flanking the sequence of interest. This is thermodynamically favored by a large excess of primers compared to the template. This step is sequence specific as primers are designed to amplify a unique portion of the template. Lastly, a thermostable polymerase extends the primers and generates two copies identical to the initial template. Annealing and extension are generally performed between 55°C and 65°C, but can proceed simultaneously. In ideal conditions, each cycle doubles the number of template copies, hence a succession of cycles allows for exponential amplification. The exponential nature of PCR and its specificity are the strength of this detection method.[94]

In the past 30 years, PCR systems have considerably evolved: faster thermal cycling, higher throughput and enhanced detection systems have enabled extremely sensitive and precise PCR amplifications in laboratory settings. However, commercial PCR remains handicapped by uncontrollable

aspects of its chemistry: primer dimmers, reagent depletion, and large reactor volume. Also, there have been multiple efforts to miniaturize PCR platforms for field and point-of-care analysis. Microfluidic platforms employing traditional PCR have competed for faster thermal cycling [95], miniaturization [96], and sensitivity [97]., with various degrees of success, as thermal cycling requires significant instrumentation for control.

We here propose and demonstrate a novel chemical cycling polymerase chain reaction (ccPCR) for DNA amplification where temperature is held constant in space and time. We use a chemical cycling that substitutes the effect of thermal cycling in traditional PCR. Other isothermal nucleic acid amplification methods have not successfully competed with PCR. Techniques such as the nucleic acid sequence based amplification (NASBA)[98] or the rolling-circle amplification[99] have more complex chemistries and lack the versatility of PCR.

Here, we present a fully functional device including simultaneous flow control and isotachophoretic focusing, and successful isothermal amplification with end-point and real time detection. ccPCR has potential for simpler chemistry and device fabrication, enhanced replication fidelity, faster amplification, more accurate quantitation and lower power consumption than traditional PCR. We demonstrate successful ccPCR amplification while simultaneously focusing products via isotachophoresis (ITP).

DNA melting corresponds to the disruption of all hydrogen bonds between the two strands. The number of hydrogen bonds between bases varies; the

free energy associated with DNA melting is therefore sequence dependent. The hydrogen bonds fully disrupt at the melting temperature T_m. The melting temperature is also a function of ion concentration and solvent. Solvents that significantly reduce the melting temperature compared to water are called denaturants (or denaturing agents). Formamide, urea and dimethylformamide (DMF) are denaturing agents commonly used in electrophoresis of nucleic acids. Because it allows for adjustment of melting temperature, formamide has been used in PCR to enhance amplification specificity.[100] However, denaturing agents have not been used for denaturation in traditional PCR as they inhibit primer annealing.

In this work we combine ITP with flow of denaturants that mimic the thermal cycling of thermal PCR. In ccPCR, we leverage the difference of electrophoretic mobilities of DNA and PCR reagents. We leverage the neutrality of denaturant agents (urea and formamide) to perform chemical cycling. We electrophoretically drive the DNA sample with ITP. Similarly to the previous chapter, this confines the DNA template into a small volume delimited by the ITP zone. Simultaneously, we control flow to generate a series of high denaturant concentration zones. These zones propagate in the microchannel in direction opposite to electromigration of DNA. The denaturant is neutral and is only transported by bulk flow, so the DNA experiences alternatively low and high concentrations. We show a schematic of the concept in Figure V-2. This process effectively replaces the thermal cycling of classical PCR associated with denaturation, which is the highest temperature

(typically 95°C). With this strategy, we therefore relax the requirement to fast heating and cooling system that require high power. We also open the possibility of performing PCR at a single temperature, with isothermal annealing and extension.

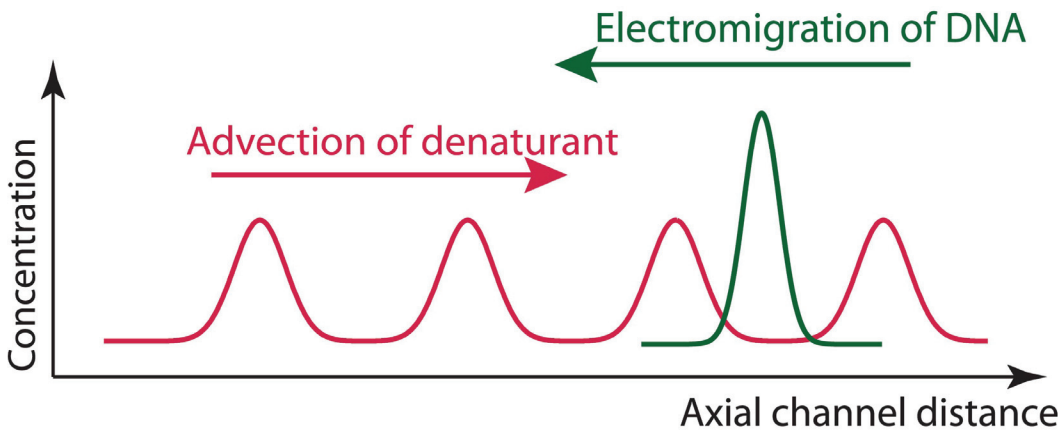

Figure V-2: Conceptual representation of ccPCR. Zones of high denaturant concentration flow in opposite direction of DNA template electromigration. The template experiences a chemical cycling that mimics the thermal cycling of classical PCR.

V.2 Methods

Chemicals and reagents

For ccPCR experiments, we prepared a stock of 10x PCR buffer containing 200 mM Tris (Sigma Aldrich, Saint Louis, MO) titrated to pH = 8.2 with hydrochloric acid and 500 mM potassium chloride. This stock was diluted to 1x and used as LE. The LE also contained 0.01% (v/v) Tween 20 (Sigma Aldrich), 5 mM magnesium chloride (EMD Biosciences, Gibbstown, NJ). 2 μM SYTO 13 fluorescent dye (Invitrogen, Carlsbad, CA), 200 μM each dNTP (New England Biolabs, Ipswich, MA), 2 μM of forward and reverse primers targeting

a fragment of the 16S rRNA gene from *E. Coli* (Operon, Huntsville, Al), and 2.5 U per 100 µL of Taq polymerase (QIAGEN, Valencia, CA). To prepare the sample solution, we dissolve the DNA template into the 100 µL of LE that additionally contains 0.5 mM of MES as spacer . The TE contains 100 mM Tris, 100 mM HEPES (Sigma Aldrich), 0.01% (v/v) Tween 20 and 2 µM SYTO 13. The denaturing agent is composed of 40% formamide (Invitrogen), 4 M urea (EMD Biosciences), 2x PCR buffer and contains 2 µM of each primer.

To measure the melting temperature of the DNA template in multiple denaturing conditions, we build dissociation curves using a real time PCR system (model Fast 7500, Applied Biosystems, Foster City, CA) on pre-amplified PCR product. The working solution for this experiment contained 1x PCR buffer, 1 µM SYTO 13, 1 ng. μL^{-1} of pre-amplified DNA, and 0 to 50% of formamide (v/v) or 0 to 4 M of urea. After an initial denaturation at 95˚C, the PCR cycler ramped the temperature from 60˚C to 95˚C at 100% ramp rate, and monitored SYTO 13 fluorescence during heating. For each sample, the instrument generated a trace of fluorescence *vs.* temperature, whose principal inflexion point gives the melting temperature T_m that we report in **Figure V-4**.

Off-chip PCR control experiments

For off-chip controls of compatibility between ITP and PCR buffers, we performed PCR on a Techne thermal cycler (modelxx, xx) with 35 two-step cycles: denaturation 1 min at 95˚C, and 2 min at 55˚C for annealing and extension. We performed reaction in 1x to 6x PCR buffer or 25 to 75 mM Tris HEPES, 1.5 mM magnesium chloride, 5 U per 100 µL *Taq* polymerase,

200 μM each dNTP and 2 μM of forward and reverse primers and 1/50 ng of template. PCR products were separated in a 2% agarose gel using a standard electrophoresis system. After separation, the gel was stained with 1x SYBR Green I and visualized on a UV transilluminator.

Chip preparation

We performed ITP and ccPCR experiments in a 34 μm wide 12 μm deep borosilicate channel with simple cross geometry as in **Figure V-3** (model NS95X, Caliper Life Science, Mountain View, CA). To passivate the glass surface during reactions, we used the silanizing agent Sigmacote (Sigma Aldrich) as described in the methods section of Chapter 1. This permanent glass coating along with Tween 20 dissolved in the working buffers reduce adsorption of polymerase to glass, which inhibits PCR.[101]

On-chip flow control

We tested multiple techniques to control flow and generate the chemical cycling. We describe and discuss these techniques in appendix C. Here, we briefly describe the flow control method we used to generate results presented in this chapter. We built an injection system leveraging an HPLC low dead volume switching valve (model C2, Vici Valco, Houston, TX) controlled with Matlab (The Mathworks). We interfaced the valve, sample reservoirs and chip with 360 μm OD, 50 μm ID fused silica capillaries (Upchurch Scientific, Oak Harbor, WA). We used NanoPorts (F-121H, Upchurch Scientific) to connect the capillaries to the chip, capillary liners and adapters to connect the

capillaries to the valve (FS1R and FS1L, Vici Valco). The ends of the capillaries are immersed in the two buffer reservoirs. We initially prime the valve with working solutions (LE and denaturant) to remove any air bubble present in the tubing system, and then screw the nanoport fitting onto the reservoir. To generate flow, we change the height of the two reservoirs (typically between 2 and 10 cm above the chip) to create the desired pressure head (properly calibrated in a separate experiment). See appendix A for additional details.

Temperature control

During the ccPCR, we maintain the temperature in the microchannel between 55 and 60˚C. The microchip stands on a copper block heated with a Peltier device (Omega Engineering, Stamford, CT) connected to a heat source (another copper block) and powered by a temperature controller (model xx, Omega Engineering). The heated copper block is machined to fit the glass chip and to allow for channel visualization with an inverted microscope. To calibrate temperature in the channel, we measured the temperature at diverse locations using rhodamine B fluorescence.[102] We verified uniformity of temperature and calibrated the controller to maintain the desired temperature in the channels during ccPCR.

Optical setup

We visualized ITP focused DNA (or chemical cycling) on-chip on an inverted epifluorescent microscope equipped with a 10x objective (Plan APO,

N.A. = 0.45); a mercury light source (Ushio, Japan); a filter cube (exciter/emitter 485/535 nm, Omega, VT); and a 0.6x demagnification lens (model RD060-CMT, Diagnostic Instruments, MI). We acquired images with a CCD camera (Cascade 512F, Roper Scientific) controlled with the software Winview32 (Princeton Instruments, Trenton, NJ).

ccPCR protocol

We initially fill the microchannels with the LE-ccPCR buffer described above. We then connect the PCR buffer and denaturant valve outlets to wells 1 and 2 respectively (**Figure IV-3**). At this time, there is no pressure drop between wells 1 to 4, so no flow in the channel. We then empty 4, add the sample solution containing the template, and apply vacuum at 3 for 5 s. This fills the reaction channel up to point A with a (finite) amount of template. We then carefully rinse 4 and pipette in 20 µL of TE. We apply a potential difference between 3 and 4 (200 V) to generate the electric field in the reaction channel. This starts the ITP process and focuses the DNA template at the interface between LE and TE. The ITP interface travels away from 3 further into the reaction channel. We then create a pressure-head in the off-chip reservoirs of denaturant and PCR buffer to generate a counter-flow in the reaction channel. When the focused zone appears in the field of view of the camera, we adjust the applied potential to balance electromigration and advection velocity. In these conditions, the focused ITP zone remains approximately at the same position during the ccPCR process. Lastly, we start the denaturant cycling using the off-chip switching valve to start the

ccPCR, and monitor fluorescence in the ITP zone by tracking the focused primer peak.

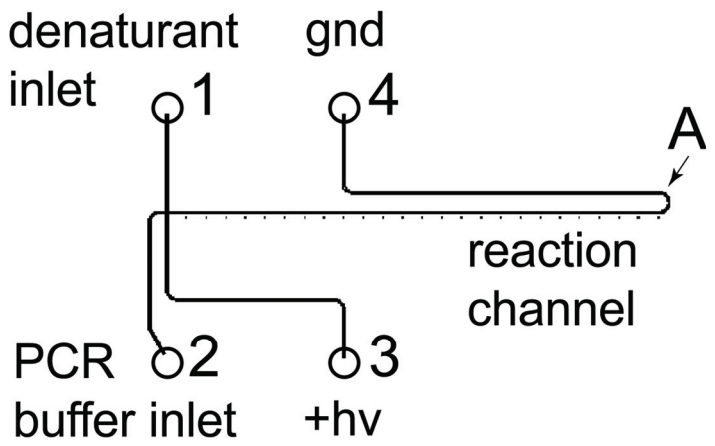

Figure V-3: Schematic of the chip used for ccPCR. Inlet 1 is connected to a denaturant reservoir via a switching valve. Inlet 2 is connected to a PCR buffer reservoir. The electric field is generated between 3 and 4 to focus the ccPCR product in the reaction channel.

V.3 Results and discussion

DNA melting temperature in denaturants

T_m decreases with formamide and urea concentrations, solvents of choice in denaturing gel electrophoresis.[103] We characterized these chemical denaturants by measuring the effect of their concentration on the melting temperature of our DNA ccPCR template. To measure melting temperatures, we built dissociation curves on our qPCR instruments using SYBR Green I fluorescence. We report the measurements of melting temperatures in **Figure V-4**. We show the dependence of the template melting temperature on urea concentration in the left graph. The melting temperature decreases with urea

concentration. We note the linear dependence of T_m with urea concentration. T_m decreases about 3˚C per mol.L^{-1} of urea. Similarly, formamide reduces the melting temperature by 0.6˚C per percent of formamide (v/v) in solution (**Figure V-4**, right graph). The dashed line shows that we can reduce the melting temperature of the template to 55˚C by using approximately 45% v/v formamide.

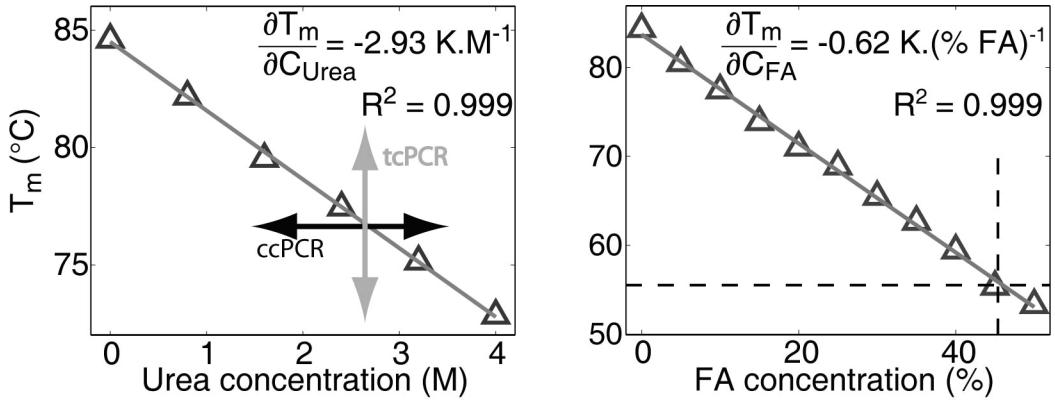

Figure V-4: Measured effect of formamide and urea concentration on melting temperature Tm of the 16S rRNA gene from E. Coli. Tm decreases with increasing urea and formamide concentrations.

Control experiments for compatibility of PCR with ITP

To verify the compatibility of PCR with ITP, we used standard ITP LE and TE as PCR reaction buffers for the amplification of the target of interest. We present sample results in Figure V-5. Here, we performed off-chip PCR using a two step cycle, denaturation at 95˚C and annealing and extension at 55˚C. Because chloride is an acceptable leading ion, we hypothesize that the traditional PCR buffer (50 mM potassium chloride, 20 mM Tric HCl) is a possible choice for LE in ccPCR conditions. As a control, we varied the

concentration of PCR buffer from 1x to 6x and verified the amplification efficiency. We show results in Figure V-5, which show that PCR buffer allows for amplification at concentration up to 3x, but inhibits amplification at 4x and above. We also verified the compatibility of a possible TE with PCR. The last three lanes in Figure V-5 show PCR using 25, 50 and 75 mM of Tris HEPES. We observe significant amplification in the three cases with a larger efficiency at 75 mM. Therefore, Tris HEPES is an acceptable TE to perform ccPCR. To summarize, we here showed that the traditional PCR buffer can be used as LE, the use of Tris HEPES at high enough concentration does not alter PCR amplification, and that amplification using a two step cycle is significant.

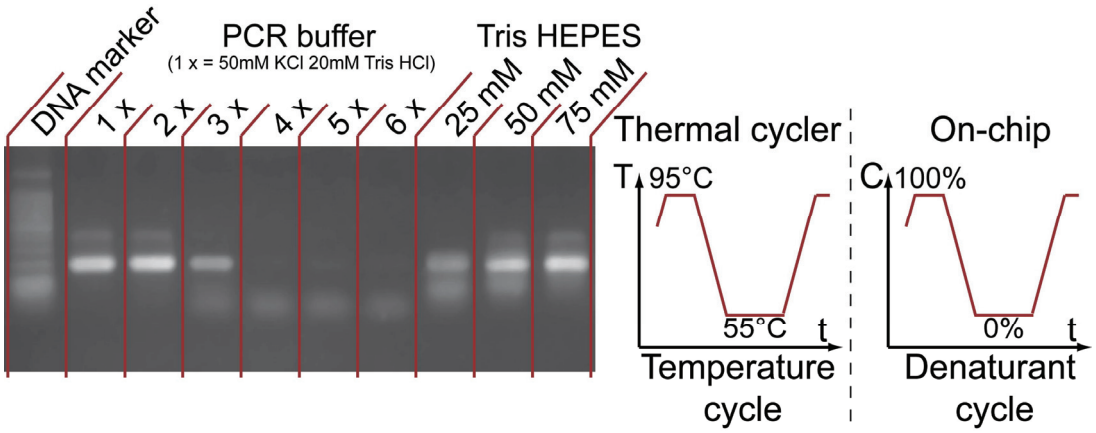

Figure V-5: Compatibility of PCR with ITP and denaturant cycling. 2% agarose gel electrophoresis of PCR products of a 2-step thermal cycle classical PCR (95°C-55°C) with increasing ionic strengths. The data shows that 3x or lower PCR buffer concentrations are required and the feasibility of a two steps thermal cycle analogous to our denaturant cycle.

Simultaneous amplification and separation of primers and reaction products

In traditional real-time PCR, primers do not yield significant fluorescence signal in reaction tubes. In ccPCR, primers focus with ITP, and despite being single stranded, they yield significant fluorescence as they preconcentrate. We leverage this residual fluorescence of focused primers to track the ITP interface when the fluorescence generated by the amplification product is below background. This allows for localization of the ITP interface during the reaction for image acquisition. With a standard chemistry, primers and PCR product focus at the same location (*i.e.* at the LE-TE interface) and the increase in fluorescence signal from the amplification reaction is biased by the continuous focusing of primers (present in the LE).

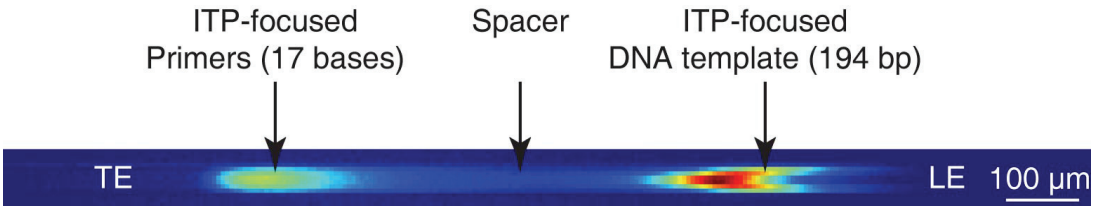

Figure V-6: Separation of primers and PCR product for localization of ITP reaction zone. A non fluorescent spacer (here benzoate) whose mobility is bracketed by the one of the primers and the DNA separates the two signal peaks, allowing for PCR product localization during ccPCR amplification.

To resolve this bias, we use a non-fluorescent spacer to separate the fluorescent signal of primers and ccPCR product. We selected a spacer that has en electrophoretic mobility larger than the one of the primers and smaller than the one of reaction product.[19] We initially introduce the spacer in the

initially injected sample (that contains the DNA template) so that the space between primer and reaction products remains constant over time.

We demonstrate this separation strategy in **Figure V-6** where we focus forward and reverse primers (fluorescent peak on the left) , and pre-amplified (off-chip) 194 bp PCR product (fluorescent peak on the right), separated by benzoate. At low cycle number, only the primer peak is detectable. During the ccPCR cycling we monitor fluorescence about 1 mm upstream the primer peak where ccPCR template and product focus.

Description of the assay

We illustrate the ccPCR process in Figure V-7. In the separation channel of the cross design chip, we initially focus a finite amount of DNA template while continuously separating it from focused primers. When the ITP interface reaches the detector's field of view, we apply pressure to the PCR buffer inlet to generate counterflow. DNA electromigrates against the flow and is held stationary upon balance of advection and electromigration velocities. We then create spatiotemporal variations of denaturant concentration using our off-chip flow control. During this process, ITP protects DNA from dispersion. The neutral denaturant clouds are unaffected by the electric field and flow through the focused polynucleotides.

When the DNA template meets a denaturant cloud, it melts into two complementary single strands (Figure V-7a). After the denaturant cloud has passed the ITP interface, the two complementary strands anneal a primer present in the LE (Figure V-7b). In the same phase, *Taq* polymerase extends

the primers to generate the two copies of the sequence of interest. We then generate a new cloud of denaturant into the reaction channel to start a new cycle.

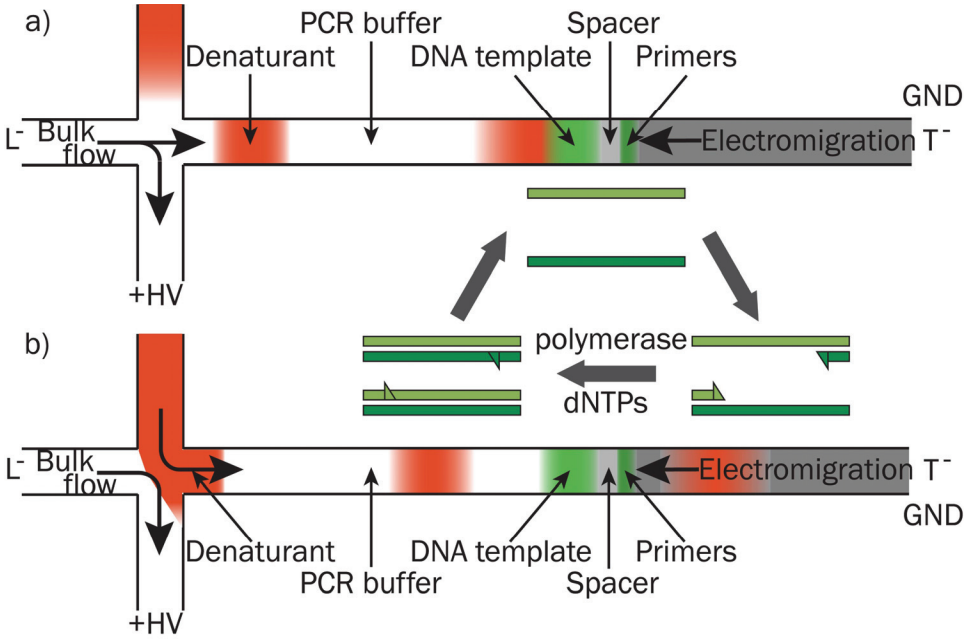

Figure V-7: Schematic of the on-chip ccPCR. DNA template (green) focuses between LE and TE with ITP. The DNA template is continuously separated from focusing primers by an electrophoretic spacer. Upon balance of flow and electromigration velocities, DNA remains stationary in the reaction channel. A flow control scheme at the cross creates discrete pulses of denaturant. a) DNA experiences a high denaturant concentration and metls into two complementary strands. b) single DNA strands anneals a primer which is then extended by a polymerase.

ccPCR results

We present two ccPCR demonstrations. In a first demonstration, we perform end-point detection after 40 cycles (**Figure V-8**); and in a second realization we monitor and report fluorescence in the ITP focused zone after each cycle in the same manner as real-time PCR (**Figure V-9**).

For the end-point demonstration, we report the fluorescence in the ITP focused template zone before the first ccPCR cycle. In **Figure V-8**, the left trace shows this signal at the level of background. We then generate the denaturing cycles. During ccPCR, we could locate the ITP zone by tracking the focused primer peak (*cf*. **Figure V-6**). After 40 ccPCR cycles, we measured fluorescent signal in the template zone, of which we show the cross-sectional averaged in the right trace of **Figure V-8**. The Gaussian-shaped peak corresponds to the focusing of ccPCR products at the ITP

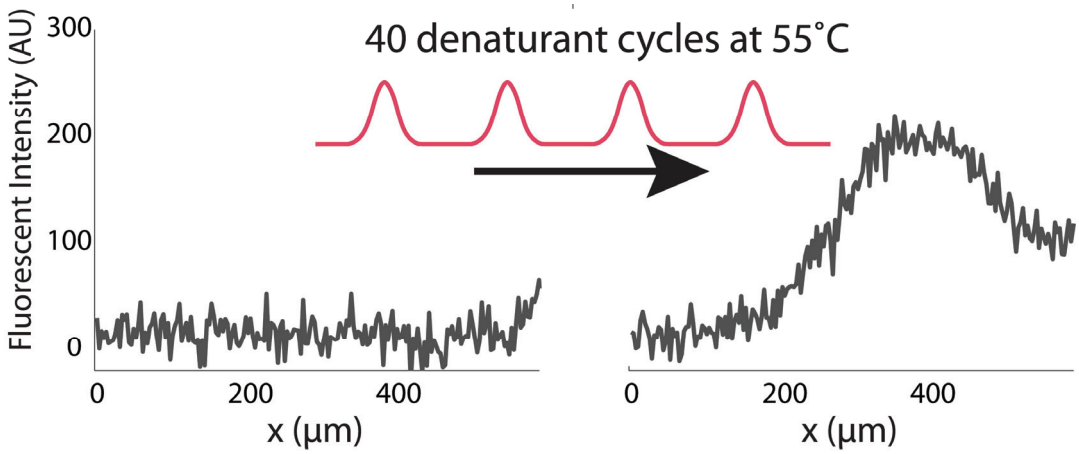

Figure V-8: Signal in the ITP-focused DNA zone before (left) and after (right) 40 ccPCR cycles. These two fluorescence profile are generated by averaging the image data over the channel cross section. Initially, the fluorescence of the template is below the limit of detection. At this stage of the ccPCR, we locate the ITP zone using the focused primers peak (no visible here, at approximately 1 mm) separated from the template zone with a spacer (MES). After 40 denaturant cycles, we measure a significant increase in the fluorescence signal in the ITP DNA zone that we attribute to ccPCR amplification product. We observe that the signal tails at $x > 500$ μm, into the spacer zone. We attribute this tailing effect to ccPCR byproducts that were only partially extended by polymerase or to primer-dimers. Applied voltage is 200 V, we measured a stationary current at approximately 1.5 μA throughout the experiment.

interface. We observe that the signal exhibits a tail diffusing into the spacer zone that we attribute to shorter reaction byproducts such as primer-dimers.

In the real-time ccPCR (**Figure V-9**), we performed the same type of measurement presented in **Figure V-8** above after each cycle, and integrated fluorescence over four standard deviations of the peak. We report the resulting curve for ccPCR with10^4 DNA copies initially focused (black squares) along with a negative control without focused template (grey circles). For the positive case, before cycle 16, the fluorescent signal is below the limit of

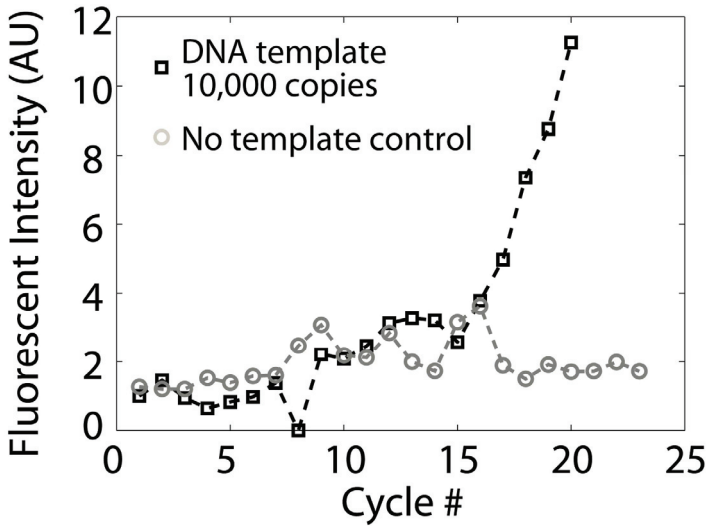

Figure V-9: Real-time ccPCR over 20 cycles. We here measure fluorescence in the ITP focused template peak after each cycle and integrate fluorescence over 4 standard deviations of the primer peak at the location of the template peak. The black square represents real time monitoring of ccPCR with initially approximately 10^4 copies in the focused zone. The grey circle curve is a negative control with no template initially focused. While the fluorescence intensity of the negative control remains at background level, the fluorescence intensity significantly increases in the ccPCR after cycle 16. We attribute this increase of fluorescence to the accumulation of focused ccPCR product, which yields a signal greater than background after cycle 16. Applied voltage is 100 V to 200 V.

detection. After cycle 16, the fluorescent signal increases significantly above background. We attribute this increase in fluorescence to the accumulation of ccPCR product after each cycle. This curve exhibits the shape of a real-time PCR curve built off-chip on a traditional thermocycler. We were not able to measure fluorescence at later cycle, and could not capture the plateau phase exhibited in off-chip real-time PCR at large cycle numbers.

V.4 Conclusion

We presented and successfully demonstrated a novel chemical cycling polymerase chain reaction (ccPCR) technique for DNA amplification in isothermal conditions. We characterized the effect of denaturants on melting temperature of our template and showed that high concentration formamide or urea allow for DNA denaturation at 55˚C. Also, we verified that ITP focusing electrolytes are compatible with PCR reactions, and that they can sustain a two step cycle (with annealing and extension in a single step). Also, we leveraged a non-fluorescent spacer to continuously separate ITP-focsued primers from ccPCR product during amplification, which allows for localization of the reaction zone. We demonstrated the ccPCR assay by amplifying a 194 bp fragment of the 16S rRNA gene from *E. Coli;* we showed end-point detection and real time monitoring of the reaction towards a quantitative ccPCR assay.

This is the first time DNA amplification by PCR has been performed isothermally, and using a chemical cycling. Performing the reaction at lower,

constant temperature relaxes the requirement for thermostable polymerase. Also, performing the reaction at constant temperature reduces the power consumption of the device compared to thermal cycling. The ccPCR combines electric field driven migration of the sample and counterflow of reactants in a microchannel, which to our knowledge has never been described.

Chapter VI. Conclusions and recommendations

In this chapter, we summarize the contributions of the work presented in this dissertation. Additionally, we give recommendations for future work and discuss potential extensions.

VI.1 Conclusions and Contributions

Purification of nucleic acids using isotachophoresis

1. We developed a method for the purification of nucleic acids from a cell lysate using ITP. We leverage the selectivity of ITP focusing to focus nucleic acids while leaving unwanted species unfocused.
2. We have used this technique for the extraction and isolation of DNA from whole blood. We initially released nucleic acids using chemical lysis and protein digestion.
3. We recovered the extracted DNA sample and verified purity by off-chip PCR. The DNA samples collected after ITP extraction were successfully and reproducibly amplified by PCR.
4. We estimated the ITP sample preparation has 30% to 70% efficiency for extraction of DNA from 2.5 nL of blood, which represents extraction from 10 to 25 white blood cells
5. We performed extraction of DNA in less than 1 min, which represents a significant speed improvement compared to benchtop and miniaturized purification techniques.

Quantification of global miRNA using selective isotachophoresis

1. We developed an assay for the quantification of global miRNA abundance in cultures and tissues. This quantification is a measurement of the cell RNA silencing activity. We leverage the selectivity and sensitivity of ITP to focus miRNA while leaving longer RNA molecules from total RNA unfocused.
2. To simultaneously reach high selectivity and sensitivity, we designed a multi-stage ITP protocol where the ITP-focused sample migrates through three stationary zones initially generated. The chemistries of the are designed to successively preconcentrate, select and detect miRNA.
3. We optimized the chemistry of the multi-stage ITP to perform quantitation of miRNA shorter than 40 nt and down to 0.3 $pg.uL^{-1}$.
4. We have validated our method by measuring and comparing miRNA abundance in cell cultures at different densities. We observed that miRNA expression increases with culture density, as previously reported.
5. We measured miRNA abundance in a wide variety of samples to survey miRNA expression in multiple tissues. In particular, we showed that E14 ES stem cells have high miRNA expression level. We also showed that the expression of oncogene transcription factor MYC decreases miRNA expression level.

miRNA profiling using isotachophoresis and molecular beacons

1. We developed an assay for the sequence specific and size selective detection of miRNA in total RNA by combining ITP and hybridization with molecular beacons. We used ITP to selectively focus miRNA simultaneously with molecular beacons that hybridize the target of interest within the ITP-focused zone.
2. We used the multi-stage ITP to perform successive preconcentration, selection and hybridization of miRNA.
3. We optimized the selectivity of the multi-stage ITP to allow for detection of miRNA without detection bias from (longer) miRNA precursors.
4. We used the ITP-hybridization assay to quantify miR-122 in liver and kidney. We successfully detected miR-122 in liver and our quantification results are consistent with measurements performed with traditional methods.

Chemical cycling polymerase chain reaction

1. We developed an assay for the isothermal amplification of DNA by chemical cycling PCR. We combined ITP focusing of DNA template and product with flow of chemical denaturants to mimic thermal cycling.
2. We characterized chemical denaturants and verified that at high enough concentration, they significantly lower the melting temperature of DNA. This shows that cycling denaturant concentration is equivalent to cycling temperature.

3. We performed a series of control experiments to verify that ITP conditions for the focusing of DNA are compatible with PCR. We also showed that these buffers were suitable for two-step PCR cycles.
4. We leverage the separation power of ITP and a non-fluorescent spacer to segregate the fluorescent signal of focused DNA template and product from the focused primers. We then use the focused primer peak to localize the reaction zone.
5. To demonstrated ccPCR amplification, we performed end-point detection and real-time monitoring. These results represent a proof-of-concept of ccPCR.

VI.2 Recommendations for future work

We list here possible extensions of the current work and future research directions

Purification of nucleic acids using isotachophoresis

1. One of the limitations of the current DNA purification protocol is its low throughput. Channels with significantly larger cross section or free flow ITP architecture (*cf*. Appendix C) would significantly improve throughput to perform purification from larger sample volumes
2. Single cell nucleic acid isolation and transport could be achieved with ITP. Extraction from a single cell could be performed by combining on-chip lysis. For example, using on-chip serial dilutions of the sample could enable single cell isolation prior lysis and extraction.

3. The current protocol is limited to extraction of DNA. A significant improvement consists in adapting the ITP purification to extraction of RNA. The main technical challenge is to reduce RNA degradation during lysis and extraction.

Quantification of global miRNA using selective isotachophoresis

1. We have only qualitatively validated the ITP assay for measurement of global miRNA abundance. A detailed quantitative study could reconcile our results with estimates from microarray data. Also, a direct comparison between microarray and ITP could lead to a standard method for normalizing miRNA profiling data.
2. Our method for the quantification of miRNA can be adapted to the purification of miRNA for subsequent analysis (*e.g.* sequencing, qPCR). Transformation could be achieved by designing system that will only collect the ITP-focused miRNA.
3. We observed that RNA quality has a significant impact on miRNA quantitation. We hypothesize that miRNA quantification can be corrected for degradation knowing the sample RNA integrity number. Such correction would be beneficial in the case of samples that rapidly degrade prior RNA preparation

miRNA profiling using isotachophoresis and molecular beacons

1. The current detection limit of the assay is on the order of 3,000 copies per cell. Further optimization of ITP chemistry and channel design could

significantly enhance sensitivity. For example, using a channel with large cross section for preconcentration and small cross section to reduce ITP zone volume is beneficial to sensitivity.[104]

2. To perform mutliplex miRNA profiling using ITP hybridization, the assay can be performed in parallel channels. This would allow for analysis of multiple samples and/or multiple targets in a single run.
3. The ITP hybridization assay can be transcribed into assay for profiling of a wide variety of nucleic acids. For example, ITP hybridization on ribosomal RNA may be efficient for the rapid detection of pathogens or virus.

Chemical cycling polymerase chain reaction

1. The current ccPCR detection system has low sensitivity. In order to perform more sensitive reaction monitoring, we recommend the use of a confocal microscope assembly to monitor fluorescence in the ITP zone
2. Currently, ccPCR has low reproducibility. We hypothesize that polymerase activity is affected by electric fields. We therefore suggest running ccPCR with electric field on during denaturation and stopping flow and field for extension. In these conditions, we use the robustness of ITP to rapidly refocus the ccPCR products when voltage is applied.
3. To increase resolution of the separation of amplification products and primers, the assay can be performed in a sieving matrix that does not inhibit PCR, for example PVP.

4. Using a non-thermostable polymerase (*e.g.* Klenow fragment of DNA polymerase I) has potential for higher amplification fidelity and relaxes the requirement for polymerase thermostability

Bibliography

1. Mariella, R., Sample preparation: the weak link in microfluidics-based biodetection. *Biomedical Microdevices* **2008,** 10, (6), 777-784.

2. He, L.; Hannon, G. J., Microrнas: Small RNAs with a big role in gene regulation. *Nat. Rev. Genet.* **2004,** 5, (7), 522-531.

3. Baker, M., MicroRNA profiling: separating signal from noise. *Nat Meth* **2010,** 7, (9), 687-692.

4. Probstein, R. F., *Physicochemical Hydrodynamics: An Introduction*. Second ed.; John Wiley & Sons, Inc.: New York, 1994; p 400.

5. Melcher, J. R.; Taylor, G. I., Electrohydrodynamics - a review of role of interfacial shear stresses. *Annual Review of Fluid Mechanics* **1969,** 1, 111-&.

6. Persat, A.; Suss, M. E.; Santiago, J. G., Basic principles of electrolyte chemistry for microfluidic electrokinetics. Part II: Coupling between ion mobility, electrolysis, and acid-base equilibria. *Lab on a Chip* **2009,** 9, (17), 2454-69.

7. Landers, J. P., *Handbook of Capillary and Microchip Electrophoresis and Associated Microtechniques*. Taylor & Francis Group, LLC, Boca Raton, FL: 2008.

8. Moore, D. S., Instrumentation for trace detection of high explosives. *Review of Scientific Instruments* **2004,** 75, (8), 2499-2512.

9. Cifuentes, A., Recent advances in the application of capillary electromigration methods for food analysis. *Electrophoresis* **2006,** 27, (1), 283-303.

10. Valaskovic, G. A.; Kelleher, N. L.; McLafferty, F. W., Attomole protein characterization by capillary electrophoresis mass spectrometry. *Science* **1996,** 273, (5279), 1199-1202.

11. Zhou, H. H.; Miller, A. W.; Sosic, Z.; Buchholz, B.; Barron, A. E.; Kotler, L.; Karger, B. L., DNA sequencing up to 1300 bases in two hours by capillary electrophoresis with mixed replaceable linear polyacrylamide solutions. *Analytical Chemistry* **2000,** 72, (5), 1045-1052.

12. Cheng, Y.-F.; Dovichi, N. J., Subattomole amino acid analysis by capillary zone electrophoresis and laser-induced fluorescence. *Science* **1988,** v242, (n4878), p562(3).

13. Simpson, P. C.; Roach, D.; Woolley, A. T.; Thorsen, T.; Johnston, R.; Sensabaugh, G. F.; Mathies, R. A., High-throughput genetic analysis using microfabricated 96-sample capillary array electrophoresis microplates. *Proceedings of the National Academy of Sciences of the United States of America* **1998,** 95, (5), 2256-2261.

14. Bousse, L.; Cohen, C.; Nikiforov, T.; Chow, A.; Kopf-Sill, A. R.; Dubrow, R.; Parce, J. W., Electrokinetically controlled microfluidic analysis systems. *Annual Review of Biophysics and Biomolecular Structure* **2000,** 29, 155-181.

15. Quirino, J. P.; Terabe, S., Exceeding 5000-fold concentration of dilute analytes in micellar electrokinetic chromatography. *Science* **1998,** 282, (5388), 465-468.

16. Jensen, P. K.; Pasa-Tolic, L.; Anderson, G. A.; Horner, J. A.; Lipton, M. S.; Bruce, J. E.; Smith, R. D., Probing proteomes using capillary isoelectric focusing-electrospray ionization Fourier transform ion cyclotron resonance mass spectrometry. *Analytical Chemistry* **1999,** 71, (11), 2076-2084.

17. Everaerts, F. M.; Beckers, J. L.; Verheggen, T. P. E. M., *Isotachophoresis : theory, instrumentation, and applications*. Elsevier Scientific Pub. Co.: Amsterdam; New York, 1976.

18. Jung, B. G.; Zhu, Y. G.; Santiago, J. G., Detection of 100 aM fluorophores using a high-sensitivity on-chip CE system and transient isotachophoresis. *Analytical Chemistry* **2007,** 79, (1), 345-349.

19. Khurana, T. K.; Santiago, J. G., Preconcentration, separation, and indirect detection of nonfluorescent analytes using fluorescent mobility markers. *Anal. Chem.* **2008,** 80, (1), 279-286.

20. Fredlake, C. P.; Hert, D. G.; Kan, C. W.; Chiesl, T. N.; Root, B. E.; Forster, R. E.; Barron, A. E., Ultrafast DNA sequencing on a microchip by a hybrid separation mechanism that gives 600 bases in 6.5 minutes. *Proceedings of the National Academy of Sciences of the United States of America* **2008,** 105, (2), 476-481.

21. Easley, C. J.; Karlinsey, J. M.; Bienvenue, J. M.; Legendre, L. A.; Roper, M. G.; Feldman, S. H.; Hughes, M. A.; Hewlett, E. L.; Merkel, T. J.; Ferrance, J. P.; Landers, J. P., A fully integrated microfluidic genetic analysis system with sample-in-answer-out capability. *Proceedings of the National Academy of Sciences of the United States of America* **2006,** 103, (51), 19272-19277.

22. Schroeder, A.; Mueller, O.; Stocker, S.; Salowsky, R.; Leiber, M.; Gassmann, M.; Lightfoot, S.; Menzel, W.; Granzow, M.; Ragg, T., The RIN: an RNA integrity number for assigning integrity values to RNA measurements. *Bmc Molecular Biology* **2006,** 7, (1), 3.

23. Gebauer, P.; Mala, Z.; Bocek, P., Recent progress in capillary ITP. *Electrophoresis* **2007,** 28, (1-2), 26-32.

24. Chen, L.; Prest, J. E.; Fielden, P. R.; Goddard, N. J.; Manz, A.; Day, P. J. R., Miniaturised isotachophoresis analysis. *Lab on a Chip* **2006,** 6, (4), 474-487.

25. Saville, D. A., THE EFFECTS OF ELECTROOSMOSIS ON THE STRUCTURE OF ISOTACHOPHORESIS BOUNDARIES. *Electrophoresis* **1990,** 11, (11), 899-902.

26. Jung, B.; Bharadwaj, R.; Santiago, J. G., On-chip millionfold sample stacking using transient isotachophoresis. *Anal. Chem.* **2006,** 78, (7), 2319-2327.

27. Khurana, T. K.; Santiago, J. G., Sample zone dynamics in peak mode isotachophoresis. *Anal. Chem.* **2008,** 80, (16), 6300-6307.

28. Khurana, T. K.; Santiago, J. G., Effects of carbon dioxide on peak mode isotachophoresis: Simultaneous preconcentration and separation. *Lab on a Chip* **2009,** 9, (10), 1377-1384.

29. Persat, A.; Marshall, L. A.; Santiago, J. G., Purification of Nucleic Acids from Whole Blood Using Isotachophoresis. *Anal. Chem.* **2009,** 81, (22), 9507-9511.

30. Xu, Z. Q.; Esumi, T.; Ikuta, N.; Hirokawa, T., High-sensitive analysis of DNA fragments by capillary gel electrophoresis using transient isotachophoresis preconcentration and fluorescence detection. *Journal of Chromatography A* **2009,** 1216, (17), 3602-3605.

31. Caslavska, J.; Thormann, W., Continuous separation and purification of proteins by recycling isotachophoresis. *Journal of Chromatography* **1992,** 594, (1-2), 361-369.

32. Park, C. C.; Kazakova, I.; Kawabata, T.; Spaid, M.; Chien, R.-L.; Wada, H. G.; Satomura, S., Controlling Data Quality and Reproducibility of a High-Sensitivity Immunoassay Using Isotachophoresis in a Microchip. *Analytical Chemistry* **2008,** 80, (3), 808-814.

33. Goet, G.; Baier, T.; Hardt, S., Micro contactor based on isotachophoretic sample transport. *Lab on a Chip* **2009,** 9, (24), 3586-3593.

34. Chambers, R.; Santiago, J. G.; Persat, A.; Schoch, R.; Ronaghi, M.; Matsumura, T., Isotachophoretic Focusing of Nucleic Acids. **2009**.

35. Persat, A.; Chivukula, R.; Mendell, J.; Santiago, J. G., Quantification of Global microRNA Abundance by Selective Isotachophoresis. *Anal. Chem, under review* **2010**.

36. Santiago, J. G.; Persat, A. Enhanced Isotachophoresis Assays Using Additives with Spatial gradients. 2010.

37. Persat, A. S., J.G., microRNA profiling by simultaneous selective isotachophoresis and hybridization with molecular beacons. *in preparation* **2010**.

38. Persat, A., Morita, T., and Santiago J.G., Towards on-chip isothermal polymerase chain reaction. *Proc. MicroTAS 2007* **2007,** 11, 56-58.

39. Persat, A.; Santiago, J. G. Performing chemical reaction involves providing two reactants, which are confined by isotachophoresis to isotachophoresis zone in liquid flow channel; and allowing to react in the zone to give product which is separated by isotachophoresis. US2010084271-A1, 2009.

40. Hong, J. W.; Quake, S. R., Integrated nanoliter systems. *Nature Biotechnology* **2003,** 21, (10), 1179-1183.

41. Wilding, P.; Shoffner, M. A.; Kricka, L. J., PCR in a silicon microstructure. *Clin Chem* **1994,** 40, (9), 1815-1818.

42. Manz, A.; Harrison, D. J.; Verpoorte, E. M. J.; Fettinger, J. C.; Paulus, A.; Ludi, H.; Widmer, H. M., Planar chips technology for miniaturization and integration of separation techniques into monitoring systems - capilary electrophoresis on a chip. *Journal of Chromatography* **1992,** 593, (1-2), 253-258.

43. Chiem, N. H.; Harrison, D. J., Monoclonal antibody binding affinity determined by microchip-based capillary electrophoresis. *Electrophoresis* **1998,** 19, (16-17), 3040-3044.

44. Boom, R.; Sol, C. J. A.; Salimans, M. M. M.; Jansen, C. L.; Wertheimvandillen, P. M. E.; Vandernoordaa, J., Rapid and simple method for purification of nucleic acids. *Journal of Clinical Microbiology* **1990,** 28, (3), 495-503.

45. Wen, J.; Legendre, L. A.; Bienvenue, J. M.; Landers, J. P., Purification of nucleic acids in microfluidic devices. *Analytical Chemistry* **2008,** 80, (17), 6472-6479.

46. Breadmore, M. C.; Wolfe, K. A.; Arcibal, I. G.; Leung, W. K.; Dickson, D.; Giordano, B. C.; Power, M. E.; Ferrance, J. P.; Feldman, S. H.; Norris, P. M.; Landers, J. P., Microchip-based purification of DNA from biological samples. *Analytical Chemistry* **2003,** 75, (8), 1880-1886.

47. Hagan, K. A.; Bienvenue, J. M.; Moskaluk, C. A.; Landers, J. P., Microchip-Based Solid-Phase Purification of RNA from Biological Samples. *Analytical Chemistry* **2008,** 80, (22), 8453-8460.

48. Marcus, J. S.; Anderson, W. F.; Quake, S. R., Microfluidic single-cell mRNA isolation and analysis. *Analytical Chemistry* **2006,** 78, (9), 3084-3089.

49. Bier, M., Recycling isoelectric focusing and isotachophoresis. *Electrophoresis* **1998,** 19, (7), 1057-1063.

50. Weber, G.; Bocek, P., Interval isotachophoresis for purification and isolation of ionogenic species. *Electrophoresis* **1998,** 19, (18), 3090-3093.

51. Kondratova, V. N.; Serd'uk, O. I.; Shelepov, V. P.; Lichtenstein, A., Concentration and isolation of DNA from biological fluids by agarose gel isotachophoresis. *Biotechniques* **2005,** 39, (5), 695-699.

52. Schoch, R. B.; Ronaghi, M.; Santiago, J. G., Rapid and selective extraction, isolation, preconcentration, and quantitation of small RNAs from cell lysate using on-chip isotachophoresis. *Lab Chip* **2009,** 9, (15), 2145-2152.

53. Kemp, B. M.; Smith, D. G., Use of bleach to eliminate contaminating DNA from the surface of bones and teeth. *Forensic Science International* **2005,** 154, (1), 53-61.

54. Rickard, E. C.; Strohl, M. M.; Nielsen, R. G., Correlation of electrophoretic mobilities from capillary electrophoresis with physicochemical properties of proteins and peptides. *Analytical Biochemistry* **1991,** 197, (1), 197-207.

55. Stellwagen, N. C.; Gelfi, C.; Righetti, P. G., The free solution mobility of DNA. *Biopolymers* **1997,** 42, (6), 687-703.

56. Radstrom, P.; Knutsson, R.; Wolffs, P.; Lovenklev, M.; Lofstrom, C., Pre-PCR processing - Strategies to generate PCR-compatible samples. *Molecular Biotechnology* **2004,** 26, (2), 133-146.

57. Ebeling, W.; Hennrich, N.; Klockow, M.; Metz, H.; Orth, H. D.; Lang, H., Porteinase K from *Tritirachium-album* limber. *European Journal of Biochemistry* **1974,** 47, (1), 91-97.

58. Bickley, J.; Short, J. K.; McDowell, D. G.; Parkes, H. C., Polymerase chain reaction (PCR) detection of Listeria monocytogenes in diluted milk and reversal of PCR inhibition caused by calcium ions. *Letters in Applied Microbiology* **1996,** 22, (2), 153-158.

59. Kim, J.; Johnson, M.; Hill, P.; Gale, B. K., Microfluidic sample preparation: cell lysis and nucleic acid purification. *Integrative Biology* **2009,** 1, (10), 574-586.

60. Weyant, R. S.; Edmonds, P.; Swaminathan, B., Effect of ionic and nonionic detergents on the Taq polymerase. *Biotechniques* **1990,** 9, (3), 308-309.

61. Shapiro, A. L.; Vinuela, E.; Maizel, J. V., Molecular weight estimation of polypeptide chains by electrophoresis in SDS-polyacrylamide gels. *Biochemical and Biophysical Research Communications* **1967,** 28, (5), 815-&.

62. Chen, X.; Cui, D. F.; Liu, C. C.; Li, H.; Chen, J., Continuous flow microfluidic device for cell separation, cell lysis and DNA purification. *Analytica Chimica Acta* **2007,** 584, (2), 237-243.

63. Nakagawa, T.; Tanaka, T.; Niwa, D.; Osaka, T.; Takeyama, H.; Matsunaga, T., Fabrication of amino silane-coated microchip for DNA extraction from whole blood. *Journal of Biotechnology* **2005,** 116, (2), 105-111.

64. Alberts, B., *Molecular biology of the cell. Reference edition*. Garland Science: New York, 2008.

65. Lu, J.; Getz, G.; Miska, E. A.; Alvarez-Saavedra, E.; Lamb, J.; Peck, D.; Sweet-Cordero, A.; Ebet, B. L.; Mak, R. H.; Ferrando, A. A.; Downing, J. R.; Jacks, T.; Horvitz, H. R.; Golub, T. R., MicroRNA expression profiles classify human cancers. *Nature* **2005,** 435, (7043), 834-838.

66. Thomson, J. M.; Newman, M.; Parker, J. S.; Morin-Kensicki, E. M.; Wright, T.; Hammond, S. M., Extensive post-transcriptional regulation of microRNAs and its implications for cancer. *Genes Dev.* **2006,** 20, (16), 2202-2207.

67. Hwang, H. W.; Wentzel, E. A.; Mendell, J. T., Cell-cell contact globally activates microRNA biogenesis. *Proc. Natl. Acad. Sci. U. S. A.* **2009,** 106, (17), 7016-7021.

68. Chu, C. Y.; Rana, T. M., Small RNAs: Regulators and guardians of the genome. *Journal of Cellular Physiology* **2007,** 213, (2), 412-419.

69. Masotti, A.; Caputo, V.; Da Sacco, L.; Pizzuti, A.; Dallapiccola, B.; Bottazzo, G. F., Quantification of Small Non-Coding RNAs Allows an Accurate Comparison of miRNA Expression Profiles. *J. of Biomed. and Biotechnol.* **2009,** Article ID 659028, 9.

70. Becker, C.; Hammerle-Fickinger, A.; Riedmaier, I.; Pfaffl, M. W., mRNA and microRNA quality control for RT-qPCR analysis. *Methods* **2010,** 50, (4), 237-243.

71. Barron, A. E.; Sunada, W. M.; Blanch, H. W., The effects of polymer properties on DNA separations by capillary electrophoresis in uncross-linked polymer solutions. *Electrophoresis* **1996,** 17, (4), 744-757.

72. Kan, C. W.; Fredlake, C. P.; Doherty, E. A. S.; Barron, A. E., DNA sequencing and genotyping in miniaturized electrophoresis systems. *Electrophoresis* **2004,** 25, (21-22), 3564-3588.

73. Gao, Q.; Yeung, E. S., A Matrix for DNA Separation: Genotyping and Sequencing Using Poly(vinylpyrrolidone) Solution in Uncoated Capillaries. *Analytical Chemistry* **1998,** 70, (7), 1382-1388.

74. Li, N.; Nguyen, A.; Diedrich, J.; Zhong, W., Separation of miRNA and its methylation products by capillary electrophoresis. *Journal of Chromatography A* **2008,** 1202, (2), 220-223.

75. Bocek, P.; Deml, M.; Janak, J., Effect of a concentration cascade of leading electrolyte on separation capacity in isotachophoresis. *J. Chromatogr., A* **1978,** 156, (2), 323-326.

76. Todorov, T. I.; Yamaguchi, Y.; Morris, M. D., Effect of urea on the polymer buffer solutions used for the electrophoretic separations of nucleic acids. *Anal. Chem.* **2003,** 75, (8), 1837-1843.

77. Cosa, G.; Focsaneanu, K. S.; McLean, J. R. N.; McNamee, J. P.; Scaiano, J. C., Photophysical properties of fluorescent DNA-dyes bound to single- and double-stranded DNA in aqueous buffered solution. *Photochem. Photobiol.* **2001,** 73, (6), 585-599.

78. Zhang, X. X.; Graves, P. R.; Zeng, Y., Stable Argonaute2 overexpression differentially regulates microRNA production. *Biochim. Biophys. Acta, Gene Regul. Mech.* **2009,** 1789, (2), 153-159.

79. Vreeland, W. N.; Williams, S. J.; Barron, A. E.; Sassi, A. P., Tandem isotachophoresis-zone electrophoresis via base-mediated destacking for increased detection sensitivity in microfluidic systems. *Anal. Chem.* **2003,** 75, (13), 3059-3065.

80. Bissels, U.; Wild, S.; Tomiuk, S.; Holste, A.; Hafner, M.; Tuschl, T.; Bosio, A., Absolute quantification of microRNAs by using a universal reference. *RNA* **2009,** 15, (12), 2375-2384.

81. Ach, R.; Wang, H.; Curry, B., Measuring microRNAs: Comparisons of microarray and quantitative PCR measurements, and of different total RNA prep methods. *Bmc Biotechnology* **2008,** 8, (1), 69.

82. Chang, T.-C.; Yu, D.; Lee, Y.-S.; Wentzel, E. A.; Arking, D. E.; West, K. M.; Dang, C. V.; Thomas-Tikhonenko, A.; Mendell, J. T., Widespread microRNA repression by Myc contributes to tumorigenesis. *Nat Genet* **2008,** 40, (1), 43-50.

83. Tricoli, J. V.; Jacobson, J. W., MicroRNA: Potential for Cancer Detection, Diagnosis, and Prognosis. *Cancer Res* **2007,** 67, (10), 4553-4555.

84. Chen, C. F.; Ridzon, D. A.; Broomer, A. J.; Zhou, Z. H.; Lee, D. H.; Nguyen, J. T.; Barbisin, M.; Xu, N. L.; Mahuvakar, V. R.; Andersen, M. R.; Lao, K. Q.; Livak, K. J.; Guegler, K. J., Real-time quantification of microRNAs by stem-loop RT-PCR. *Nucleic Acids Research* **2005,** 33, (20), 9.

85. Varallyay, E.; Burgyan, J.; Havelda, Z., MicroRNA detection by northern blotting using locked nucleic acid probes. *Nat. Protocols* **2008,** 3, (2), 190-196.

86. Tyagi, S.; Kramer, F. R., Molecular beacons: Probes that fluoresce upon hybridization. *Nature Biotechnology* **1996,** 14, (3), 303-308.

87. Santangelo, P. J.; Nix, B.; Tsourkas, A.; Bao, G., Dual FRET molecular beacons for mRNA detection in living cells. *Nucleic Acids Research* **2004,** 32, (6).

88. Kibbe, W. A., OligoCalc: an online oligonucleotide properties calculator. *Nucl. Acids Res.* **2007,** 35, (suppl_2), W43-46.

89. Squires, T. M.; Quake, S. R., Microfluidics: Fluid physics at the nanoliter scale. *Reviews of Modern Physics* **2005,** 77, (3), 977-1026.

90. Marras, S. A. E.; Kramer, F. R.; Tyagi, S., Efficiencies of fluorescence resonance energy transfer and contact-mediated quenching in oligonucleotide probes. *Nucleic Acids Research* **2002,** 30, (21).

91. Dubertret, B.; Calame, M.; Libchaber, A. J., Single-mismatch detection using gold-quenched fluorescent oligonucleotides. *Nature Biotechnology* **2001,** 19, (4), 365-370.

92. Chang, J.; Nicolas, E.; Marks, D.; Sander, C.; Lerro, A.; Buendia, M. A.; Xu, C.; Mason, W. S.; Moloshok, T.; Bort, R.; Zaret, K. S.; Taylor, J. M., miR-122, a mammalian liver-specific microRNA, is processed from hcr mRNA and may downregulate the high affinity cationic amino acid transporter CAT-1. *RNA Biol* **2004,** 1, (2), 106-13.

93. Sarasin-Filipowicz, M.; Krol, J.; Markiewicz, I.; Heim, M. H.; Filipowicz, W., Decreased levels of microRNA miR-122 in individuals with hepatitis C responding poorly to interferon therapy. *Nat Med* **2009,** 15, (1), 31-33.

94. Saiki, R. K.; Gelfand, D. H.; Stoffel, S.; Scharf, S. J.; Higuchi, R.; Horn, G. T.; Mullis, K. B.; Erlich, H. A., Primer-Directed Enzymatic Amplification of DNA with a Thermostable DNA-Polymerase. *Science* **1988,** 239, (4839), 487-491.

95. Giordano, B. C.; Ferrance, J.; Swedberg, S.; Huhmer, A. F. R.; Landers, J. P., Polymerase chain reaction in polymeric microchips: DNA amplification in less than 240 seconds. *Analytical Biochemistry* **2001,** 291, (1), 124-132.

96. Liu, J.; Enzelberger, M.; Quake, S., A nanoliter rotary device for polymerase chain reaction. *Electrophoresis* **2002,** 23, (10), 1531-1536.

97. Beer, N. R.; Hindson, B. J.; Wheeler, E. K.; Hall, S. B.; Rose, K. A.; Kennedy, I. M.; Colston, B. W., On-chip, real-time, single-copy polymerase chain reaction in picoliter droplets. *Analytical Chemistry* **2007,** 79, (22), 8471-8475.

98. Compton, J., Nucleic acid sequence-based amplification. *Nature* **1991,** 350, (6313), 91-92.

99. Fire, A.; Xu, S. Q., Rolling Replication of Short DNA Circles. *Proceedings of the National Academy of Sciences of the United States of America* **1995,** 92, (10), 4641-4645.

100. Varadaraj, K.; Skinner, D. M., Denaturants or cosolvents improve the specificity of PCR amplification of a G + C-rich DNA using genetically engineered DNA polymerases. *Gene* **1994,** 140, (1), 1-5.

101. Shoffner, M. A.; Cheng, J.; Hvichia, G. E.; Kricka, L. J.; Wilding, P., Chip PCR .1. Surface passivation of microfabricated silicon-glass chips for PCR. *Nucleic Acids Research* **1996,** 24, (2), 375-379.

102. Ross, D.; Gaitan, M.; Locascio, L. E., Temperature measurement in microfluidic systems using a temperature-dependent fluorescent dye. *Analytical Chemistry* **2001,** 73, (17), 4117-4123.

103. Fischer, S. G.; Lerman, L. S., Length-Independent Separation of DNA Restriction Fragments in 2-Dimensional Gel-Electrophoresis. *Cell* **1979,** 16, (1), 191-200.

104. Bahga, S. S., Kaigala, G.V., Bercovici, M., Santiago, J.G., High sensitivity indirect chemical detection using on-chip isotachophoresis with variable cross-section geometry. *under review, Electrophoresis* **2010**.

105. Cui, H. C.; Huang, Z.; Dutta, P.; Ivory, C. F., Automated electric valve for electrokinetic separation in a networked microfluidic chip. *Anal. Chem.* **2007,** 79, (4), 1456-1465.

106. Turgeon, R. T.; Bowser, M. T., Micro free-flow electrophoresis: theory and applications. *Analytical and Bioanalytical Chemistry* **2009,** 394, (1), 187-198.

107. Matsumura, T.; Persat, A.; Santiago, J. G., On-chip Purification of Nucleic Acid using isotachophoresis. **2009**, in preparation.

108. Huang, S. J.; Wang, H. Y.; Carroll, C. A.; Hayes, S. J.; Weintraub, S. T.; Serwer, P., Analysis of proteins stained by Alexa dyes. *Electrophoresis* **2004,** 25, (6), 779-784.

109. Penrod, S. L.; Olson, T. M.; Grant, S. B., Whole particle microelectrophoresis for small viruses. *Journal of Colloid and Interface Science* **1995,** 173, (2), 521-523.

110. Sigma-Aldrich Detergents for Cell Lysis. http://www.sigmaaldrich.com/life-science/proteomics/protein-sample-preparation/individual-reagents/cell-lysis-detergents.html

Appendix A. Flow control for chemical cycling PCR

We here present and compare the different methods to control on-chip flow in the ccPCR experiments. We tested three different flow control strategies: pressure control with a switching valve, pressure control with a sequencer and initial loading of chemical cycles in a PDMS-glass device.

Pressure-driven flow

Hydrostatic pressure and switching valve

We used hydrostatic pressure to generate flow in the microchannel and an off-chip valve to control injection of denaturant. This method is described in detail in the methods section of Chapter V. We here give additional practical details on the setup and on calibration of the injection.

We show a picture of the setup in figure A-1. Its main components include the chip, connected via a capillary and Nanoports to the valve. The reservoir of denaturant is connected to the valve with capillary A. The reservoir of PCR buffer (not visible in the figure) is connected directly to the chip with capillary B. The surface of the reservoirs are placed 2 to 5 cm above the level of the chip to create the pressure-head.

To calibrate the denaturant injection, we dissolve rhodamine B in the denaturant and visualize flow at the chip intersection. We adjust the level of the reservoirs so that the when the valve is in “PCR buffer” position, the interface between denaturant and PCR buffer remains stationary in its

injection channel, (*i.e.* no flow) and when the valve is in "denaturant" position, the denaturant flows into the main reaction channel. With this setup, we could inject denaturant clouds traveling at about 1 $mm.s^{-1}$.

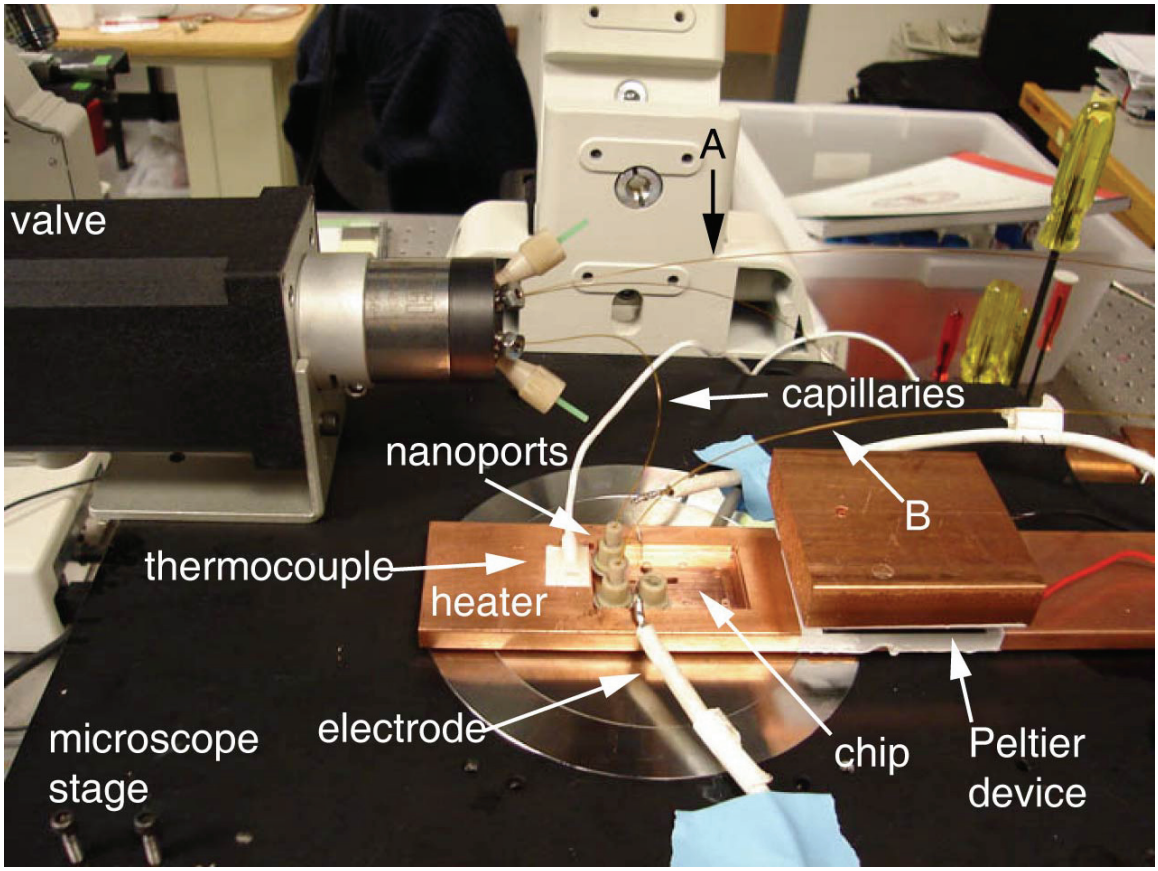

Figure A-1. ccPCR flow control setup. The injection is performed using pressure-head created between the reservoirs and the chip. The denaturant reservoir is connected to the valve with capillary A and the PCR buffer is connected to the chip with capillary B. The switching valve allows for injection of denaturant on-chip. The chip stands on a copper heater that is machined to allow for visualization. Temperature is maintained between 55˚C and 60˚C with a Peltier device connected to a temperature controller (thermocouple allows for feedback control).

Pressure-driven flow – pressure controller

We have explored alternatives to the hydrostatic pressure-head to generate ccPCR flow. In particular, we tested a software controlled

microfluidic flow sequencer (MFCS, Fluigent, Paris, France). The sequencer independently controls air pressure in tubes containing the reagents and that are connected to the chip. Each of the tube is connected to the microchip via 100 μm ID PEEK tubing and Nanoport microfluidic connections (Upchurch Scientific, Oak Harbor, WA). The flow calibration is performed the same way as the previous method, with the pressure adjusted on the software provided with the pressure controller.

We note that other pressure controllers can be used there, for example the Mensor 6000, but we found that the MFCS was most convenient as it offers regulation of pressure in the 1 psi range. and can simultaneously control eight pressure outputs.

PDMS device for initial loading of denaturant cycles

We have performed preliminary experiments on a PDMS device that allows for initial creation of the denaturant cycles prior ccPCR. This scheme does not require simultaneous ITP and flow control, which greatly simplifies the ccPCR process.

We use a two-layer PDMS device with a network of valves that can be activated in two positions: a first injection position which allows for denaturant injection, and a ccPCR position that enables ITP though the chemical cycles.

The chip was fabricated at ths Stanford Microfluidics Foundry. The PDMS chip is plasma bonded to glass. We show the Autocad drawing of the chip in figure A-2. We designed the chip to create a total of 40 denaturant cycles,

injected in each of the U-turns of the main channel (between point c and d of the bottom right inset).

All initial injection procedure are performed manually with 1 mL syringes, and valve pressurization is performed with a pump set to 25 psi.

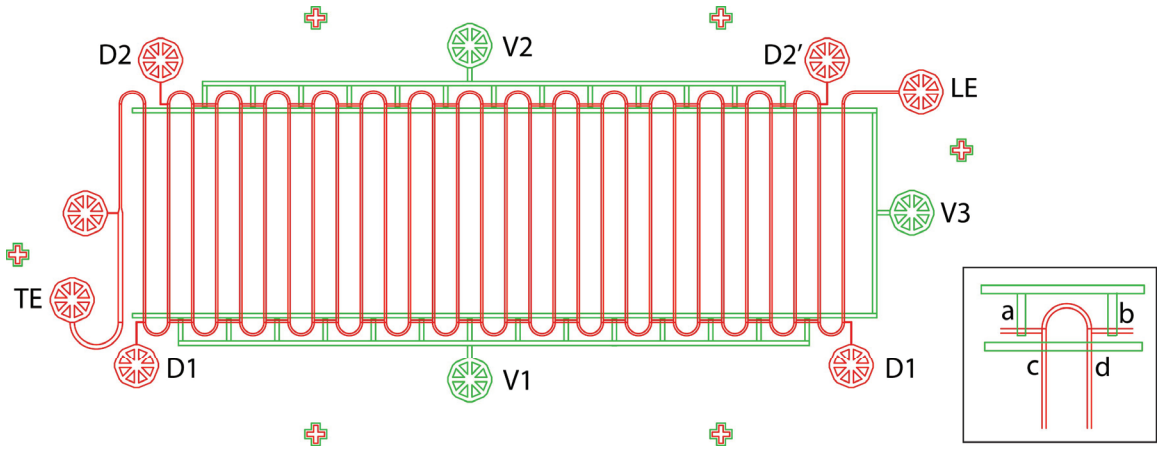

Figure A.2. Multi-layer PDMS-glass device for ccPCR with initial loading of denaturant cycles. The red channel corresponds to the flow layer and the green channels correspond to the control layer. Initially, we fill all flow channels with LE. We apply 25 psi to V3 so that the main serpentine channel is closed at the interception c and d in the inset. Using a syringe pump, we inject denaturant in the turns of the channel (between c and d). Simultaneously, we inject the DNA sample in the wide channel from the TE reservoir. We then release pressure in V3 and apply 25 psi to V1 and V2 to close the connecting channels at intersections a and b in the inset. We place the TE in the TE reservoir and finally apply the electric field between TE and LE reservoirs.

Initially, the serpentine channel is filled with the LE-PCR buffer. We then pressurize V3 to isolate flow in the turns by closing the vales at point c and d (in the inset). We then inject the denaturant at D1 and D@ into the turns through the connecting channels (passing point a and b). At the same time, we will the wise channel connected to the TE reservoir with the DNA template solution. Once the turns are fully filled with denaturant and the template is loaded, we remove pressure from V3 and pressurize V1 and V2. This closes

the small channels connecting the turns (at point a and b in the inset), allowing generation of an electric field in the main reaction channel. We then place THE in the TE reservoir and apply a potential difference between LE and TE to initiate ITP. In such conditions (and under reduced electroosmostic flow), the denaturant cycles remain stationary in the reference frame of the laboratory. The ITP interface therefore experiment denaturing conditions in the turns and annealing and extension conditions in the straight part of the channel.

Appendix B. Injection protocol for multi-stage ITP: additional recommendations

We described the strategy to prepare the chip for miRNA quantitation and molecular beacon assay in detail in Chapter III and IV. In this appendix, we provide additional practical details to setup the multi-stage ITP.

Chip and zone length

The off-the-shelf chip design (model NS260, Caliper LS) is shown in Figure III-6 (reproduced below in Figure B-1 for convenience). The multiple branches of this chip are ideal for initially setting up various LE zones. For quantification of microRNA, we chose to perform ITP in 2 cm of LE1 (1 to A), 4 cm to LE2 (A to B) and 8 mm of LE3 (B to the detector). This injection protocol allows for high selectivity for miRNA. In applications requiring where sensitivity must be privileged over selectivity, increasing the length of LE1 will be beneficial (for example by vacuuming from 5 instead of 3).

Effect of intersections on focused sample

The focused ITP sample passing an intersection may suffer loss of mass and dispersion.[105] Moreover, leading ions present in the branch may leak into the main channel, possibly disrupting ITP. To solve this, we create the LE zones so that there is a slight flow into the branching channel (for example, from A to 3). To do this, we deliver a larger volume (10 µL) of solution in 1 and 8 compared to the other reservoirs (5 µL). The resulting difference of fluid level generates a slight pressure driven flow into the branches connecting.

We note that this induces loss of sample at the intersection, but we found that this loss was small and reproducible.

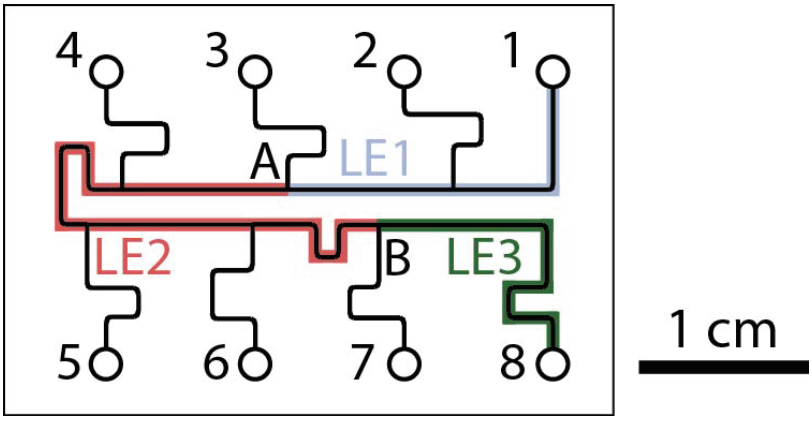

Figure B-1: Design of the caliper NS260 borosilicate glass microchip. Before each experiment, we fill the microchannels with LE1, 2 and 3 according the sequence described in Table III-3. Channel width is not to scale. The three LE zones are highlighted for clarity

Vacuum

We used a single vacuum line (GAST pump) to generate the LE zones. We use a 3 way fitting to split the line and use 200 µl pipette tips (without filter) to connect the line to the plastic caddy holding the chip. We place the two resulting vacuum lines on the reservoirs (here 3 and 7). We switch the pump on to generate vacuum. If the ionic strength or polymer concentration varies significantly between LEs, the interface can be visualized at the intersection from their difference in index of refraction. Finally, the release of vacuum is key to get reproducible LE zones. Both line must be removed from the reservoir simultaneously to avoid disruption of the LE zones. For example, if the vacuum was first released at 3, then at 7, this would induce significant flow

of LE1 into the LE2 zone, and affect the subsequent ITP dynamics. For the same reasons, when rinsing the TE reservoir (1) with water before adding the sample, we recommend to use only a light vacuum.

Rinsing between experiments

PVP has relatively low viscosity compared to other traditional capillary electrophoresis matrices like hydroxyethyl cellulose or linear polyacrylamide. Such matrix is relatively easy to load in microchannels and does not require powerful vacuum. However, we recommend not rinsing the channels with water between experiments. Rinsing all polymer solution from the channel and subsequent refilling can take up to 6 min in our protocol, which considerably reduces experiment throughput without gain. We suggest to use the matrix itself to perform rinsing. This step takes 2 min (or less), cleans possible contamination from previous experiment (RNA or TE ions left in the channel). Also, it continuously maintains conditions for reduced electroosmotic flow.

Appendix C. Free Flow Isotachophoresis for fractionation of nucleic acids and viruses

The content of this appendix is the result of an ongoing collaboration with Klint Rose at the Lawrence Livermore National Laboratories. The goal of this project is to build a free flow isotachophoresis module to separate nucleic acids from viruses in a biological sample (*e.g.* nasal rinse or blood). We here present the preliminary results that initiated this project.

Introduction

Sample preparation becomes more tedious for contaminated samples. Detection of a virus or bacteria in a biological fluid requires further sample preparation, which is typically performed using traditional benchtop techniques. Currently, there is no system that allows for fully automated sample preparation for the detection of pathogens. In particular, respiratory pathogens are particularly difficult to prepare for analysis as their concentration is low and the noise induced by other species is large.[1] In the scope the development of a versatile, size based fractionation system for the preparation of aerosol pathogens, we developed and demonstrated an ITP unit able to filter sub-micrometer size species. We demonstrated the efficacy of this filtration module by fractionating a larger volume of a mixture of DNA and MS2 bacteriophage virus. This module offers the possibility to perform sample fractionation but can also be adapted to increase the throughput of the ITP-based nucleic acid purification described above.

We propose an ITP free flow electrophoresis (FFE) device to increase the throughput of ITP purification (described in chapter II) by orders of magnitude (to 0.1 ml/min). FFE is based on electrophoretic separation where the electric field is applied perpendicularly to a sample flow stream.[106] For the first time, we combine FFE with ITP so that species flow in one dimension while continuously being focused and segregated via ITP in a second dimension. Downstream collection streams allow us to extract purified species. We here propose to adapt this approach to collect, preconcentrate, and fractionate target biological compounds into sharp, focused streams. Specifically, we will use free flow ITP to selectively extract DNA from complex samples.

We show the principle of the free flow ITP device on figure C-1. We apply flow to a four-inlet, three-outlet chamber. The two pairs of slanted inlet and outlet channels on the peripheries are connected to off-chip electrodes with high conductivity buffers. The top inlet has high conductivity TE, and the bottom high conductivity LE. These outer high conductivity sheath flows act as nearly constant voltage “nodes” or “buses” (“liquid electrodes”) allowing a largely transverse field across the center TE/LE stream. This allows us to move electrodes to traditional, vented, end-channel electrodes to avoid interference by electrolysis or electrochemical reactions.[107] We inject the sample (in LE) in one inner (horizontal) inlet and TE in another and these merge before entering the focusing chamber (not shown). Anionic species present in the sample will migrate towards the LE liquid electrode, and focus if and only if LE and TE bracket their mobility. The careful selection of TE and

LE allows highly specific focusing of nucleic acids in the stream. The focused stream can then be directed into a narrow outlet (horizontal) channel while the rest of the sample is collected in two other outlet channels. We designed a prototype device based on this concept and discuss it below.

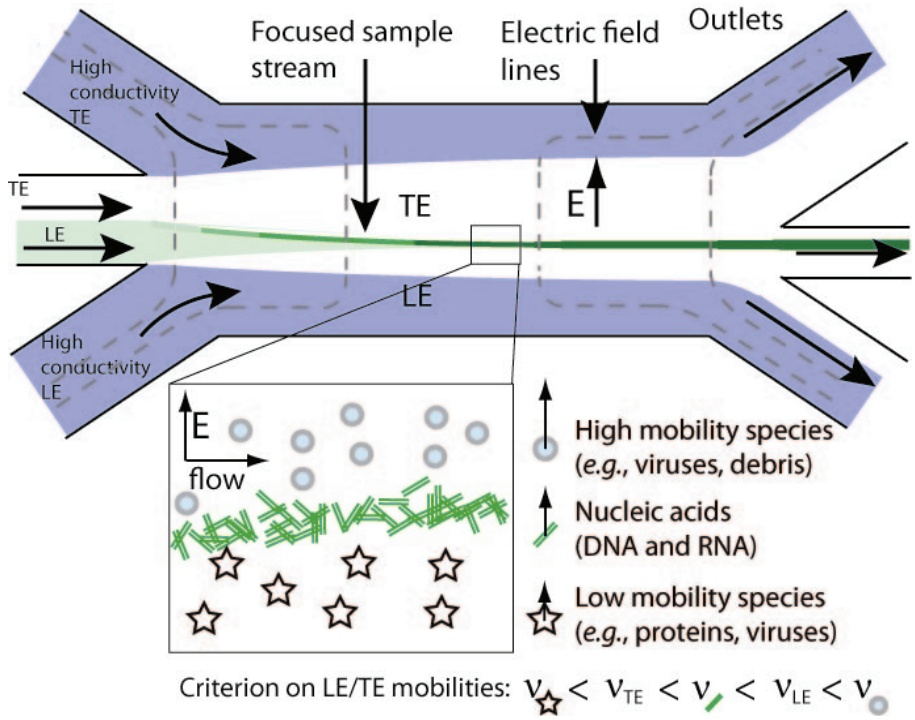

Figure C-1: Schematic representation of our free flow ITP nucleic acid extraction system. The device is composed of a four inlet, four outlet channels. A "liquid electrode" concept is applied wherein high conductivity sheath flows (in grey) of TE (topmost) and LE (bottommost) are used to apply a transverse electric field to a pre-stratified sample stream (near center with horizontal inlet) consisting of TE (top center) and a mixture of LE and sample (bottom center). The dashed lines correspond to a schematic of electric field lines. Sample flows directly from left to right by pressure driven flow. Species migrate in order of increasing electrophoretic mobilities v (close-up view on bottom left). Only species with mobilities between those of the LE and TE will focus in a sharp stream. An outlet collection channel allows extraction of the nucleic acid after focusing; the two other outlets allow recovery of alternately low and high mobility species purified from nucleic acids.

Preliminary experiments demonstrating ITP-based extraction.

On-chip ITP extraction of DNA from nasal rinse sample. We have completed proof-of-principle experiments demonstrating the efficacy of ITP-based selective extraction of extracellular DNA from nasal rinse. We collected

a nasal rinse from a healthy patient using a commercial rinse solution (Ayr) and performed a series of ITP based extractions including negative controls as shown in Figure C-2.

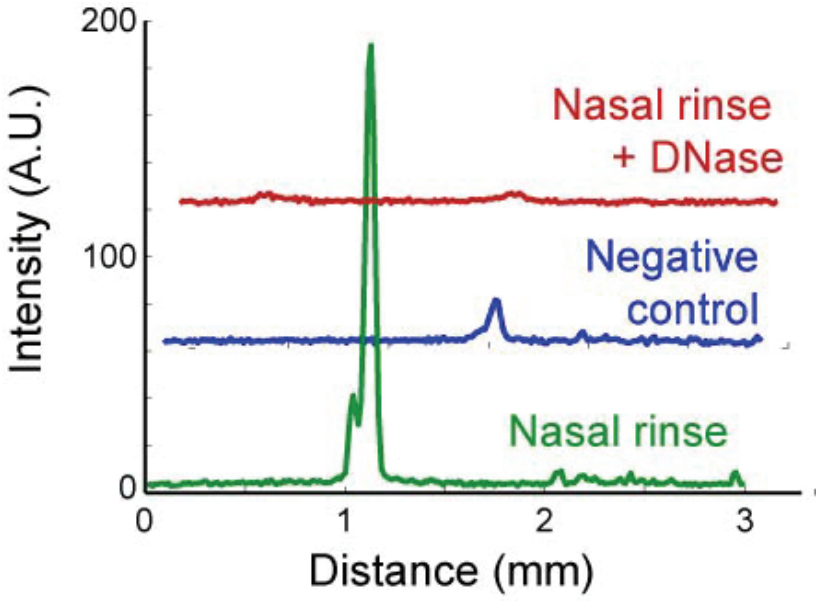

Figure C-2: Signals (staggered) from ITP extractions of nucleic acids from a nasal rinse from a healthy patient. Each curve shows the channel-cross-sectional-averaged fluorescence from DNA intercalating dye. The bottom curve shows ITP where the LE is the nasal rinse. It shows significant signal compared to the negative control. The top trace corresponds to ITP of the same nasal rinse after DNA digestion by DNase.

The channel is first filled with the nasal rinse sample. The cathode reservoir is then filled with a solution of TE. Upon application of an electric field, the fluorescent sample focuses at the interface between LE and TE. As shown in the figure, pretreatment of the sample with DNase (enzyme specifically digesting DNA) shows that the fluorescent peak is DNA. This experiment shows we can extract nucleic acids from a complex biological sample via ITP.

Preliminary experiments demonstrating free flow ITP-based extraction. We have built an initial prototype of our ITP-based FFE extraction system as depicted in Figure C-1 and completed a series of preliminary experiments demonstrating its efficacy. Using this prototype, we performed a set of experiments where we verified focusing of DNA. As shown in Figure C-3, a 1 kbp DNA ladder focuses in a sharp and concentrated stream. We were able to perform this experiment with a sample flowing at 100 $\mu L.min^{-1}$, enabling processing of 1 mL of sample in 10 min.

Demonstration of ITP chemistry for fractionation of viruses from DNA by free flow ITP. We performed a classical on-chip ITP assay with a sample containing MS2 bacteriophage and a 1 kbp ladder. We labeled MS2 with the red fluorescent dye Alexa Fluor 594. This yields a mixture of tagged viruses and free dye.[108] We show ITP separation results in the inset of Figure C-4. This experiment demonstrates the potential of ITP to specifically purify and fractionate viruses from DNA and proteins. A spacer focuses between the virus and a zone containing both tagged DNA and the labeling byproducts. The choice of this spacer is based on the known mobilities of the MS2 bacteriophage and DNA.[55, 109]

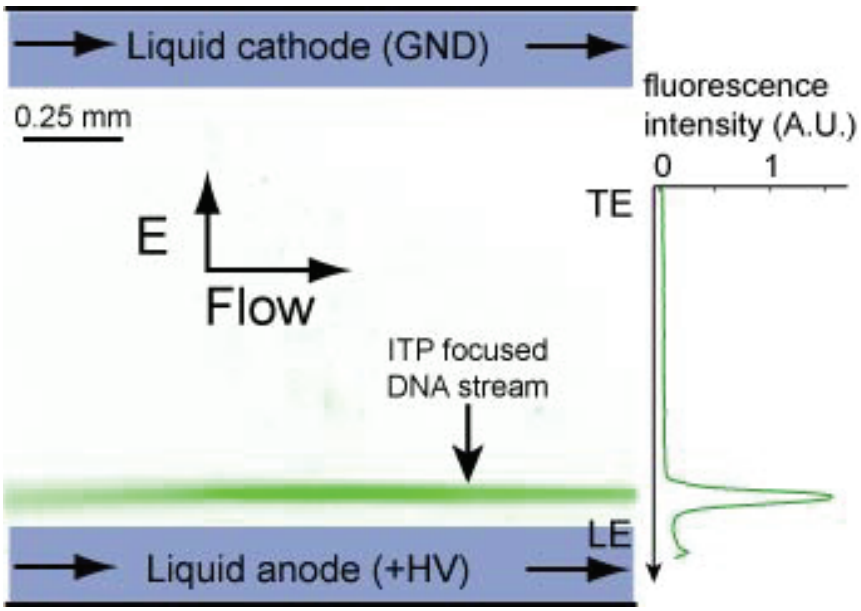

Figure C-3: DNA focusing experiment in our free flow ITP device. The high conductivity TE and LE "liquid electrode" sheath streams are respectively 1M HEPES and 0.5 M Tris hydrochloride, flowing at 20 $\mu L.min^{-1}$. Stratified TE and LE flow in the inner inlet channels at 40 $\mu L.min^{-1}$; these are respectively 20 mM HEPES and 10 mM Tris hydrochloride containing a DNA ladder. DNA focuses in a sharp stream. The plot on the right shows axial average of the fluorescent signal.

We also performed experiments demonstrating the ability of our FFE ITP device to focus, fractionate, and extract DNA from a virus stream. We filter out DNA from a sample containing MS2 bacteriophage. We show a sample result on Figure C-4. We diluted the labeled viruses and DNA into the LE buffer. Distinct emission wavelengths of the tagged virus and DNA allow separate visualization of their respective concentration fields. We show results of the FFE ITP filtration experiment in Figure C-4. Upon application of an electric field, DNA and free fluorophores focus into a sharp stream between TE (HEPES ions) and LE (chloride ions). MS2 bacteriophage has lower mobility than the TE and consequently does not focus. This results in the

unfocused “tail” region (on the left side of the axial-averaged fluorescence signal) which will be separated from the DNA using a spacer ion as in the inset.

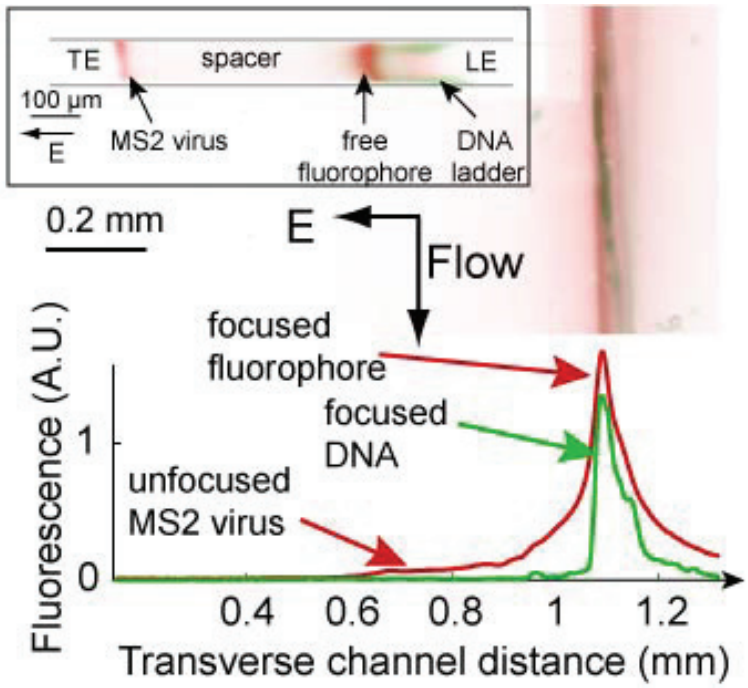

Figure C-4: Preliminary results demonstrating focusing of DNA while avoiding focusing of virus stream via free flow ITP. LE contains tagged MS2 bacteriophage and DNA. At the top, is a composite image of green (DNA) and red (free fluorophore and virus) fluorescence. Below, the plot shows axial fluorescence average for each green and red emission wavelengths. Visualization in the green shows a strong peak corresponding to DNA focusing. In the red, the strong peak corresponds to free dye. The red fluorescent “step” signal between about 0.6 and 0.9 mm is due the unfocused, low-mobility virus. The top left inset shows ITP separation of MS2 virus and DNA and free dye with the aid a spacer ion. LE contains a DNA ladder and HEPES used as spacer. Free dye focuses at the same place as the DNA.

Appendix D. Compatibility of chemical lysis with ITP

We here present multiple lysis methods and discuss their compatibility with ITP. We describe the most common and widely applicable lysis methods, but multiple alternate protocols can be found in the literature, in particular for particularly difficult lysis.

Detergents

Detergents are commonly used for multiple lysis protocols. They have the ability to disrupt the cell membrane, and sometimes require mechanical grinding. The choice of detergent will depend on the cell type. For example, cells with weak membranes can be disrupted with a zwitterionic detergent, while tougher cells require the use of a charged detergent (which solubilizes lipid bilayers more effectively). A drawback of the use of charged detergents is the possible denaturation of proteins in the cell (however this is acceptable when preparing of nucleic acids).

The zwitterionic detergent series Triton X is widely used for mild lysis protocols, for example for disruption of white blood cells (*cf*. protocol in Chapter II). Other zwitterionic detergents include CHAPS, Brij 35, TWEEN. For tougher lysis, for example for bacteria or yeast, ionic detergents such as sodium dodecyl suflate (SDS) are more efficient disruption agents. A more comprehensive list of lysis agents can be found on the Sigma Aldrich website.[110]

Chaotropic agents

Commercial kits for the extraction of nucleic acids generally use a reagent that allows for simultaneous lysis and phase separation of nucleic acids and proteins. Chaotropic salts destabilize protein interactions and therefore disrupt cell walls (and simultaneously effectively denature proteins). Commonly, high concentration guanidine salts (*e.g.* 6 M guanidine hydrochloride) are used as chaotropes for cell lysis. These high concentration salts are typically used in conjunction with solvents with poor solubility (phenol, isopropanol, chloroform) for phase separation of proteins from nucleic acids.

These reagents are extremely attractive for benchtop nucleic acid purification as they simultaneously lyse and avoid nucleic acid degradation (*e.g.* RNase degradation) but their on-chip implementation remains complex as it involves the control of multiple phases (liquid-liquid or solid-liquid).

Compatibility with ITP

In table D.1, we compare the different types of chemical lysis methods for combination with ITP based purification of nucleic acids. The most practically lysis method for such combination is the use of neutral detergents. We note that numerous additives can be used along with detergents to increase lysis performance (*e.g.* proteinase K, lyzozyme).

Lysis methods	Advantages	Drawbacks	ITP compatibility	Typical concentrations
zwitterionic (neutral) detergents	generally simple chemistry (detergent + buffer) enable use of additives (proteinase K or lysozyme)	weak lysis (not applicable to bacteria) does not denature proteins (in particular RNase and histones) may require heating	Yes	Triton X100: 0.1% for blood lysis
ionic detergents	strong lysis (*e.g.* for bacteria) potentially denature proteins	inhibit PCR may require heating	Require dilution of lysate (>10 fold)	SDS: 2.5% w/v
chaotropic salts	strong lysis inhibit nucleic acid degradation	generally require phase separation inhibit PCR	Require dilution of lysate (>100 fold)	4 M guanidinium thiocyanate
hypotonic buffers	simple chemistry	very weak lysis, rarely applicable	Yes	5 mM sodium phosphate

Table D.1. Summary of advantages and drawbacks of chemical lysis techniques and compatibility with ITP